From acute to persisting damage: CHK2 is crucial for sustaining the p53 response

vom Fachbereich Biologie

der Technischen Universität Darmstadt

zur Erlangung des Grades

Doctor rerum naturalium

(Dr. rer. nat.)

Dissertation

von Laura Friedel

Erstgutachter: Prof. Dr. Alexander Löwer

Zweitgutachter: Prof. Dr. Markus Löbrich

Darmstadt 2022

Friedel, Laura: From acute to persisting damage: CHK2 is crucial for sustaining the p53 response

Darmstadt, Technische Universität Darmstadt

Jahr der Veröffentlichung der Dissertation auf TUprints: 2022

Tag der mündlichen Prüfung: 29.04.2022

CONTENT

ABSTRACT

The choice between life and death is one of the most vital decisions a cell has to make when challenged with different sources of stress. This choice is confounded by variable cellular states, which change throughout the stress response due to both, input from the environment and countermeasures initiated by the cell. The transcription factor p53 is a crucial player orchestrating the cellular response to DNA damage. It not only decides whether a cell should live or die, but it also arrests the cell cycle to provide time for the DNA repair machinery to restore the integrity of the genome. In response to DNA double-strand breaks, p53 shows a series of uniform pulses of accumulation lasting over several hours. In this time, the status of the genome is changing significantly: While during the first pulse the cell is challenged with newly emerged breaks, during the second and the following pulses many breaks have been repaired with only complex breaks and lesions in heterochromatic regions remaining.

In this thesis, I investigated whether this change in the status of the genome is reflected in the p53 response. Using live-cell microscopy and pharmacological inhibitors, I provide evidence that the immediate response to acute damage and the sustained response to persisting damage are mediated by two different though interconnected upstream signals: The kinase ATM is crucial to initiate the p53 response and to respond to new DNA damage detected by the cell. Furthermore, active ATM is essential for the initial activation of the checkpoint kinase CHK2. However, sustained activity of ATM is dispensable for both, sustained oscillations of p53 and maintaining CHK2 activity. In contrast, continuous input by CHK2 is crucial for sustaining the p53 response. I could provide first indications that CHK2 modulates p53 levels by inducing the degradation of the negative regulator MDMX thereby destabilizing MDM2. To investigate the impact of these different upstream networks on p53's function as a transcription factor, the posttranslational modification (PTM) state, kinetics of promoter binding and target gene transcription were assessed for the immediate response (1st pulse) and the sustained response (2nd pulse). I could show that p53's PTM state changes between the first and second pulse. Comparing the binding of p53 across different loci, no gene-specific patterns of promoter binding were observed. However, we observed gene-specific patterns of transcription which varied particularly for the second pulse. By altering the time-varying PTM state of p53, we were able to modulate both promoter binding and gene-specific patterns of target gene transcription. All in all, I provide evidence that the immediate and the sustained p53 response are mediated by different upstream signals inducing time-varying posttranslational modifications that in turn modulate target-specific gene transcription. Consequently, my work provides first indications that different molecular barcodes might allow differentiating between acute and persisting breaks.

ZUSAMMENFASSUNG

Die Wahl zwischen Überleben und Tod ist eine der zentralen Entscheidungen, die Zellen in Gegenwart von verschiedenen Stressoren treffen müssen. Diese Wahl ist umso heikler, da die Grundlage der Entscheidung, der Zustand der Zelle selbst, sich im Laufe der zellulären Stress-Antwort fortwährend verändert. Dies liegt zum einen daran, dass zusätzliche Einflüsse aus der Umwelt die Prozesse beeinflussen können. Zum anderen initiiert die Zelle selbst Gegenmaßnahmen, um potenziell gefährliche Auswirkungen abwehren zu können. Der Transkriptionsfaktor p53 ist ein wichtiger Teil der zellulären Stress-Antwort: Er koordiniert die Reaktion auf DNA-Schäden und entscheidet darüber, ob eine Zelle überlebt oder sterben muss. Darüber hinaus kann er auch ein Anhalten des Zellzyklus initiieren, um ausreichend Zeit zu schaffen, in der die DNA-Reparaturmaschinerie die Integrität des Genoms wiederherstellen kann. Wenn DNA-Doppelstrandbrüche in der Zelle auftreten, zeigt p53 eine Serie von gleichförmigen Pulsen der Akkumulation, welche je nach Schadensdosis über mehrere Stunden anhalten können. In dieser Zeit verändert sich der Zustand des Genoms signifikant: Während im Verlauf des ersten Pulses eine Vielzahl an neuen DNA-Brüchen vorlag, sind viele dieser Brüche während des zweiten Pulses bereits repariert und nur komplexe Brüche sowie Läsionen in Regionen des Heterochromatins verbleiben.

In dieser Dissertation habe ich untersucht, wie sich diese Veränderung im Zustand des Genoms in der p53 Antwort widerspiegelt. Unter Verwendung von Lebendzell-Mikroskopie und pharmakologischen Inhibitoren konnte ich zeigen, dass die unmittelbare p53 Antwort auf akuten Schaden und die anhaltende Antwort auf bestehende Schäden durch zwei unterschiedliche jedoch vernetzte vorgeschaltete Signale vermittelt werden: Die Kinase ATM ist entscheidend, um die p53 Antwort zu initiieren und auf neu detektierte DNA-Schäden zu reagieren. Darüber hinaus ist aktives ATM essenziell für die initiale Aktivierung der *checkpoint* Kinase CHK2. Eine fortwährende Aktivierung von ATM ist allerdings entbehrlich sowohl für anhaltende Oszillationen von p53 als auch für die Aufrechterhaltung von aktivem CHK2. Im Gegensatz dazu war kontinuierliche Aktivität von CHK2 jedoch essenziell, um andauernde p53 Pulse zu generieren. In ersten Experimenten konnte ich zeigen, dass CHK2 die p53 Level moduliert, indem es die Degradierung des negativen Regulators MDMX induziert und so MDM2 destabilisiert. Um herauszufinden, wie diese verschiedenen Netzwerke die Funktion von p53 als Transkriptionsfaktor beeinflussen, wurden seine posttranslationalen Modifikationen (PTM), die Kinetiken der Promotor-Bindung sowie die Transkription der Zielgene während der unmittelbaren Antwort (1. Puls) und der anhaltenden Antwort (2. Puls) untersucht. Ich konnte zeigen, dass die vorliegenden PTM zwischen dem ersten und dem zweiten Puls wechseln. Ein Vergleich der Bindung von p53 an Promotoren der verschiedenen Zielgene zeigte keine Gen-

spezifischen Muster. Allerdings beobachteten wir Gen-spezifische Muster bei der Transkription. Hierbei traten die Unterschiede vorrangig während des zweiten Pulses auf. Durch Veränderung der vorliegenden PTM konnten wir sowohl die Promotor-Bindung als auch die spezifischen Transkriptionsmuster modulieren. Alles in allem zeige ich in dieser Arbeit, dass die unmittelbare und die anhaltende p53 Antwort durch verschiedene vorgeschaltete Signale vermittelt werden. Diese Signale wiederum induzieren spezifische PTM, die infolgedessen im Verlauf der Antwort variieren und die Transkription spezifischer Zielgene beeinflussen. Somit zeigt meine Arbeit, dass mithilfe von solchen molekularen Barcodes zwischen neuem, akutem Schaden und bereits vorhandenem Schaden unterschieden werden kann.

CONTRIBUTIONS

The research presented here in this thesis was conducted in the group of Alexander Loewer at the Technical University in Darmstadt. Parts of the introduction were published in a similar form as a review (Friedel and Loewer, 2022). Most of the experimental data shown in this thesis was conceived, performed and analyzed by me. To push the impact of my study beyond the borders of my own research expertise, I combined my experimental data with mathematical modeling conducted by Raphael Löffler, Isabella Mender and Barbara Drossel (TU Darmstadt). Figures derived from this collaboration are clearly marked in the respective section.

Moreover, I teamed up with Dhana Friedrich (Humboldt University, Berlin) to explore p53's role as a transcription factor. The data resulting from this collaboration has already been published (Friedrich *et al.*, 2019). In the present study, smFISH data was provided by Dhana Friedrich. This experimental contribution is clearly indicated in the individual figures.

Finally, excellent technical assistance was provided by Petra Snyder who also supported the conduction of the live-cell microscopy experiment shown in Figure 3.7.4C and D.

1 INTRODUCTION

1 INTRODUCTION

In our daily life, we are often confronted with stressful situations. To overcome these situations, we have developed specific skills and techniques. Similarly, the cells in our body are challenged by distinct kinds of stress as well. One of the most critical conditions our cells have to face are lesions in the blueprint of life, the DNA. Up to 10^5 spontaneous DNA alterations can arise per day and cell (Hoeijmakers, 2009; Ciccia and Elledge, 2010). Additionally, exogenous sources like ionizing (IR) or ultraviolet (UV) radiation lead to thousands more lesions. The probably most dangerous lesions of the DNA are double-strand breaks (DSB). They arise upon exposure to IR, for instance when taking medical X-ray images, or naturally during replication, when single-strand breaks (SSB) or base modifications collide with the replication fork (Helleday *et al.*, 2007). If not taken care of, these lesions can lead to chromosomal aberrations and the formation of cancer. Consequently, our cells have sophisticated tools available to counteract these genomic insults. The two main pathways facilitating DNA DSB repair are homologous recombination (HR) and non-homologous end-joining (NHEJ) (Ciccia and Elledge, 2010; Jeggo, Geuting and Löbrich, 2011). During NHEJ, DSB ends are bound within seconds by the heterodimer KU70/80, which then recruits the DNA-dependent protein kinase catalytic subunit (DNA-PKcs) together forming the DNA-PK holoenzyme. Binding of DNA-PK to the break ends as well as distinct auto-phosphorylation steps control processing of the ends (Ciccia and Elledge, 2010; Chang *et al.*, 2017). Finally, the re-ligation of the ends is facilitated by XRCC4/LIG4 and XLF. While NHEJ is available in all cell cycle phases, the use of HR is limited to S- and G2-phase as this pathway requires a sister chromatid as a template for repair. During HR, DSB are recognized by the Mre11-Rad50-NBS1 (MRN) complex recruiting several factors that together induce extensive DSB end resection (Ciccia and Elledge, 2010; Liu and Kong, 2021). The thereby generated single-stranded DNA (ssDNA) overhangs are coated with replication protein A (RPA) which is subsequently replaced by the recombinase RAD51 mediating strand invasion into complementary sequences. In the following, different sub-pathways can be used to finalize repair.

Upon genotoxic stress, cells do not only take care of repairing the damage. They also have to make an appropriate decision about the cell fate depending on the severity of the damage: cells have to choose between proliferation and arrest or sometimes even between survival and death. Wrong choices can have severe consequences: if damaged and genetically altered cells decide to proliferate instead of inducing apoptosis, cancer can arise. One of the proteins in charge of such vital decisions is the guardian of the genome, p53.

1.1 Call the guardian: The tumor suppressor p53

P53 is activated by a variety of different stresses ranging from nutrient deprivation and hypoxia to damage of our genome (Kruiswijk, Labuschagne and Vousden, 2015). As a transcription factor (TF), p53 controls the expression of several hundreds of genes (Fischer, 2017) and is thereby able to induce cell fates ranging from cell cycle arrest to senescence and apoptosis upon DNA damage (Murray-Zmijewski, Slee and Lu, 2008). Among these targets are CDKN1A (involved in cell cycle arrest) and BAX (involved in apoptosis). Many tumors have mutations either of p53 itself or of members of its signaling pathway, underlining its importance as a tumor suppressor (Muller and Vousden, 2013). To prevent inappropriate induction of senescence or cell death, the p53 response is regulated on several levels (Figure 1.1.1). On a first level, the p53 response in the cell is tightly controlled through its activating pathways. These pathways are directly connected to the DNA damage response machinery and thereby allow a sensitive and precise response to genotoxic stress (Blackford and Jackson, 2017).

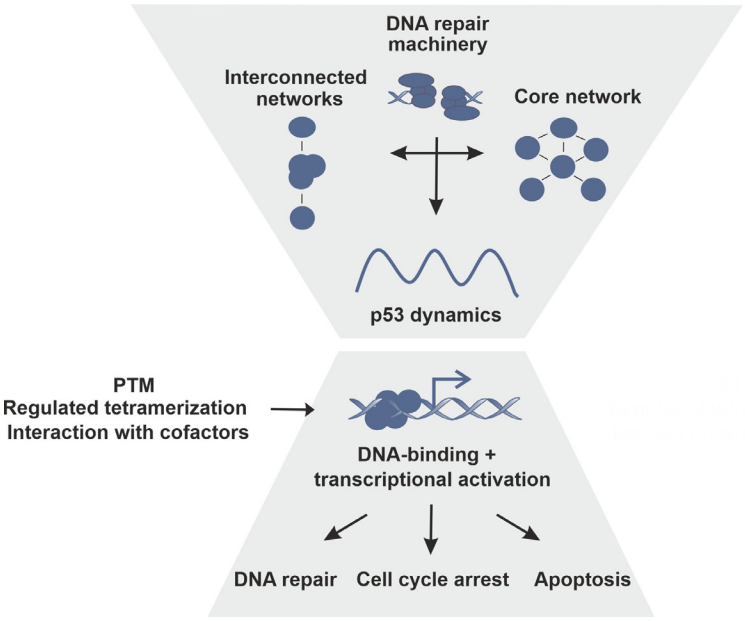

Figure 1.1.1: Regulatory levels of the p53 response.

The p53 response to DNA damage is regulated and adjusted on several levels. As a first layer, a tightly regulated interplay of canonical regulators in combination with crosstalk to other signaling pathways allows a damage-specific response. The resulting p53 dynamics are decoded on the promoter level. In this step, several mechanisms allow the diversification of the single p53 input signal. Using different patterns of PTM as well as controlled oligomerization and interaction with cofactors, the expression of distinct target genes and different cellular outcomes can be induced.

1.2 The meat of the matter: An interplay of positive and negative regulators constitutes the core of the p53 network

Under non-stressed conditions, p53 levels in the cell are kept low preventing inappropriate expression of its targets. P53's main negative regulator is the E3 ubiquitin ligase MDM2. P53 and MDM2 interact via their N-terminal domains facilitating ubiquitination and subsequent proteasomal degradation of p53 (Rodriguez *et al.*, 2000; Li *et al.*, 2003; Chi *et al.*, 2005). Additionally, MDM2 is a direct target of p53 creating a negative feedback loop (Barak *et al.*, 1993; Wu *et al.*, 1993). The importance of this interaction was highlighted by studies with MDM2 deficient mice showing that embryonic lethality in *MDM2* null mice can be rescued by deletion of p53 (Jones *et al.*, 1995; Luna, Wagner and Lozano, 1995).

When the cell encounters genotoxic stress, the MRN complex is recruited to the lesions and in turn, recruits the kinase ATM. In its inactive form, ATM is present as an inactive homodimer (Kastan and Bakkenist, 2003; Bakkenist and Kastan, 2004) (Figure 1.2.1A).

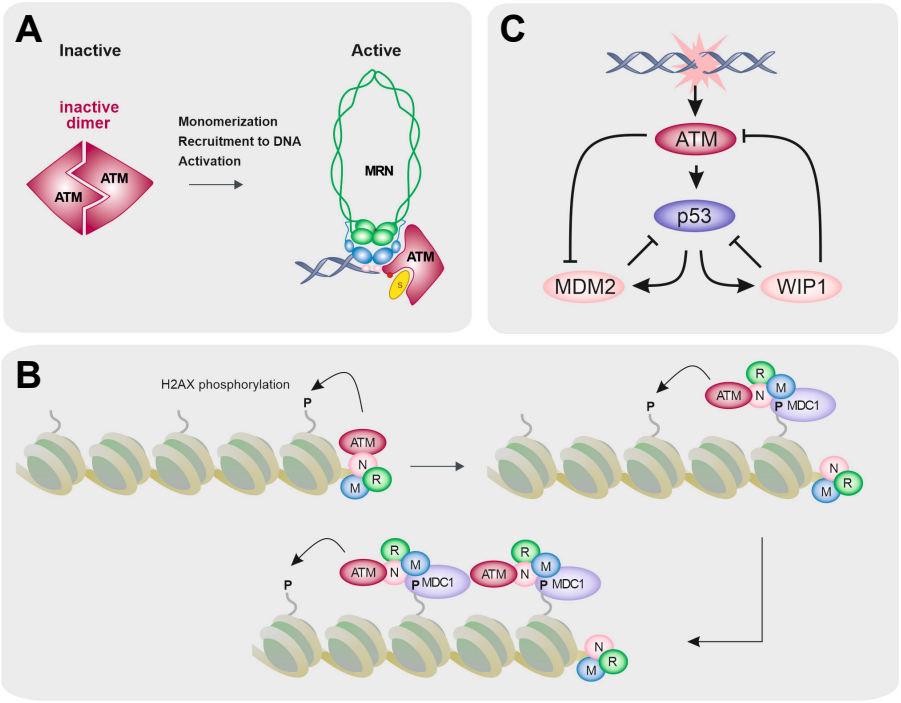

Figure 1.2.1: Activation of the p53 response via the kinase ATM.

A. Activation of the kinase ATM in response to DNA damage. In the absence of stress, ATM forms inactive noncovalent dimers. In response to DNA damage, the Mre11-Rad50-Nbs1 (MRN) complex facilitates the monomerization and activation of ATM. Rad50 in blue, Mre11 in green, Nbs1 in pink. Adapted from Paull, 2015. **B.** ATM and MDC1 mediated phosphorylation of histone H2AX. M: MRE11; R: RAD50; N: NBS1. MRN complex promotes activation of ATM which in turn phosphorylates H2AX. MDC1 binds to γH2AX which leads to the recruitment of more MRN and ATM. Modified according to West and Attikum, 2006. **C.** Schematic overview of the p53 network in response to DSB. Upon genotoxic stress, the kinase ATM mediates the stabilization and activation of p53. P53 can then induce the expression of its target genes including the negative regulators WIP1 and MDM2. These two proteins terminate the p53 response.

Upon retention at the break side, the MRN complex facilitates the monomerization and activation of the kinase (Lee and Paull, 2004). During activation, ATM undergoes auto-phosphorylation on several residues including S1981, which can be used as a marker for ATM activation (Kastan and Bakkenist, 2003; for detailed reviews see Paull, 2015; Lee and Paull, 2021)). Active ATM phosphorylates histone variant H2AX that allows the recruitment of other proteins participating in the DNA damage response like MDC1. In turn, MDC1 tethers more MRN to the break site, which again promotes the activation of ATM and thereby enhances H2AX phosphorylation (Figure 1.2.1B) (Lou *et al.*, 2006; Stucki and Jackson, 2006). This positive feedback loop facilitates the spreading of phosphorylated H2AX (γH2AX) over several megabase-pairs and promotes rapid, switch-like activation of ATM (Rogakou *et al.*, 1999).

Besides H2AX and several other proteins, activated ATM also rapidly phosphorylates p53 on S15 disturbing the interaction between p53 and MDM2 (Lees-Miller *et al.*, 1992; Shieh *et al.*, 1997; Banin *et al.*, 1998; Canman *et al.*, 1998). In addition, ATM modifies MDM2 on S395 inducing the degradation of the E3 ubiquitin ligase (Khosravi *et al.*, 1999; Maya *et al.*, 2001; Stommel and Wahl, 2004). The stabilization of p53 combined with the destabilization of the negative regulator MDM2 leads in total to an accumulation of p53 in the nucleus (Figure 1.2.1C). The TF can then promote the expression of its target genes, mediating the cellular response to damage. Among the target genes are negative regulators of p53 such as MDM2 and the phosphatase WIP1 (encoded by the gene PPM1D), which limit p53 accumulation (Barak *et al.*, 1993; Wu *et al.*, 1993; Fiscella *et al.*, 1997). WIP1 dephosphorylates several proteins involved in the DNA damage response as p53, ATM and MDM2 (Lu, Nguyen and Donehower, 2005; Shreeram *et al.*, 2006) thereby facilitating the degradation via MDM2.

ATM belongs to the family of PI3K-like kinases (PIKK). Two other crucial players of the DNA damage response belong to this family as well and were reported to modify p53. DNA-PKcs is an important key player during NHEJ (see section 1) that also mediates phosphorylation of p53 on S15 (Lees-Miller, Chen and Anderson, 1990; Lees-Miller *et al.*, 1992) (Figure 1.2.2). Interestingly, DNA-PKcs also phosphorylates ATM leading to a decreased activity of the kinase (Zhou *et al.*, 2017). Consequently, inhibition of DNA-PKcs was shown to cause an amplified p53 response due to hyperactive ATM (Finzel *et al.*, 2016). The third kinase of the PIKK family modifying p53 is ATR (Lakin, Hann and Jackson, 1999; Tibbetts *et al.*, 1999). Upon UV radiation or in response to DSB during HR, DNA lesions exhibit long stretches of single-stranded DNA. These stretches are coated with RPA leading to the binding of ATRIP, which in turn facilitates the recruitment and activation of ATR in a TOPBP1 and 9-1-1 (RAD9-HUS1-RAD1) dependent manner (Zou and Elledge, 2003; Ball *et al.*, 2007; Mordes and Cortez, 2008) (Figure 1.2.2). As with ATM and DNA-

PKcs, active ATR phosphorylates p53 on S15 contributing to its stabilization post DNA damage (Lakin, Hann and Jackson, 1999; Tibbetts *et al.*, 1999).

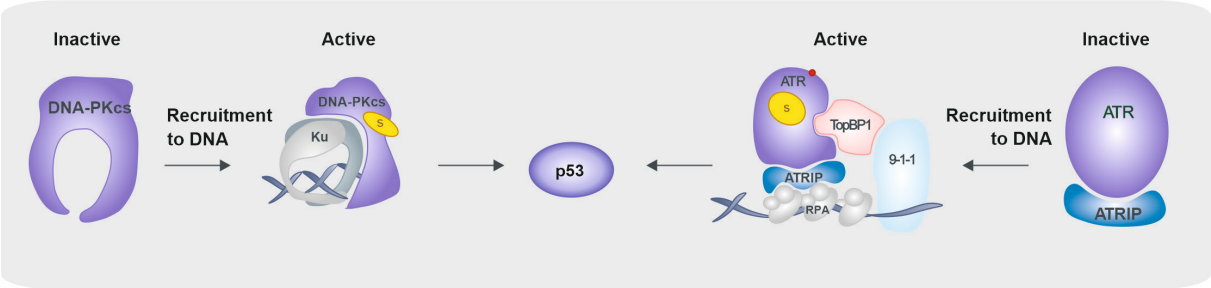

Figure 1.2.2: The PI3K-like kinases DNA-PKcs and ATR phosphorylate p53 in response to genotoxic stress.

In response to DNA DSB, DNA-PKcs localizes at DNA ends with the KU70/80 heterodimer forming the DNA-PK holoenzyme. ATR is bound to the cofactor ATRIP (ATR-interacting protein) in its inactive state. After exposure of RPA coated single-stranded DNA, the ATR-ATRIP complex is recruited to the DNA break site. The activator protein TopBP1 is recruited to the site of damage via interaction with the 9-1-1 (RAD9-HUS1-RAD1) complex. Both, ATR and DNA-PKcs can then phosphorylate p53 on S15 contributing to its stabilization post DNA damage. Adapted from Paull, 2015.

Besides S15, several other residues in p53's N-terminal domain are phosphorylated in the course of the DNA damage response. The checkpoint kinase CHK2 is activated in response to DNA damage and in turn, phosphorylates dozens of other proteins including p53. Thereby, CHK2 influences different cellular responses with the most well-known one being the induction of cell cycle arrest at G1/S and G2/M via Cdc25A and Cdc25C (Matsuoka, Huang and Elledge, 1998; Falck *et al.*, 2001). ATM activates CHK2 by phosphorylation of T68 and other residues in the C-terminal SQ/TQ cluster (SCD) domain of CHK2 (Figure 1.2.3A). These modifications induce dimerization of CHK2: Two CHK2 monomers bind via their SCD and forkhead-associated (FHA) domains (Ahn *et al.*, 2000; Xu, Tsvetkov and Stern, 2002; Buscemi *et al.*, 2006; Zannini, Delia and Buscemi, 2014). Dimerization facilitates auto-phosphorylation of CHK2 on several residues located especially in the T-loop as T383, T387 and S516 (Figure 1.2.3B) (Schwarz, Lovly and Piwnica-worms, 2003; Wu and Chen, 2003; Zannini, Delia and Buscemi, 2014). This auto-phosphorylation event finally promotes the dissociation into two active monomers. Studies suggested that active CHK2 phosphorylates p53 on S20 and thereby contributes to preventing the degradation of p53 (Chehab *et al.*, 1999; Hirao *et al.*, 2000).

In addition to MDM2 and WIP1, the homolog of MDM2, MDMX, has been connected to the p53 network as a negative regulator. Despite high structural similarity to MDM2 (Figure 1.2.3C), MDMX itself only has weak intrinsic E3 ubiquitin ligase activity (Badciong and Haas, 2002; Chen, 2012). However, it forms heterodimers with MDM2 through their RING domains thereby increasing both the stability and E3 ubiquitin ligase activity of MDM2 (Sharp *et al.*, 1999; Linares *et al.*, 2003; Wade and Wahl, 2010; Pei, Zhang and Zheng, 2012) (Figure 1.2.3C). Through the formation of these heterodimers, MDMX indirectly enhances p53 degradation. Additionally,

recent studies indicated that MDMX negatively regulates p53's transcriptional activity by masking the transactivation domain as well as by inhibiting its sequence-specific binding to DNA (Francoz *et al.*, 2006; Wei *et al.*, 2016; Huang *et al.*, 2018). In response to damage, MDMX is phosphorylated on several residues including S403 via ATM as well as S342 and S367 via CHK2 (Chen *et al.*, 2005; Okamoto *et al.*, 2005).

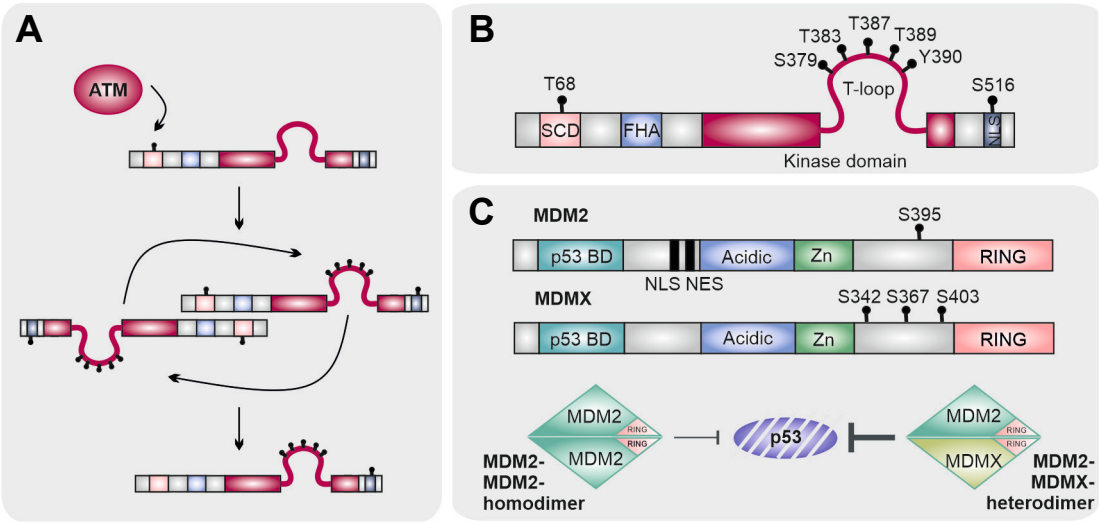

Figure 1.2.3: Activation of CHK2 in response to DNA damage.

A. Under non-stressed conditions, CHK2 resides as a monomer in the nucleus. In response to genotoxic stress, CHK2 is phosphorylated on T68 and other sites via the kinase ATM. These modifications induce dimerization of CHK2, which subsequently facilitates auto-phosphorylation of several residues in the T-loop of the kinase domain as well as S516 in the nuclear localization signal (NLS). These autophosphorylation steps induce the dissociation into active monomers. Adapted according to Zannini, Delia and Buscemi, 2014. **B.** CHK2 protein domains and selected phosphorylation sites. SCD: SQ/TQ cluster domain; FHA: forkhead-associated domain; NLS: nuclear localization signal. Adapted according to Guo *et al.*, 2010; Zannini, Delia and Buscemi, 2014. **C.** Upper part: Protein domains of MDM2 and MDMX and selected phosphorylation sites. MDM2(S395) as well as MDMX(S403) are phosphorylated by ATM in response to DNA damage, MDMX(S342) and (S367) are phosphorylated by CHK2. P53 BD: p53 binding domain. According to Chen, 2012. Lower part: MDM2 forms heterodimers with MDMX. These heterodimers are more stable and more effective ubiquitin ligases enhancing degradation of p53. According to Wade and Wahl, 2010; Chen, 2012.

These modifications induce ubiquitination via MDM2 and subsequently, lead to the degradation of the negative regulator. Similar to MDM2, MDMX deficient mice show embryonic lethality that can be rescued with a p53 null background underlining the importance of MDMX as a negative regulator (Parant *et al.*, 2001; Migliorini *et al.*, 2002).

This interplay of positive and negative regulators constitutes the core of the p53 network. However, it only represents one of several layers of regulation that enable cells to generate specific responses.

1.3 Keep it going: Generation of sustained p53 oscillations

In response to high levels of DSB, p53 shows not only one but a series of pulses of accumulation (Lahav *et al.*, 2004). Early studies of the temporal changes of p53 levels in individual breast

carcinoma cells revealed that these pulses are uniform with fixed amplitude and duration (Bar-Or *et al.*, 2000; Lahav *et al.*, 2004; Geva-Zatorsky *et al.*, 2006; Hamstra *et al.*, 2006). While the features of p53 pulses do not generally reflect the severity of the stress, the number of pulses that are triggered in response to genotoxic stress increases with the damage dose, indicating that p53 dynamics encode the strength of the input. However, even isogenic cells in the same environment show variations in their p53 dynamics and sister cells soon lose their correlation most likely due to bursty gene transcription and the resulting stochastic changes in mRNA and protein abundance (Geva-Zatorsky *et al.*, 2006). This heterogeneity in the response emphasizes the importance of measuring p53 dynamics in individual cells. Moreover, p53's complex dynamical behavior raises the question, which molecular network can generate these sustained oscillations.

A useful tool to explore the mechanisms behind experimental observations is mathematical modeling. Early approaches to model the oscillatory behavior of p53 focused on the p53-MDM2 feedback (Figure 1.3.1A). Modeling of this feedback loop using ordinary differential equations (ODE) could reproduce pulsatile p53 dynamics though with a dampening of the oscillations over time (Bar-Or *et al.*, 2000; Tiana, Jensen and Sneppen, 2002; Monk, 2003; Batchelor and Loewer, 2017). These models indicated that time delays due to transcription, splicing and protein synthesis of the negative regulator MDM2 can drive oscillations. To determine how the model responds to changes in parameter values, bifurcation analysis can be performed (Figure 1.3.1A, lower panel). In our case, upon low input signals the system remains in a stable steady state (Mönke *et al.*, 2017). Once the signal strength surpasses a critical value, the system enters a limit cycle through a Hopf bifurcation and oscillations start. However, the amplitudes of the oscillations depend on the input strength: Right at the critical threshold the amplitude is zero and subsequently rises with the signal strength (Mönke *et al.*, 2017). Consequently, a decrease in signal intensity over time, as observed after DNA damage due to DNA repair, will lead to damped oscillations in this model.

To produce uniform pulses independent of the signal strength as observed in single cells, subsequent models coupled a positive feedback to the negative p53-MDM2 loop (Figure 1.3.1B). The positive feedback introduces bistability into the system: p53 can be either high or low (Figure 1.3.1B, lower panel). The negative feedback breaks the stability of the steady-state leading to oscillations between the states (Ciliberto *et al.*, 2005; Eliaš and Maxnamara, 2021). For such a negative-positive feedback system, input signals above a critical threshold immediately lead to high amplitude pulses (Mönke *et al.*, 2017). Different positive feedbacks were suggested: autocatalytic p53, p53 mediated inhibition of MDM2, transcriptional feedback via PTEN and AKT or a positive feedback on ATM, where ATM is modeled as a switch that is

either 'on' or 'off' (Ciliberto *et al.*, 2005; Ma *et al.*, 2005; Wee and Aguda, 2006; Zhang *et al.*, 2007; Xia and Jia, 2010).

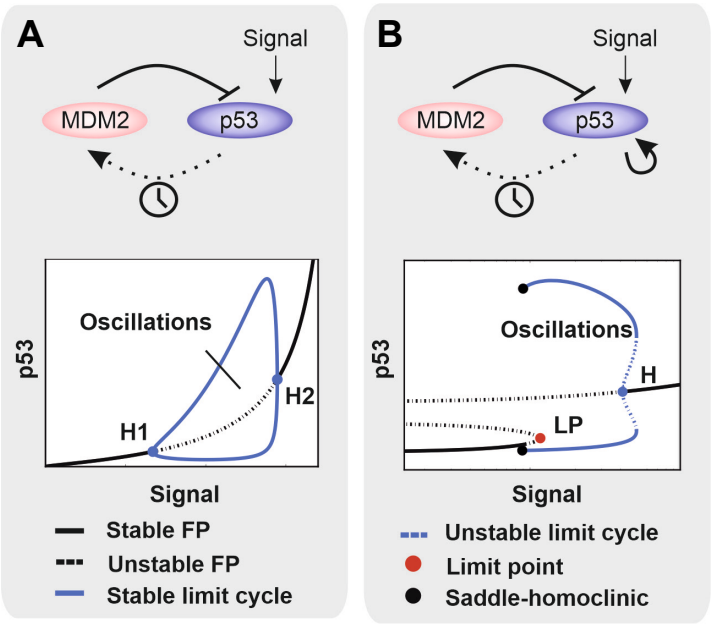

Figure 1.3.1: Modelling of the p53 pathway based on one negative feedback.

A. Network scheme based on the negative feedback between p53 and MDM2. Clock indicates time delay in the production of MDM2. Modified according to (Mönke *et al.*, 2017; Eliaš and Maxnamara, 2021). The lower panel shows the respective bifurcation diagram. Two supercritical Hopf bifurcations (H1 and H2) border the limit cycle regime. According to (Mönke *et al.*, 2017). **B.** Network scheme based on a positive feedback coupled to the negative feedback between p53 and MDM2. The lower panel shows the respective bifurcation diagram. Upon increasing signal strength, the system enters a limit cycle with full amplitudes. According to (Mönke *et al.*, 2017).

A study comparing different network architectures suggested that a second negative feedback between a p53 target and the upstream signaling might be involved in the formation of uniform p53 pulses in response damage (Figure 1.3.2A) (Geva-Zatorsky *et al.*, 2006). This model predicted pulsatile dynamics of the upstream kinase ATM driving p53 oscillations. A consecutive study using MCF7 cells demonstrated that active ATM shows at least two pulses preceding the p53 pulses. Furthermore, they identified the phosphatase WIP1 as an important factor for uniform pulsatile dynamics as it builds the negative feedback between p53 and ATM. Consequently, the study proposed that sustained pulses are triggered via repeated initiation by ATM: As long as damage persists in the cell, ATM is reactivated and can induce a new p53 pulse (Batchelor *et al.*, 2008).

Interestingly, already low degrees of damage or transient input signals can trigger a full p53 pulse. For instance, damage occurring during proliferation induces spontaneous p53 pulses with the same characteristics as pulses that are formed in response to externally induced DSB (Loewer *et al.*, 2010). This excitability of the p53 network allows it to react with high sensitivity to all levels of damage.

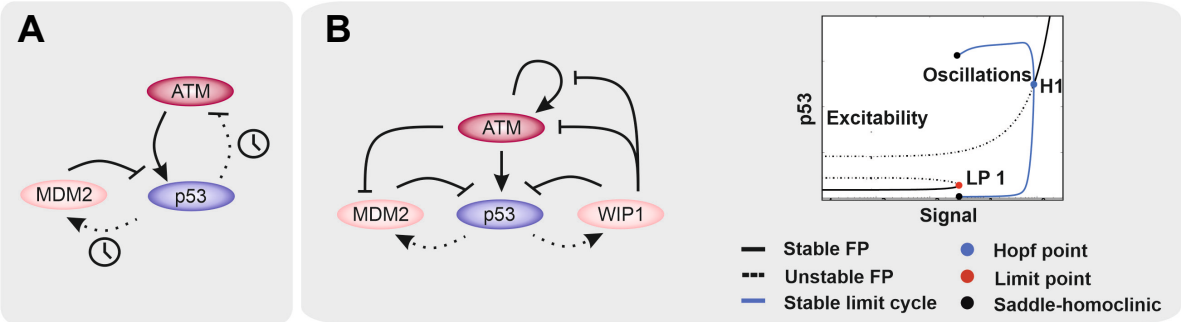

Figure 1.3.2: Modelling of the p53 pathway based on two negative feedbacks.

A. Coupling of the p53-MDM2 negative feedback with a second negative feedback between p53 and the kinase ATM. Modified according to (Batchelor *et al.*, 2008; Eliaš and Maxnamara, 2021). **B.** Left: Network scheme containing two negative feedbacks and one positive feedback on ATM. Dashed lines indicate slow rate interactions. Right: Respective bifurcation diagram. As long as the input strength is low, the system resides in the excitable regime. Upon sufficient input strength, the system enters a limit cycle with large amplitudes. Modified according to (Mönke *et al.*, 2017).

Remarkably, no discrete threshold in the number of DSB was found for inducing a p53 pulse. Individual cells with a similar number of DSB exhibited different p53 dynamics depending on the state of a given cell (Loewer *et al.*, 2013). These cell-specific activation thresholds occurred in genetically identical cells of the same type and could be explained by variability in WIP1 protein levels (Mönke *et al.*, 2017). As WIP1 removes modifications of p53 and MDM2 that are required for p53 accumulation, cells with higher levels of WIP1 needed higher levels of active ATM and consequently more DSB to induce a p53 pulse.

To reproduce sustained oscillations, as well as isolated pulses as observed under basal conditions, a recent model by Mönke et al., combined the coupled negative feedbacks with an additional positive feedback provided by the switch-like activation of ATM (see activation of ATM in section 1.2) and the rapid degradation of MDM2 (Figure 1.3.2B) (Mönke *et al.*, 2017). In the model, WIP1 modulates the input by ATM not only by dephosphorylating ATM and p53 but also by removing phosphorylations from γH2AX, NBS1 and MRE11, which are involved in the positive feedback facilitating ATM activation. Upon sufficient levels of ATM activation, the system can trigger a full pulse (Figure 1.3.2B, lower panel). This *all-or-nothing* response allows a highly specific and sensitive answer to input signals of different strengths. When the system receives sustained input above a certain threshold, it changes from an excitable regime to sustained oscillations. To account for the observed cellular heterogeneity in pulse numbers, the model was further augmented with a stochastic process describing DSB repair (Mönke *et al.*, 2017).

To put it in a nutshell, the current models suggest that sustained p53 pulses are triggered by recurrent activation of ATM as long as DNA lesions are sensed by the cell. The uniform and excitable nature of these pulses is mediated by a negative feedback between p53 and the upstream signaling via the phosphatase WIP1 and a positive feedback on the kinase ATM, which

are coupled to the delayed negative feedback between MDM2 and p53 (Figure 1.3.2B). Consequently, every p53 pulse that is triggered in response to DNA DSB relies on the activity of kinase ATM.

1.4 P53's dynamics: a key to understanding the encoding of individual stress levels

As previously reviewed by Purvis and Lahav (Purvis and Lahav, 2013), the dynamics of proteins are defined as the change of their level, their localization or of other features over time. Several TFs show complex dynamical behaviors after activation. The resulting patterns range from transient and sustained responses to periodic activation. For instance, NF-κB, ERK and NFAT4 (NFATC3) exhibit repeated pulses of cytoplasmic to nuclear translocation upon defined stimuli (Shankaran *et al.*, 2009; Tay *et al.*, 2010; Yissachar *et al.*, 2013). TF dynamics contribute to encoding the kind and strength of stimuli and control subsequent cellular responses. Using single-cell measurements and image analysis, the specific features of these dynamics can be quantified. Relevant features in the context of p53 include the amplitude and width (duration) as well as the timing of accumulation (Figure 1.4.1A).

In contrast to the pulsatile dynamics in response to DSB-inducing ionizing radiation (Figure 1.4.1B), p53 shows different dynamics after UV radiation or treatment with chemotherapeutic drugs (Batchelor *et al.*, 2011; Paek *et al.*, 2016). Treatment with the chemotherapeutic drug cisplatin, for example, induces a constant accumulation of p53 (Figure 1.4.1B). While the underlying mechanism for these altered dynamics is not well understood, the p53 response to UV radiation has been characterized in molecular detail. Here, only one single pulse is formed that increases in amplitude and duration with increasing dose (Figure 1.4.1B). This can be explained by the observation that in contrast to DSB-inducing IR, UV radiation results in the exposure of single-stranded DNA as a repair intermediate, which leads to the activation of the kinase ATR. As the ATR- and ATM-driven p53 networks have different topologies of their negative feedbacks, also the resulting p53 dynamics differ (Batchelor *et al.*, 2011).

But what is the purpose of this complex dynamical behavior? It was shown by pharmacological and genetic perturbations that p53 dynamics determine gene expression programs and define cell fates (Purvis *et al.*, 2012; Borcherds *et al.*, 2014). While a pulsatile response leads to cell cycle arrest, a sustained p53 response activates different sets of genes and induces senescence (Figure 1.4.1C). Consistently, a further study indicated that low levels of the chemotherapeutic drug etoposide induced pulsatile dynamics and cell cycle arrest, while high doses led to a strong monotonic increase and apoptosis (Chen *et al.*, 2013).

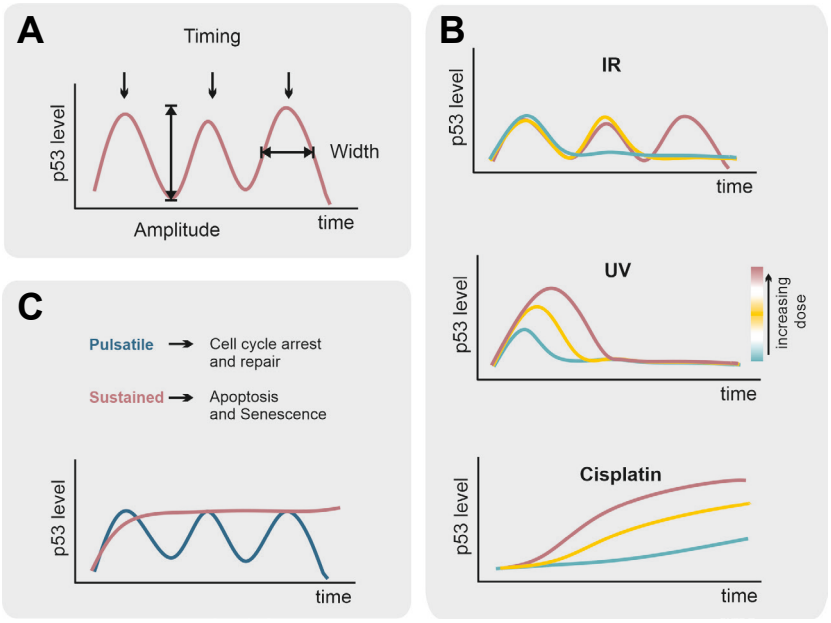

Figure 1.4.1: p53 dynamics in response to different stimuli.

A. In response to DNA DSB, p53 shows a series of pulses with fixed amplitude and duration. Relevant features of the pulses are the amplitude, timing and duration. **B.** Upon IR, the number of pulses increases with the damage dose. After UV radiation, only a single pulse is formed whose amplitude and duration increase with the degree of damage. Upon cisplatin treatment, the p53 levels increase over time. **C.** P53 dynamics control cell fate. In response to DNA DSB, p53 shows a series of pulses with fixed amplitude and duration. In contrast, certain chemotherapeutic drugs induce sustained high levels of p53. While pulsatile dynamics lead to cell cycle arrest and repair, high sustained levels are associated with terminal cell fates like apoptosis and senescence.

In this context, it was proposed that for the induction of apoptosis in response to cisplatin treatment, the p53 levels must exceed a time-dependent threshold (Paek *et al.*, 2016). All things considered, p53 is robustly induced by various levels of damage, while its complex dynamics allow cell- and stimulus-specific responses.

1.5 Promoter puzzles: The different mechanisms enabling gene-specific target gene expression

To enable cells to take appropriate fate decisions, the cell has to translate the information about the kind and degree of damage encoded in TF dynamics into the expression of specific genes. Transcription itself, one of the most vital mechanisms in our body, is a highly complex process. A variety of different factors assembles and interacts with each other to facilitate the expression of the gene in question. Gene-specific TF like p53 bind to distinct response elements (RE) in cis-regulatory regions of their targets. P53's RE comprise of two decamers with the consensus sequence RRRCWWGYYY (R = purine, W = A/T, Y = pyrimidine base) that are separated by spacers (El-Deiry *et al.*, 1992; Funk *et al.*, 1992). Some RE harbor more than two decamers (so-called cluster sites) and some genes have more than one binding site for p53 (Bourdon *et al.*, 1997; Saramäki *et al.*, 2006). The specific *cis*-regulatory architecture, location and sequence of the RE influences the overall affinity of p53 to the binding site (Riley *et al.*, 2008). Interestingly,

the affinity of p53 to its distinct RE varies widely between the different target genes: While pro-apoptotic genes are associated with binding sites exhibiting low affinity to p53, genes involved in growth arrest were connected to high-affinity RE. Derived from this finding, the 'affinity model' suggested that the nuclear p53 concentration would control the expression of specific genes (Vousden, 2000). However, as so often in biological systems, the explanation of specific expression of target genes is far more complicated. Consequently, no systematic connection between p53 levels, binding to promoters of pro-apoptotic genes and the initiation of apoptosis were found (Kaeser and Iggo, 2002; Smeenk *et al.*, 2011; Hafner *et al.*, 2019). Which other mechanisms could contribute and explain the expression of specific cell-fate associated genes?

1.5.1 Joined forces: Oligomerization modulates site-specific binding

One crucial factor may be the oligomerization status of p53. Under basal conditions, most p53 molecules in the cell form dimers (Gaglia *et al.*, 2013). Upon DNA damage, two p53 dimers rapidly form tetramers that bind DNA (Wang *et al.*, 1995; Gaglia *et al.*, 2013). The oligomerization process itself is crucial for the transcriptional activity of p53 and might contribute to the decision between survival and death. Mutations in the oligomerization domain strongly impair DNA binding and mutants that lack the ability to form oligomers are transcriptionally inactive (Davison *et al.*, 1998; Kawaguchi *et al.*, 2005; Imagawa *et al.*, 2009). In this context, the oligomerization status itself might regulate which set of genes is activated (Weinberg *et al.*, 2005). p53 mutants that only form dimers induced the transcription of genes involved in growth arrest, whereas pro-apoptotic genes were only triggered by tetrameric p53, which may be connected to the affinity of the corresponding p53-binding sites (Weinberg *et al.*, 2005; Riley *et al.*, 2008). Similarly, mutations that impair cooperative binding to the DNA due to changes in the quaternary structure of the p53 tetramer also show altered cellular outcomes: While high DNA-binding cooperativity is crucial for p53 dependent apoptosis, it is dispensable for the induction of arrest (Schlereth *et al.*, 2010, 2013; Timofeev *et al.*, 2013). Considering the important role of oligomerization, it is crucial to understand how the oligomerization process is regulated. Interestingly, even though tetramerization of p53 is triggered rapidly after induction of DNA damage, the process is independent of the rise in total p53 levels (Gaglia *et al.*, 2013). One way to control the formation of p53 oligomers are PTM. In this context, PTM of residues located in the oligomerization domain were shown to alter p53's oligomeric conformation. For instance, phosphorylation on S392 triggers tetramerization of p53 while this effect is reversed by additional phosphorylation of S315 (Sakaguchi *et al.*, 1997; Muller *et al.*, 2018). Another way to regulate the formation of tetramers is the interaction with proteins modulating the oligomerization process. Proteins of the S100 family associate with the tetramerization domain of monomeric/dimeric p53 and abrogate the formation of tetramers (Fernandez-Fernandez,

Veprintsev and Fersht, 2005). Similarly, the multifunctional protein p32 (encoded by C1QBP) was shown to interfere with p53's tetramerization (Ghate *et al.*, 2019). This way, p32 inhibits DNA binding, occupancy at target genes and p53 dependent transcription.

1.5.2 Special decorations: The role of PTMs for the expression of specific genes

P53 consists of six protein domains: Two intrinsically disordered transactivation domains (TAD), a proline-rich domain (PRD), a DNA binding domain (DBD), the oligomerization/ tetramerization domain (OD) and an intrinsically disordered C-terminal regulatory domain (Liu, Tavana and Gu, 2019). Literally, every domain undergoes modifications ranging from phosphorylation to O-GlcNAcylation (Liu, Tavana and Gu, 2019). These PTM modulate many processes in the p53 response. For instance, as mentioned in section 1.2, phosphorylation of residues in the TAD of p53 has a stabilizing effect on the TF. Additionally, the modification of specific residues modulates the expression of certain sets of target genes. One example of how PTM influence target gene expression is -as described in the previous section- the modulation of oligomerization. However, many more processes are modulated by the modification of specific residues.

For instance, acetylation, on the one hand, competes with ubiquitination for the same residues increasing the stability of p53 (Nakamura and Roth, 2000; Rodriguez *et al.*, 2000; Ito *et al.*, 2002). On the other hand, this modification was also shown to modulate p53's activity. The role of acetylation for promoter binding and activation of target gene transcription has been steadily studied over the past decade. P53 is acetylated on several lysine residues predominantly in the C-terminal domain including K320, K370 and K382 by p300 (Gu and Roeder, 1997; Sakaguchi *et al.*, 1998; Saito *et al.*, 2002) (Figure 1.5.1). The C-terminal parts of p53 control site-specific DNA binding and are important for structural features of the DNA-binding domain (Laptenko *et al.*, 2015). Early studies indicated that acetylation of the C-terminus enhances site-specific DNA binding (Gu and Roeder, 1997; Sakaguchi *et al.*, 1998; Luo *et al.*, 2004; Zhao *et al.*, 2006) while others have shown that acetylation of p53 induces transcription by recruitment of co-activators or facilitating histone acetylation instead (Barlev *et al.*, 2001). Loss of acetylation at one site can be compensated by other sites, while simultaneous loss of acetylation at eight lysine residues completely blocks p53 dependent activation of both growth arrest and apoptosis (Tang *et al.*, 2008). Consequently, acetylation is deemed indispensable for p53 activation. In this context, single-cell studies have shown that p53 binds only transiently to chromatin and that its bound fraction and residence time increases after DNA damage-dependent acetylation on its C terminus (Loffreda *et al.*, 2017).

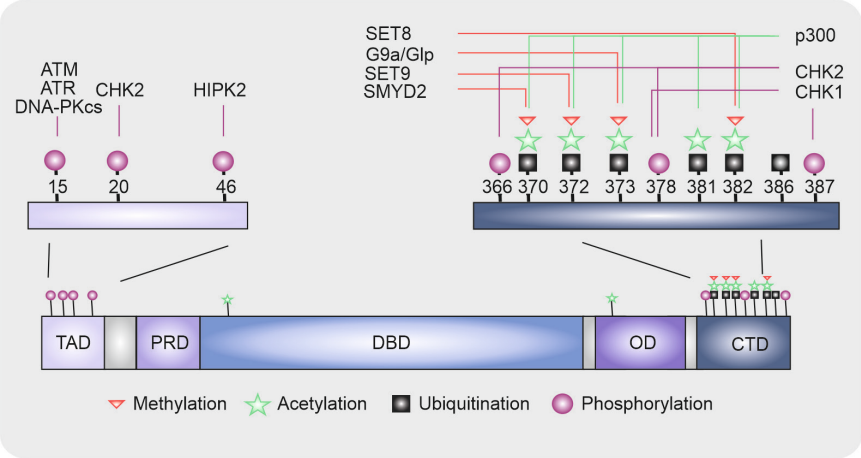

Figure 1.5.1: Domain structure of p53 and selected PTM.

P53 is phosphorylated on several residues in the transactivation domain (TAD). S15 and S20 are phosphorylated by ATM, ATR and DNA-PKcs or CHK2. S46 is phosphorylated by HIPK2. The C-terminal domain (CTD) harbors several lysine residues that are acetylated or methylated. PRD: Proline-rich domain; DBD: DNA binding domain; OD: oligomerization domain. Modified according to Hafner *et al.*, 2019.

However, does the acetylation state of p53 also allow the expression of specific genes involved in distinct cell fate programs? Knights et al. proposed that p53 acetylation cassettes coordinate gene expression in response to DNA damage (Knights *et al.*, 2006). Acetylation of K320 blocks the phosphorylation of important serine residues on the N-terminus and restricts activation to high-affinity p53-binding sites that are involved in arrest. In contrast, K373 acetylation induces phosphorylations on the N-terminus and triggers binding to low-affinity-binding sites such as those found in pro-apoptotic genes. Interestingly, also lysine residues in the DNA-binding domain were found to be acetylated after DNA damage. K120 is acetylated by MOZ (KAT6A), hMOF (KAT8) and TIP60 (KAT5) (Sykes *et al.*, 2006; Tang *et al.*, 2006; Rokudai *et al.*, 2013) upon exposure to different kinds of DNA damage. Modification of this residue was shown to be crucial for p53-mediated apoptosis and senescence rather than growth arrest. Importantly, acetylation of p53 does not only have direct effects on its DNA-binding capabilities but influences target gene expression also via an indirect mechanism. On the promoter of distinct p53 targets, p53 forms a complex with MDM2 (Minsky and Oren, 2004; Arva *et al.*, 2005; Ohkubo *et al.*, 2006), which represses transcription. Acetylated p53 does not recruit MDM2 to these promoters and is, therefore, able to activate transcription (Tang *et al.*, 2008). Besides its role in the choice of the correct cellular outcome, acetylation of p53 also serves as a filtering mechanism for non-severe intrinsic damage. During proliferation, p53 shows single accumulation pulses similar to pulses occurring after high degrees of externally induced damage. However, these pulses do not result in a full damage response due to the lack of an activating p53 PTM profile. Consequently, acetylation functions as a fine-tuning mechanism to filter p53 pulses induced by transient damage frequently occurring in proliferating cells (Loewer *et al.*, 2010).

Several lysine residues that are acetylated were shown to be modified by methyltransferases as well (Chuikov *et al.*, 2004; Huang *et al.*, 2006; Shi *et al.*, 2007) (Figure 1.5.1). For instance, K370 is methylated by SMYD2 (also known as KMT3C) repressing p53 mediated transcription of CDKN1A and MDM2 (Huang *et al.*, 2006). Additionally, K382 is mono-methylated by SET8 (KMT5A), which suppresses p53 dependent expression of CDKN1A (Shi *et al.*, 2007). In response to DNA damage, the expression of SET8 was shown to be decreased indicating that the DNA damage response machinery is able to regulate SET8 mediated methylation. In contrast, methylation of K372 by SET7/9 (KMT7) in response to DNA damage leads to transcriptional activation and stabilization of p53 (Chuikov *et al.*, 2004; Ivanov *et al.*, 2007). Interestingly, K372 methylation was shown to impair inhibitory methylation of K370 (Huang *et al.*, 2006). One can conclude that the balance between acetylation and methylation of certain residues might modulate target expression.

In addition to acetylation and methylation, also phosphorylation of certain residues was connected with the modulation of p53's activity. For example, phosphorylation at S46 by the kinase HIPK2 is associated with the induction of genes involved in apoptosis (Hofmann *et al.*, 2002; Smeenk *et al.*, 2011). Upon treatment with chemotherapeutics inducing apoptosis, binding of p53 pS46 is increased on the promoter of pro-apoptotic genes (Smeenk *et al.*, 2011). In addition to the TAD, several residues in the CTD are phosphorylated by CHK2 and CHK1 in response to DNA damage (Ou *et al.*, 2005). Phosphorylation on S378 can be detected even in the absence of stress but is further enhanced when the cell encounters DNA lesions. Interestingly, pS378 has an inhibitory effect on acetylation of K373 and K382 (Ou *et al.*, 2005). However, this effect can be counteracted by additional phosphorylation of S366 and T387. Remarkably, even though phospho-mimetic mutations S366D and T387D showed enhanced promoter binding, this did not lead to higher target gene expression for all targets. In line, mutation of S366 and T387 to alanine did not affect CDKN1A expression while the expression of BAX was strongly reduced (Ou *et al.*, 2005). Furthermore, phosphorylation of S366, S378 and T387 creates a binding motif for 14-3-3 (Rajagopalan *et al.*, 2008, 2010). 14-3-3 is a family of adapter proteins consisting of seven isoforms: β, γ, ε, η, σ, τ and ζ (Falcicchio *et al.*, 2020). Binding of 14-3-3 γ and ε was suggested to trigger tetramerization of p53 and to thereby modulate DNA binding (Rajagopalan *et al.*, 2008, 2010).

Besides PTM and oligomerization, other factors contribute to a specific target gene expression. For example, p53 interacts with other TFs as well as with several coregulators that modify the surrounding chromatin structure to specifically induce defined cell fate programs (Hafner *et al.*, 2019; Sammons *et al.*, 2020). One important example is the acetyltransferase p300. Phosphorylation of p53's TAD in response to DNA damage enhances binding to p300 and

recruits the acetyltransferase to chromatin. In turn, p300 acetylates not only p53 but also the adjacent chromatin landscape (Miller Jenkins *et al.*, 2012; Hafner *et al.*, 2019).

When considering these different layers of regulation, it is important to keep in mind that they do not act in isolation, but instead, synergize to precisely control p53's activity. For instance, PTMs alter the oligomerization status while the modification patterns themselves can be changed between p53 pulses. In turn, PTMs alter the stability of p53 and can thereby shape p53 dynamics. Interestingly, the oligomerization process seems to be independent of the accumulation of p53 after genotoxic stress and tetrameric p53 was even shown to be less stable than monomeric or dimeric forms (Gaglia *et al.*, 2013; Fischer *et al.*, 2016). However, certain PTMs, such as phosphorylation of S20 or acetylation on K320, depend on tetramerization of p53, indirectly linking the oligomerization status of p53 with the TF's dynamics (Sakaguchi *et al.*, 1998; Shieh, Taya and Prives, 1999).

1.5.3 More than just noise? The role of transcriptional bursting

Even isogenic cells show a high degree of variability during transcription (Suter *et al.*, 2011). For instance, the target of p53, PPM1D, shows a broad distribution in mRNA abundance under basal conditions (Mönke *et al.*, 2017). One factor contributing to this heterogeneity is transcriptional bursting (Fig. 1.5.2). Due to stochastic activation and inactivation of the promoter, mRNAs are not continuously transcribed. Instead, gene expression switches between transcriptionally inactive (OFF) and active (ON) states, during which a variable number of transcripts are generated (Figure 1.5.2A) (Nicolas, Phillips and Naef, 2017).

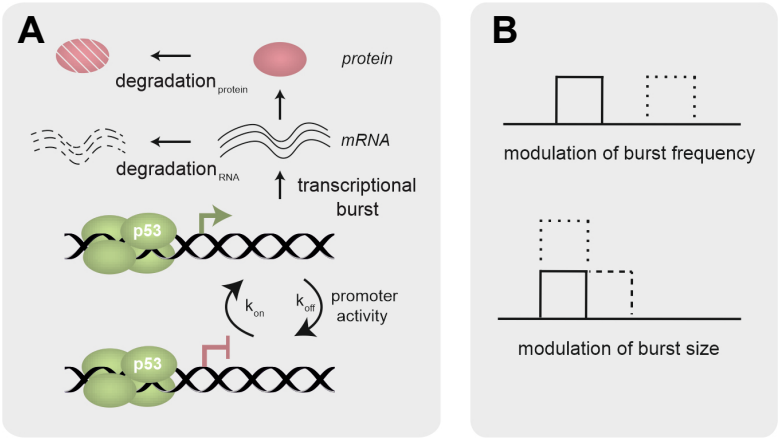

Figure 1.5.2: Schematic overview of stochastic gene expression.

A. Promoters are activated and inactivated with specific rate constants k_{on} and k_{off} leading to bursts of transcription. The resulting mRNAs and proteins decay with the rates δ_{RNA} and $\delta_{protein}$. **B.** Transcriptional bursting kinetics can be described by two parameters: The burst frequency (bf), the frequency of the promoter being in an active state, and the burst size (bs), the number of RNA molecules produced per burst. Modified according to Friedrich *et al.*, 2019.

Two parameters modulate the amount of RNAs that are produced over time: The number of transcripts produced during one burst (burst size) and the frequency of target promoter activation (burst frequency) (Figure 1.5.2B) (Golding *et al.*, 2005; Suter *et al.*, 2011; Friedrich, 2019). Transcriptional bursting can not only lead to differences in the behavior of individual cells within a population, diverse bursting patterns for different genes also allow a high variability in gene expression (Kumar, Singh and Kulkarni, 2015; Tunnacliffe and Chubb, 2020). One impressive example is a study by Tunnacliffe *et al.* They analyzed a gene family encoding 17 identical actin proteins that are distributed throughout the genome for their bursting profiles (Tunnacliffe, Corrigan and Chubb, 2018). Remarkably, the distinct genes showed a broad variety in bursting patterns. To elucidate whether these diverse bursting dynamics are determined by the promoter sequence or the chromatin environment, they exchanged the upstream regulatory region of two actin genes with the most different bursting patterns. Interestingly, switching of the promoter sequence also led to switching of the bursting dynamics. This indicates that the upstream sequence rather than the genomic context determine transcriptional bursting patterns, a hypothesis that was supported by other studies as well (Hendy *et al.*, 2017). Furthermore, studies could show that different stimuli can induce different transcriptional patterns of the same gene (Molina *et al.*, 2013).

How does the binding of TF modulate transcriptional bursting of a distinct gene? Via 3D orbital tracking (3DOT), both, transcriptional dynamics and the binding of TF can be examined at the same time. With this approach, TF binding and the start of a transcriptional burst could be directly correlated (Donovan *et al.*, 2019; Stavreva *et al.*, 2019; Tunnacliffe and Chubb, 2020). Moreover, studies with the glucocorticoid receptor (GR) indicated that the dwell time of the TF and the bound fraction can modulate burst size and burst frequency (Stavreva *et al.*, 2019). Consequently, one can conclude that transcriptional bursting is a promising cellular mechanism for the diversification of target gene expression despite having the same input from the respective TF. However, little is known about the role of transcriptional bursting in the p53 response and its impact on the expression of specific target genes remains to be elucidated.

2 AIM OF THE STUDY

2 AIM OF THE STUDY

P53 is a crucial player in the response to DNA damage: Controlling cell fate decisions, p53 can induce arrest and repair but also terminal outcomes like apoptosis and senescence when the degree of damage is too severe. In response to DSB, p53 shows characteristic pulsatile dynamics of accumulation in the nucleus. By combining experimental data as well as mathematical modeling, previous studies proposed that every pulse is generated by the same network interactions: Via the MRN complex, DNA DSB induce the activation of ATM which in turn promotes its own activation by a feed-forward loop and stabilizes p53 (Mönke *et al.*, 2017). However, while the p53 dynamics seem to be uniform throughout the DNA damage response, the underlying status of the genome is changing continuously over time. DSB are rapidly marked within minutes after the lesion occurred. Within the first hours, most of the breaks are repaired with a smaller fraction of breaks remaining that have higher damage complexity or occurred in less accessible chromatin regions (Jeggo, Geuting and Löbrich, 2011). Consequently, the cell is confronted with many new breaks (acute damage) during the first pulse, while during the second pulse only a significantly smaller number of breaks remains.

Here, I want to elucidate whether this change in the status of the genome is reflected in the p53 response and whether the immediate p53 response to acute damage and the sustained response to persisting damage differ with regard to the underlying mechanisms and role for the final cell fate decision. To this end, I explore how the p53 dynamics and the core network respond to recurrent detection of new DSB. Furthermore, the role of key players of the p53 network for the immediate and sustained response is investigated by combining time-lapse live-cell microscopy with the application of specific small molecule inhibitors. This allows controlling the activities of network members in a timely precise manner while closely monitoring the p53 response in individual cells. Finally, I want to elucidate whether pulses of the immediate and the sustained p53 response differ with regard to their PTM state or binding properties to distinct promoters and how these differences modulate target gene expression.

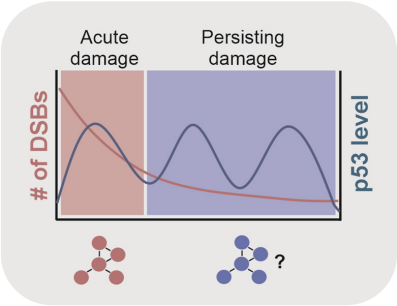

Figure 2.1.1: Do the immediate and the sustained p53 response differ with regard to their underlying mechanisms?

In this thesis, I investigate the interplay of regulators mediating the immediate and sustained p53 response and how these regulators modulate p53's PTM state, DNA binding dynamics and target gene expression.

3 RESULTS

3 RESULTS

When the cell senses DNA damage, it not only has to take care of restoring the lesions. It also has to decide for an appropriate outcome ranging from simply arresting the cell cycle to give time for repair to the induction of terminal cell fates like apoptosis. Doing this, the cell has to dynamically integrate inputs from the environment and respond to changes in its state, as only all these pieces of information together allow for an appropriate decision. In the following, I will unravel possible differences between the p53 response to acute, newly emerged lesions and the response to persisting breaks allowing the cell to differentiate between old and new genomic insults.

3.1 ATM is involved in the response to acute damage

In a first step, the damage status of the genome was changed in the course of the p53 response: To investigate whether a recurrent detection of new breaks alters the p53 dynamics, cells were repeatedly confronted with newly induced DSB. As p53 dynamics are highly variable even in isogenic cells, we systematically approached this question via live-cell time-lapse microscopy using the small cell lung carcinoma cell line A549 expressing a fluorescent p53 reporter (Chen *et al.*, 2013; Finzel *et al.*, 2016). To induce DSB repeatedly in a timely precise manner, the radiomimetic drug Neocarcinostatin (NCS) was used. To compare several conditions, the median nuclear fluorescence intensity of p53 was analyzed. In response to 0.2 µg/mL NCS, A549 cells showed a regular and rather synchronous pulsatile response (Figure 3.1.1A). Re-damaging cells after 1 h with the same dose of NCS (Figure 3.1.1A) led to an increase in the amplitude of the first pulse. Interestingly, the amplitudes of the 2nd and 3rd pulse were unchanged (Figure 3.1.1B). Comparing a single initial dose of 0.4 µg/mL with sequential usage of 2x0.2 µg/mL NCS, the latter showed a similar increase in the amplitude compared to a single dose of 0.2 µg/mL (Figure 3.1.1A and B). These observations show on the one hand that the amplitude of the first pulse increases in a dose-dependent manner in A549 cells, while the amplitude of the second pulse is fixed. On the other hand, we see that even when the p53 response has already started, the occurrence of new damage can lead to alterations of the dynamics. After the peak of the first pulse, p53 levels decrease due to a p53-induced increase in MDM2 and WIP1 levels. Can new damage alter the p53 dynamics under these circumstances as well? To address this question, cells were damaged with an initial dose of 0.2 µg/mL NCS and a second dose of 0.2 µg/mL NCS was added after p53 reached its peak level (2.5 h). Remarkably, this led to an immediate rise of p53 levels, a dynamical behavior that could also be observed in individual cells (Figure 3.1.1C and E).

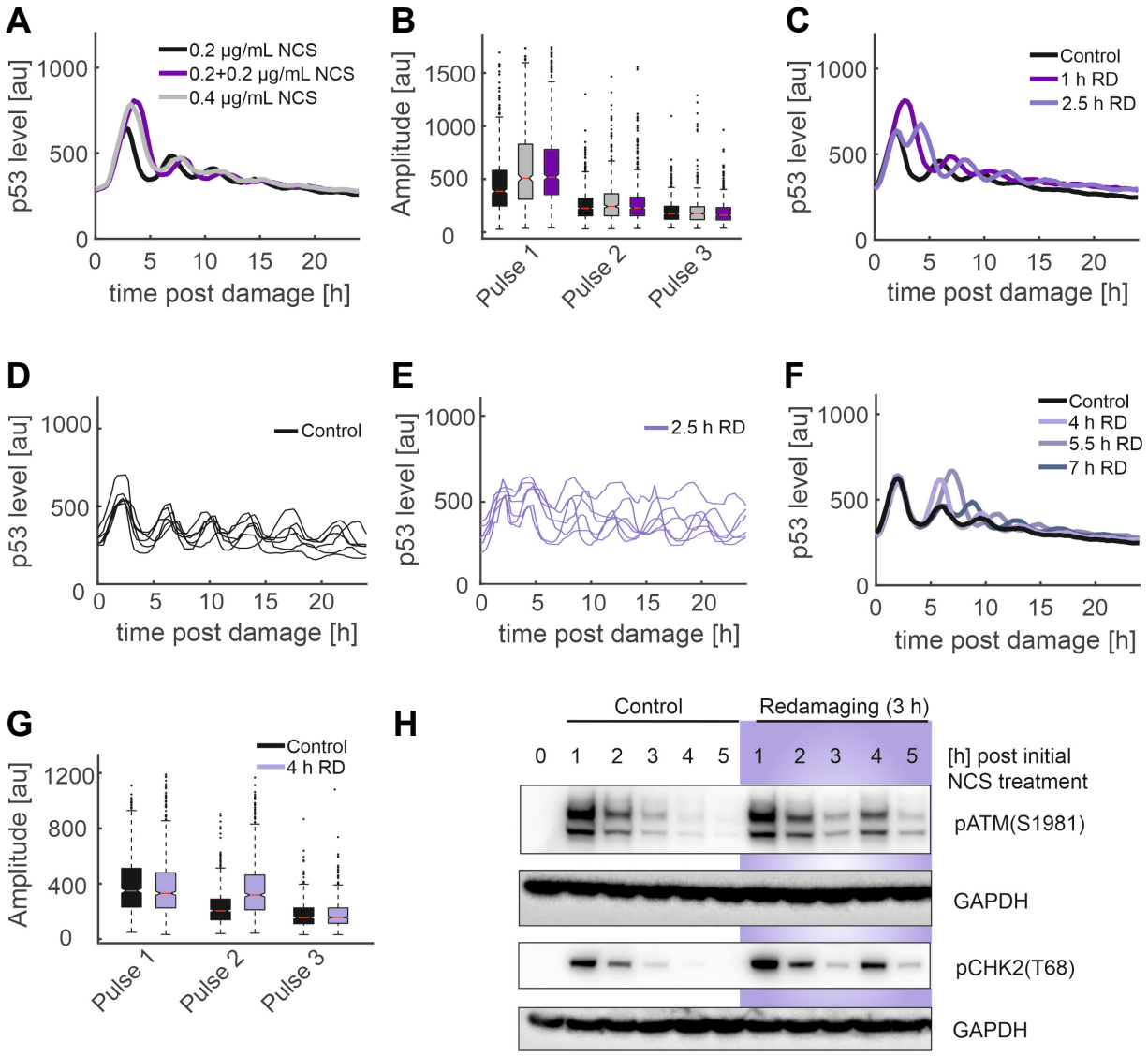

Figure 3.1.1: Re-damaging leads to an increase in p53 levels.

A. A549 reporter cells were treated with 0.2 µg/mL, 0.4 µg/mL Neocarcinostatin (NCS) or were re-damaged 1h after an initial treatment with 0.2 µg/mL NCS. Cells were followed using live-cell time-lapse microscopy. Trajectories show the median nuclear fluorescence intensity of p53. The number of cells analyzed per condition as well as the threshold used for pulse analysis can be found in Table 7.4.1 and Table 7.4.2. **B.** Quantification of the amplitude of the first three pulses. Distribution is displayed by boxplots. Here and in the following figures, median values are shown as red lines. Boxes include data within the interquartile range (IQR). Length of whiskers corresponds to maximum and minimum values with a maximal length of 1.5x the IQR. Outliers are represented as dots. Notches display 5% confidence intervals for the median. **C-G.** A549 reporter cells were treated with 0.2 µg/mL NCS and re-damaged (RD) 1 h, 2.5 h, 4 h, 5.5 h and 7 h after an initial treatment with 0.2 µg/mL NCS. Trajectories in **C** and **F** show the median nuclear fluorescence intensity of p53. **D-E.** shows the response of six representative single cells without single NCS treatment (**D**) or upon re-damaging after 2.5 h (**E**). The number of cells analyzed per condition as well as the threshold used for pulse analysis can be found in Table 7.4.1 and Table 7.4.2. **G.** shows the quantification of the amplitude of the first three pulses upon re-damaging after 4 h. **H.** A549 WT cells were treated with 0.2 µg/mL or re-damaged 3 h after an initial treatment with 0.2 µg/mL NCS. Cells were harvested at indicated time points and pCHK2(T68) and pATM(S1981) levels were assessed via western blotting. GAPDH was used as a loading control.

Taken together, one can conclude that the detection of new damage during the first pulse leads to an immediate increase in p53 levels independent of the levels of its negative regulators. Is this

true throughout the response? Comparing the amplitude of the first and the following pulses in control cells, the first pulse had a higher amplitude than the following pulses (Figure 3.1.1B). Interestingly, re-damaging cells in the trough (4 h) after the first pulse led to an increase in the amplitude of the second pulse resulting in an amplitude similar to the level of the first pulse (Figure 3.1.1F and G). The amplitude of the third pulse remained unaltered. Similar to what I observed during the first pulse, re-damaging during the rising phase of the second pulse (5.5h) led to an increase of the amplitude, while re-damaging after the peak (7 h) led to an immediate rise of the p53 levels (Figure 3.1.1F).

To elucidate the molecular basis for the immediate response to new damage, I took a closer look at the activity of the kinase ATM. As a read-out for ATM activity both ATM auto-phosphorylation at S1991 as well as phosphorylation of CHK2 at T68 were assessed via western blotting (Figure 3.1.1H). Re-damaging after 3 h led to an immediate reactivation of the kinase indicating an important role for ATM in the response to acute damage. Together the observations indicate that cells are able to quickly respond to new damage and adjust the p53 response accordingly.

3.2 ATM is dispensable for the sustained response

To further characterize the role of ATM in the course of the p53 response, I chose to inhibit the kinase using a small molecule inhibitor. Two structurally related inhibitors were tested: KU55933 and its improved analog KU60019. As a readout for ATM activity, ATM autophosphorylation at S1991 and phosphorylation of CHK2 at T68 were measured using western blotting. Both inhibitors reduced phosphorylation on both residues to background levels (Figure 3.2.1A). Due to its lower IC_{50} for ATM, KU60019 was chosen for the following experiments and will be referred to as ATMi. All experiments in Figure 3.2.1 were performed as well with KU55933 showing consistent results (data not shown). First, ATM was inhibited before IR and the p53 levels were monitored in individual cells in response to genotoxic stress (Figure 3.2.1B). While control cells showed a regular pulsatile behavior (Figure 3.2.1B), for the inhibitor-treated cells no regular pulses could be observed (Figure 3.2.1B), in line with its role for responding to acute damage. Remarkably, when ATM was inhibited 1 h after IR, not only the first pulse was completed but also the following pulses were induced. Plotting the p53 dynamics of all tracked cells in form of a heat-map indicates an even more regular pulsatile behavior (Figure 3.2.1C). Quantification of the duration, amplitude and timing of the pulses confirmed that the characteristic features of the following pulses are unchanged (Figure 3.2.1D).

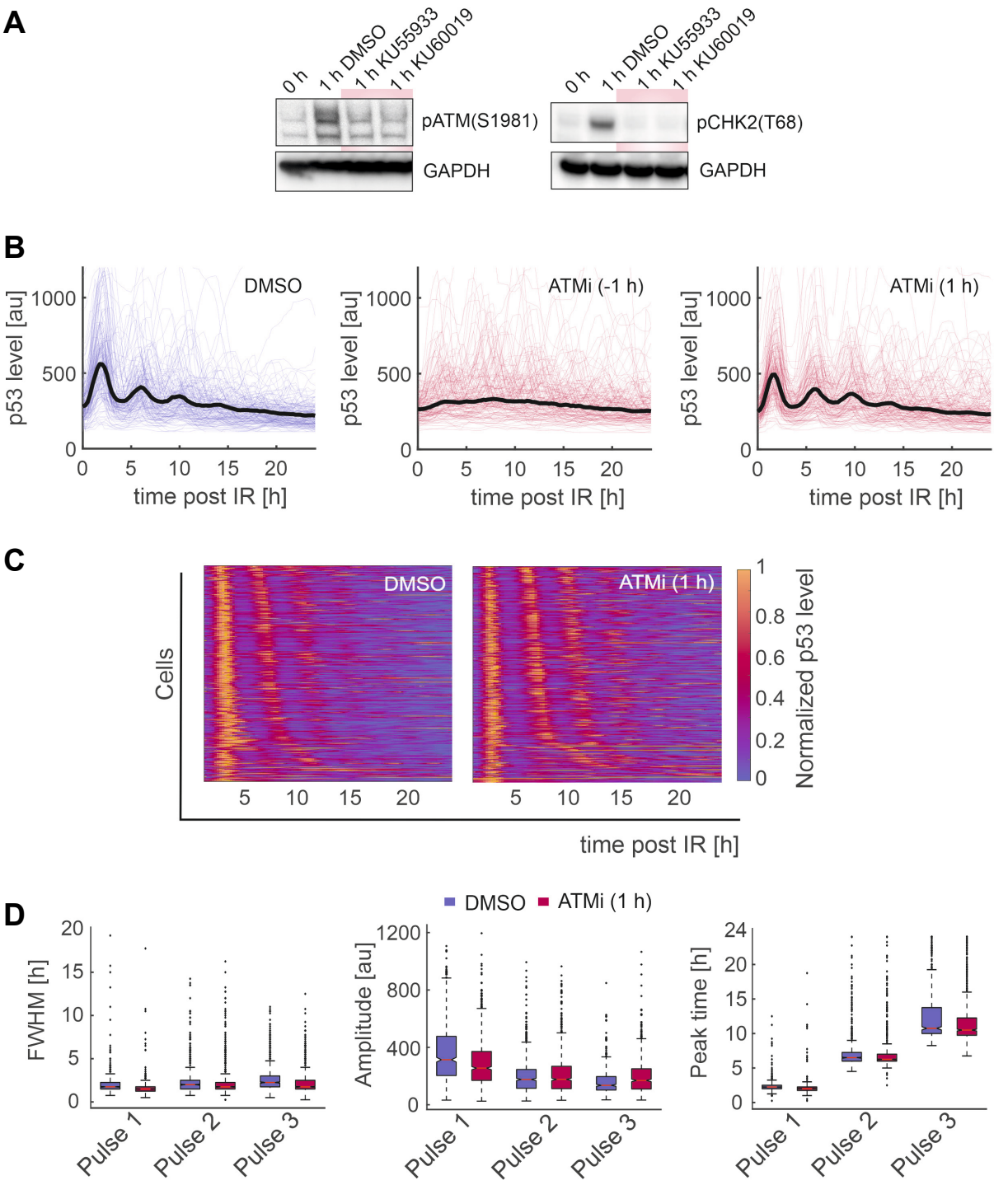

Figure 3.2.1: ATM is dispensable for the sustained p53 response.

A. A549 WT cells were treated with the ATM inhibitors KU55933 or KU60019 1 h before irradiation with 5 Gy X-rays (IR). Cells were harvested at indicated time points after IR and pCHK2(T68) and pATM(S1981) levels were assessed via western blotting. GAPDH was used as a loading control. **B.** A549 reporter cells were treated with the ATM inhibitor KU60019 1h before and 1 h after 5 Gy IR, respectively. Cells were followed using live-cell time-lapse microscopy. Thick black lines show the median nuclear fluorescence intensity of p53, thin lines represent a random subset of 100 single cells. The number of cells analyzed per condition as well as the threshold used for pulse analysis can be found in Table 7.4.1 and Table 7.4.2. **C.** Heatmap of p53 levels. Each trajectory was min-max-normalized. Cells are sorted by the timing of the second pulse. **D.** Quantification of the timing, amplitude and duration (FWHM: full-width at half-maximum) of the first three pulses.

To validate these findings, I analyzed the dynamics of endogenous p53 via Western Blotting and observed similar dynamics after treatment with an ATM inhibitor 1 h post IR compared to control cells (Figure 3.2.2A).

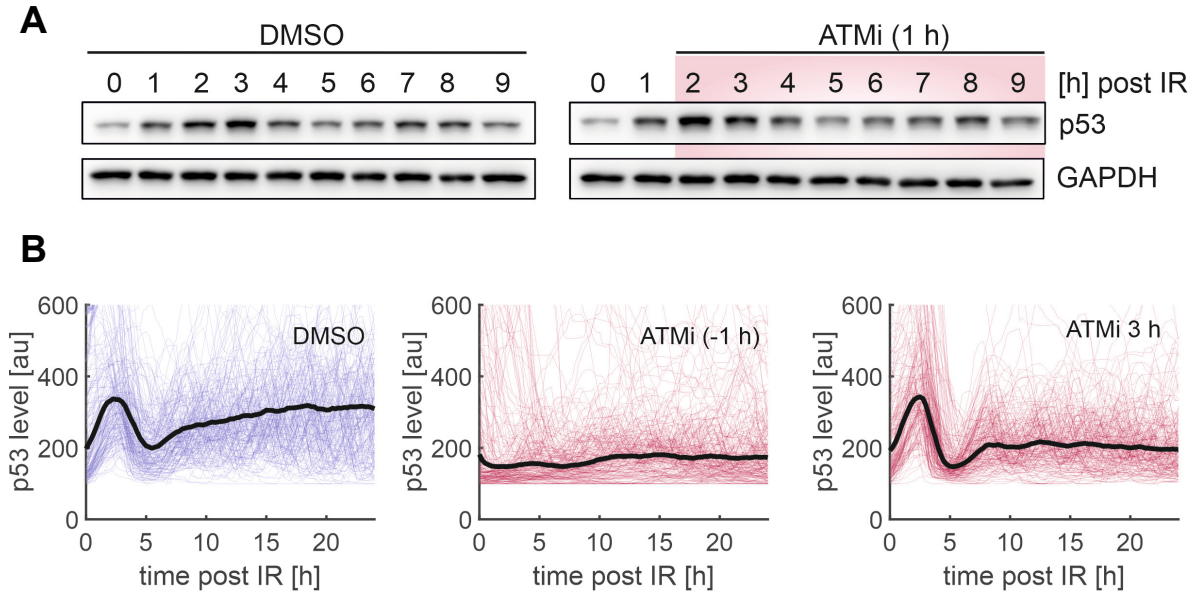

Figure 3.2.2: Response after ATM inhibition can be validated on population level and in MCF10A cells.

A. A549 WT cells were treated with an ATM inhibitor 1 h post 5 Gy irradiation (IR). Cells were harvested at indicated time points after IR and p53 levels were assessed via western blotting. GAPDH was used as a loading control. **B.** MCF10A reporter cells were treated with an ATM inhibitor 1 h before and 3 h after 5 Gy IR, respectively. Cells were followed using live-cell time-lapse microscopy. Thick black lines show the median nuclear fluorescence intensity of p53, thin lines represent a random subset of 100 single cells. The number of cells analyzed per condition can be found in Table 7.4.1.

Previous studies have shown that p53 dynamics differ across cell lines (Stewart-Ornstein and Lahav, 2017). To confirm that the observed effect is conserved in different cell lines, I verified these results in an MCF10A reporter cell line (Sheng *et al.*, 2019) (Figure 3.2.2B). In this cell line, p53 was tagged heterozygously at the endogenous locus with a fluorescent protein. Interestingly, in both cell lines, ATM inhibition resulted in a more regular pulsatile behavior (Figure 3.2.2B and Figure 3.2.1B). Together, the results show that while ATM is crucial for initially triggering the p53 response, it is dispensable for the sustained p53 response indicating that another kinase besides ATM is involved in sustaining the p53 dynamics.

3.3 CHK2 is crucial for sustaining the p53 response

In addition to ATM, other kinases from the PI3K like kinase family are activated in response to genotoxic stress and were reported to phosphorylate p53 (Lees-Miller *et al.*, 1992; Tibbetts *et al.*, 1999). To investigate whether ATR and/or DNA-PK activity are crucial for sustaining the p53 response, I inhibited their activity using small molecule inhibitors (Figure 3.3.1). However,

neither inhibition of DNA-PKcs nor ATR alone (Figure 3.3.1A) nor in combination with ATM (Figure 3.3.1B and C) led to qualitative changes in the sustained p53 response. Note that DNA-PKcs inhibition alone leads to hyperactivation of ATM causing an amplified first p53 pulse (Finzel *et al.*, 2016).

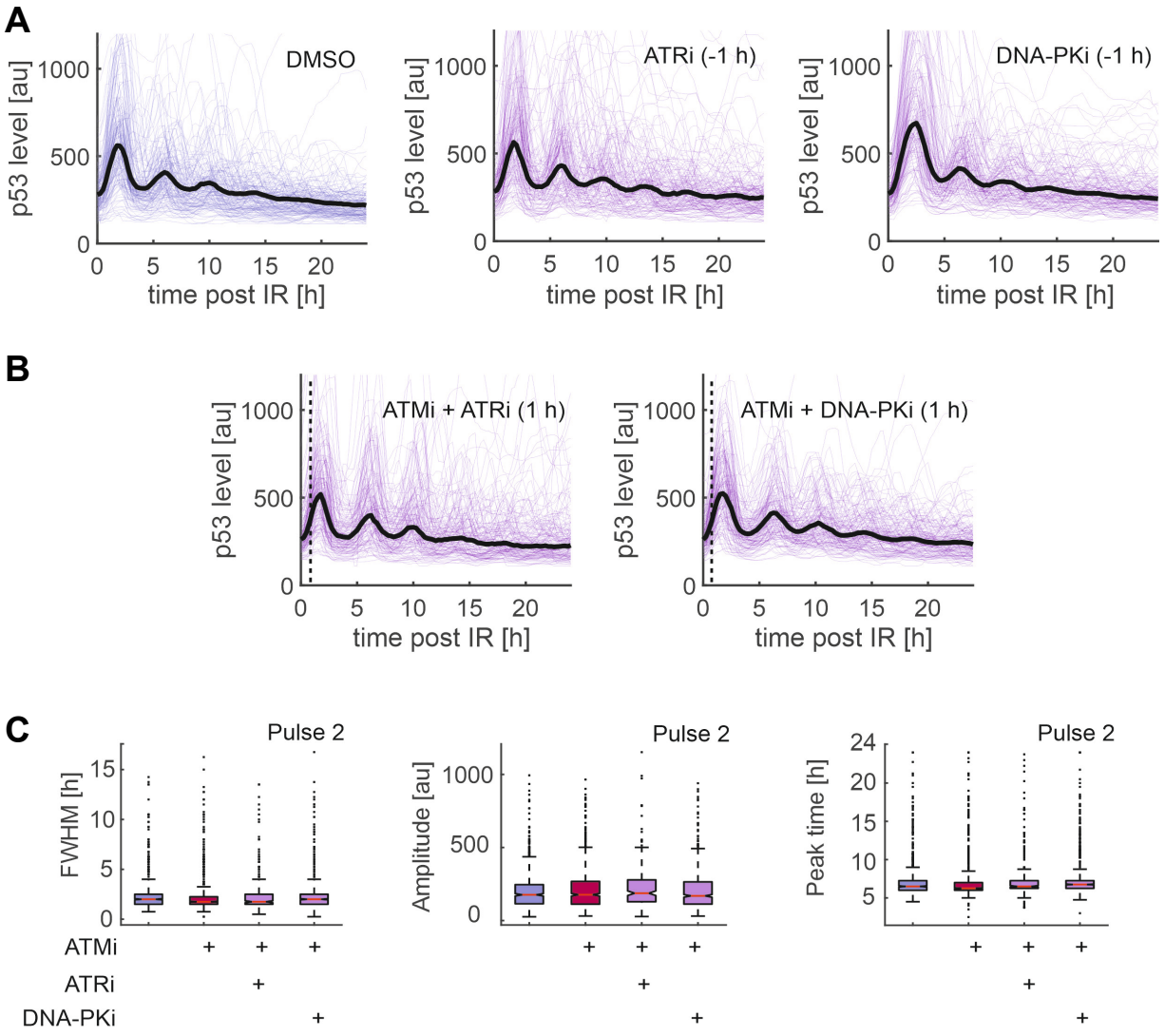

Figure 3.3.1: ATR and DNA-PK are dispensable for the sustained response.

A. A549 reporter cells were treated with ATR and DNA-PK inhibitors 1 h prior to 5 Gy irradiation (IR). Cells were followed using live-cell time-lapse microscopy. Thick black lines show the median nuclear fluorescence intensity of p53, thin lines represent a random subset of 100 single cells. The number of cells analyzed per condition as well as the threshold used for pulse analysis can be found in Table 7.4.1 and Table 7.4.2. **B.** Cells were treated with ATR and DNA-PK inhibitors in combination with an ATM inhibitor 1 h after 5 Gy IR. The dashed line indicates the time point of inhibitor addition. The number of cells analyzed per condition can be found in Table 7.4.1. **C.** Quantification of the timing, amplitude and duration (FWHM: full-width at half-maximum) of the second pulse.

The previous findings indicate that initial ATM activity is crucial to initiate the p53 response. Therefore, in the next step, we took a closer look at CHK2, a checkpoint kinase that is activated by ATM and reported to phosphorylate p53 (Hirao *et al.*, 2000). Interestingly, inhibition of CHK2

before or after radiation strongly impaired the sustained p53 response (Figure 3.3.2A). Sorting the single cells according to the timing of the second pulse revealed broad variation in the timing of the second pulse with an increased fraction of cells that did not respond with a second pulse at all (Figure 3.3.2B). Quantification of the features showed that while the first pulse is unaltered in amplitude, timing and duration, for the sustained response cells showed a remarkable delay in the timing of the second pulse, as well as a broader distribution in the duration of the second pulse and a slight decrease in the amplitude (Figure 3.3.2C).

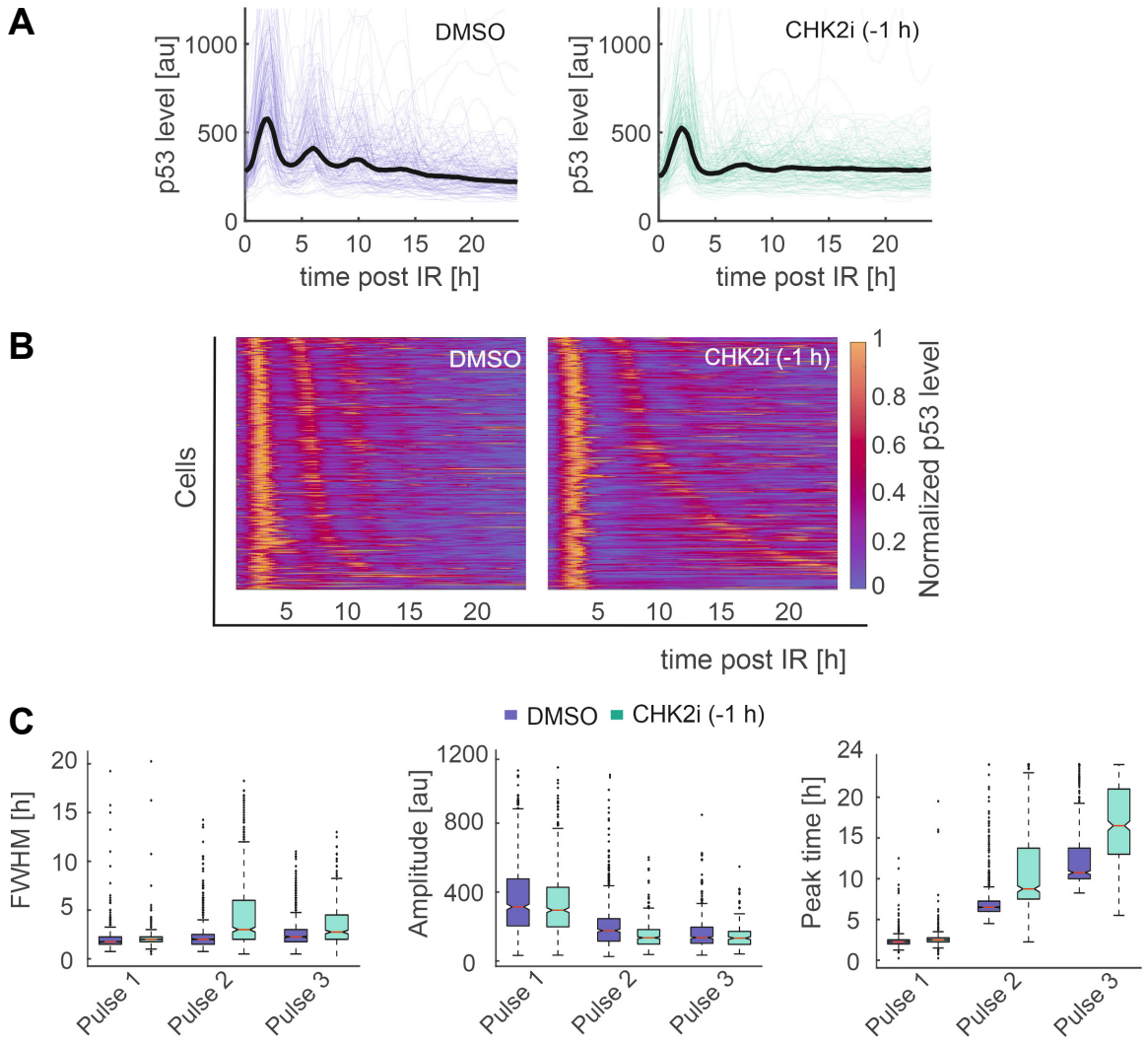

Figure 3.3.2: CHK2 is crucial for sustaining the p53 response.

A. A549 reporter cells were treated with a CHK2 inhibitor 1 h prior to 5 Gy IR. Cells were followed using live-cell time-lapse microscopy. Thick black lines show the median nuclear fluorescence intensity of p53, thin lines represent a random subset of 100 single cells. The number of cells analyzed per condition as well as the threshold used for pulse analysis can be found in Table 7.4.1 and Table 7.4.2. **B.** Heatmap of p53 levels. Each trajectory was min-max-normalized. Cells are sorted by the timing of the second pulse. **C.** Quantification of the timing, amplitude and duration (FWHM: full-width at half-maximum) of the first three pulses.

To verify the role of CHK2 for the sustained p53 response, these observations were confirmed on population-level via Western blotting and in MCF10A cells (Figure 3.3.3A and B). To exclude off-target effects of the inhibitor, the results were verified using an siRNA against CHK2 (Figure 3.3.3C). Double siRNA treatment 120h and 72h before the experiment reduced the mRNA levels to 33%. To consider effects mediated by divergent culturing conditions and the siRNA transfection process itself, two different controls were carried along: One condition where cells were seeded and cultured as the siRNA treated samples (untreated), as well as one condition, where a non-targeting control siRNA was added instead of the CHK2 siRNA. Again, I observed a delay of the second pulse and a strongly impaired sustained p53 response.

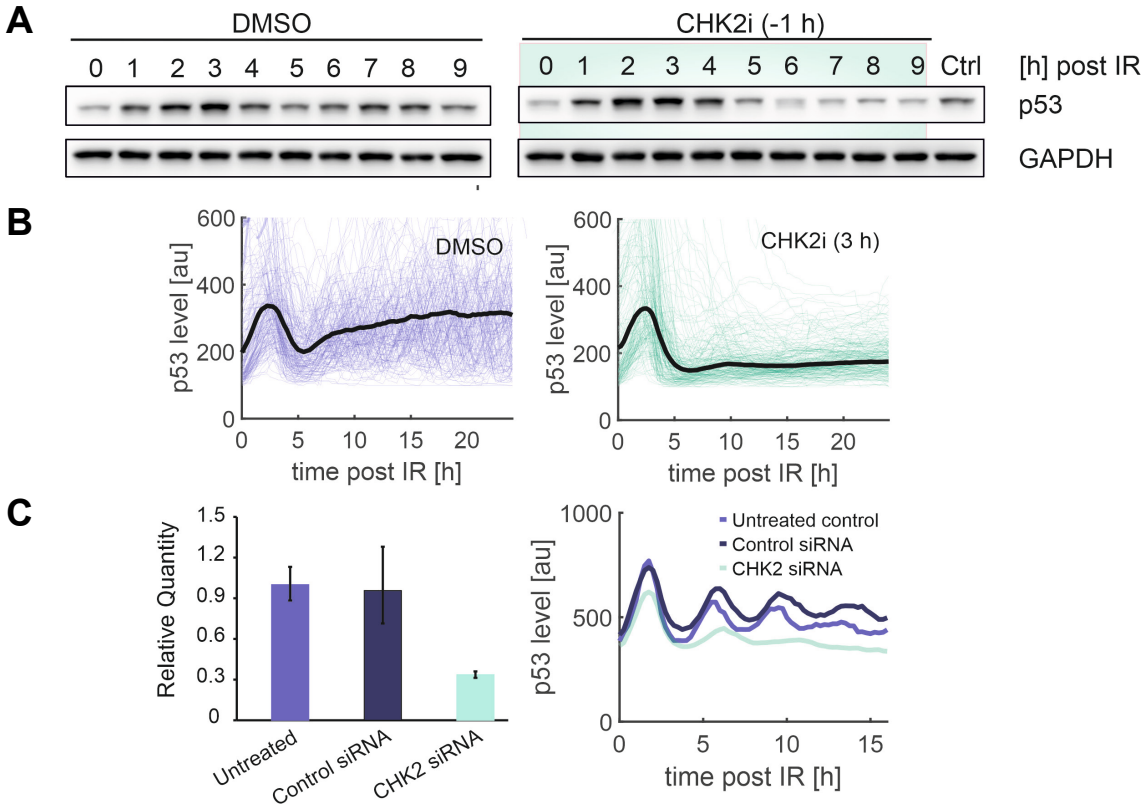

Figure 3.3.3: Response after CHK2 inhibition can be validated on population level and in MCF10A cells.

A. A549 WT cells were treated with the CHK2 inhibitor 1 h prior to 5 Gy irradiation (IR). Cells were harvested at indicated time points after IR and p53 levels were assessed via western blotting. GAPDH was used as a loading control. **B.** MCF10A reporter cells were treated with the CHK2 inhibitor 3 h after 5 Gy IR. Cells were followed using live-cell time-lapse microscopy. Thick black lines show the median nuclear fluorescence intensity of p53, thin lines represent a random subset of 100 single cells. The number of cells analyzed per condition can be found in table S1. **C.** A549 reporter cells were transfected with an siRNA targeting CHK2 or a control siRNA. Levels of CHK2 mRNA were measured via qRT-PCR (left panel). The ΔΔCt method was used to calculate relative gene expression, β-Actin was used as a housekeeping gene for the calculation of ΔCt. Error bars represent the RQmin and RQmax values obtained with three technical replicates. CHK2 depleted cells were tracked via live-cell time-lapse microscopy (right panel). Trajectories show the median nuclear fluorescence intensity of p53. The number of cells analyzed per condition can be found in Table 7.4.1.

Studies have shown that the cell cycle phase influences the DNA damage response. The DNA itself, the amount and the packing vary drastically in the different phases. Additionally, distinct repair pathways are available and different kinases are active (Hustedt and Durocher, 2017).

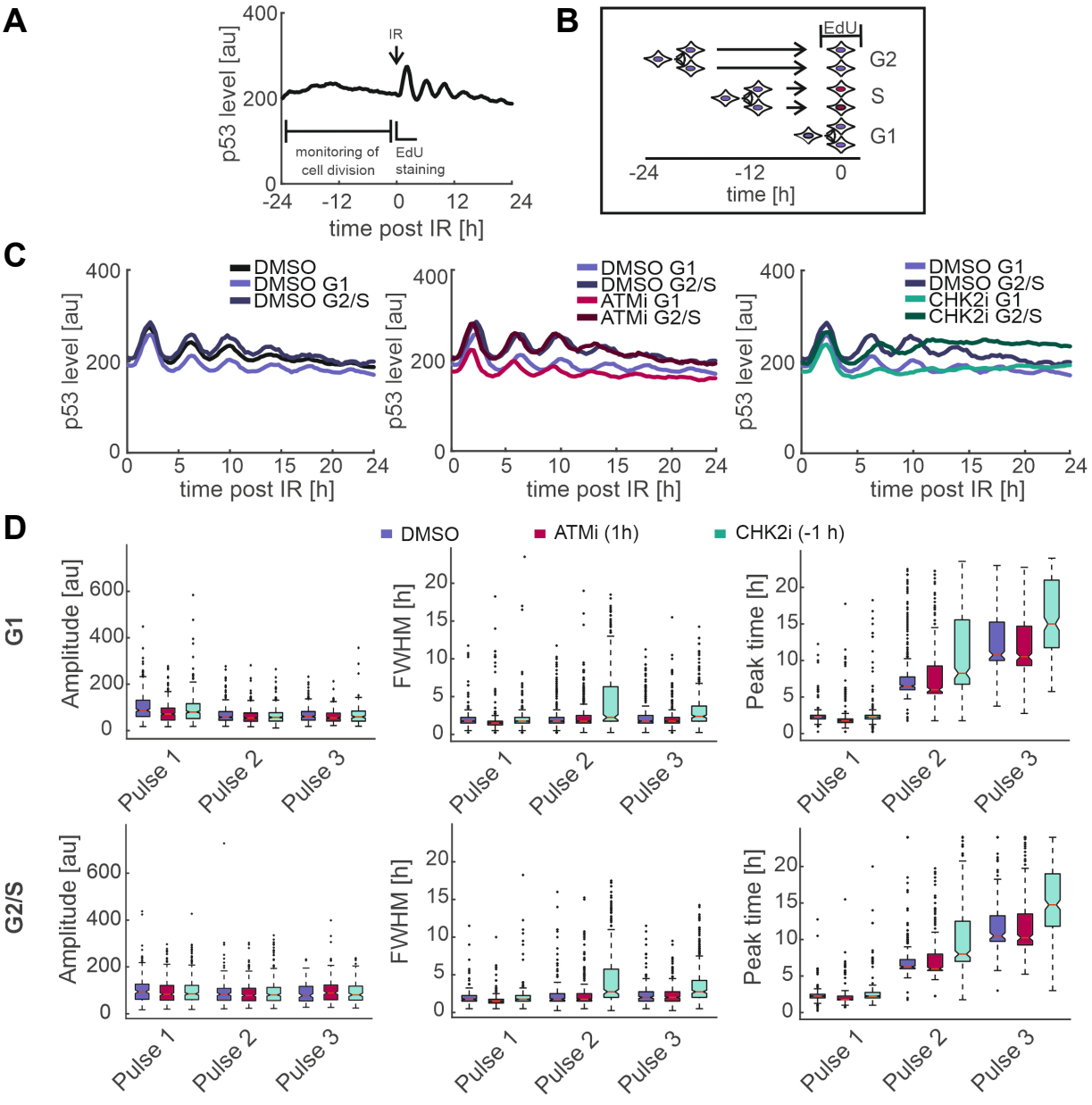

Figure 3.3.4: Effect of CHK2 inhibition is independent of the cell cycle phase.

A-B. Determination of the cell cycle phase at the time of irradiation (IR) by computational analysis and EdU staining. **A.** Cell division is monitored for 24 h before IR. Shortly before IR, S-phase cells are marked by incorporation of EdU. **B.** Cells dividing before the EdU-positive S-phase cells are sorted as G2-phase cells. Cells dividing after the S-phase cells were sorted as G1-phase cells. Modified according to Sheng, 2017. **C.** A549 reporter cells were sorted according to their cycle phase at the time of IR and treated with an ATMi inhibitor 1 h post IR or a CHK2 inhibitor 1 h prior to IR. Trajectories show the median nuclear fluorescence intensity of p53. **D** Quantification of the timing, amplitude and duration (FWHM: full-width at half-maximum) of the first three pulses. The number of cells analyzed per condition as well as the threshold used for pulse analysis can be found in Table 7.4.1 and Table 7.4.2.

To exclude that the observations after ATM and CHK2 inhibition differ in the different cell cycle phases, cells were grouped into G1 and G2/S-phase. To this end, I monitored cell division 24 h prior to IR. Previous studies have shown that the cell cycle phase can be derived from the timing of the last division event before IR (Figure 3.3.4A and B) (Toettcher *et al.*, 2009; Sheng, 2017). For instance, G2 phase cells have passed through the whole cell cycle since their last division. Accordingly, the last division before IR must have been several hours ago. In contrast, G1-phase cells most likely divided within a few hours before IR while S-phase cells should divide with a timing between G1 and G2-phase cells (Figure 3.3.4B). This computational analysis of cell division events was supplemented with 5- ethynyl-2'-deoxyuridine (EdU)-staining. The thymidine analogue EdU is incorporated during DNA replication and consequently, staining for EdU allows a faithful detection of S-phase cells. For this purpose, cells were sorted according to their EdU signal and S-phase cells were determined via an edge detection algorithm (Supplementary Figure 7.5.1A). For this population of EdU positive cells, the median division time before IR was calculated. Cells that divided before this threshold were sorted as G2-phase cells, cells that divided afterwards were sorted as G1-phase cells (Supplementary Figure 7.5.1B). As the number of G2-phase cells was considerably smaller than the group of G1 and S-phase cells, G2-phase cells were grouped together with S-phase cells.

Both, G1 and G2/S-phase cells showed a regular pulsatile behavior after ATM inhibition and a delayed and impaired sustained p53 response after CHK2 inhibition (Figure 3.3.4C and D), indicating that the observed effect is independent of the cell cycle phase. Interestingly, p53 levels are slightly higher in G2/S-phase compared to G1 (Figure 3.3.4C). Combined inhibition of ATM and CHK2 almost completely abolishes the sustained p53 response in G1 phase, but only has a smaller additional effect in G2/S-phase cells compared to single inhibition of CHK2, indicating an additional contribution of another kinase in these cell cycle phases (Figure 3.3.5A and B).

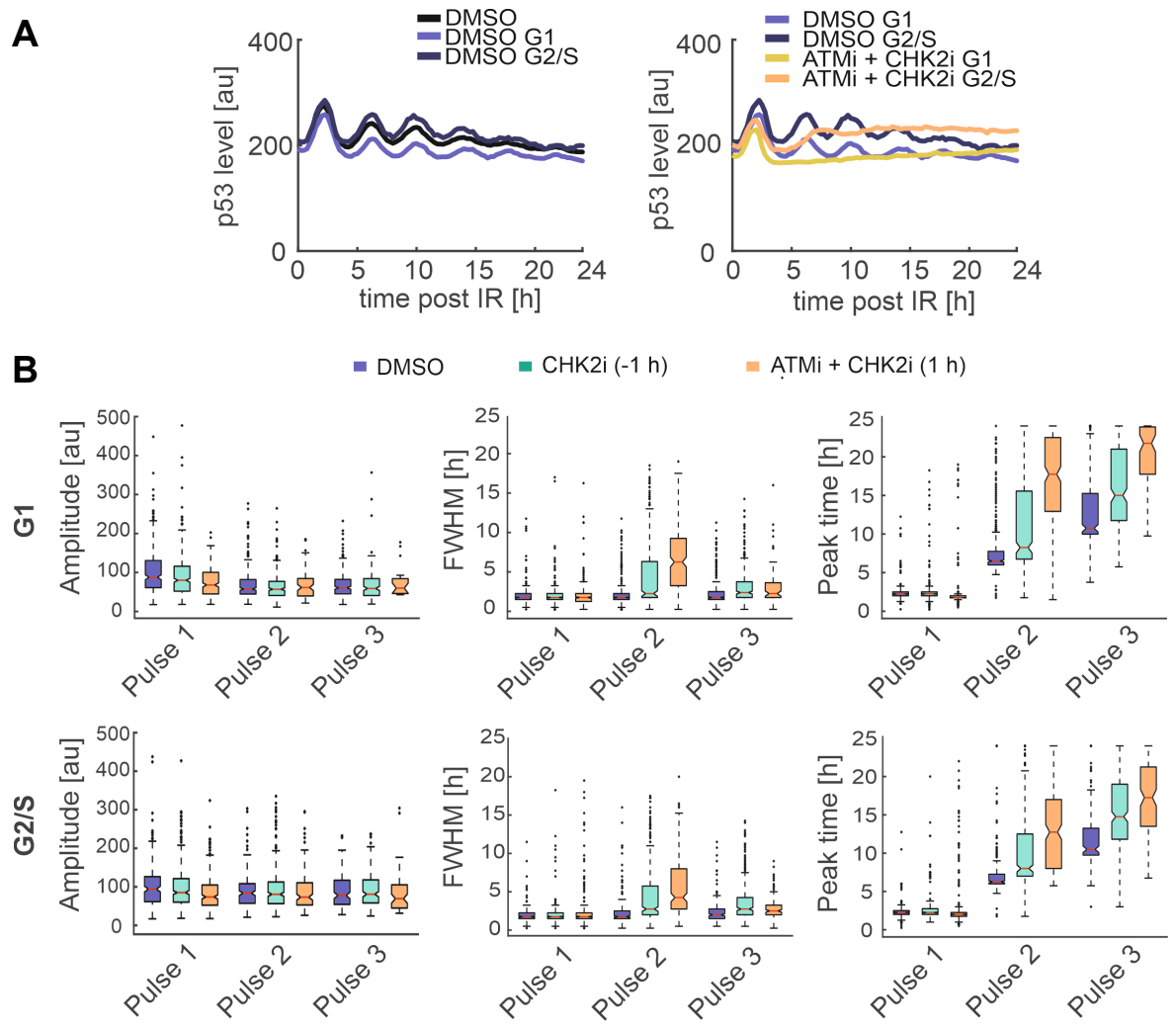

Figure 3.3.5: p53 dynamics upon combined inhibition of ATM and CHK2 indicate the contribution of another kinase in S/G2-phase.

A. A549 reporter cells were sorted according to their cycle phase at the time of IR and treated with an ATMi and CHK2i inhibitor 1 h post IR. Trajectories show the median nuclear fluorescence intensity of p53. **B.** Quantification of the timing, amplitude and duration (FWHM: full-width at half-maximum) of the first three pulses. The number of cells analyzed per condition as well as the threshold used for pulse analysis can be found in Table 7.4.1 and Table 7.4.2.

Together, the results demonstrate that while ATM triggers the immediate p53 response to acute damage (first pulse), CHK2 is needed to sustain the response (following pulses) thereby responding to persisting damage. To test this hypothesis, DNA DSB were induced using the radiomimetic drug NCS and the cells were treated with an ATM inhibitor (1 h post IR) or CHK2 inhibitor (1 h prior IR), respectively. After the first pulse was completed, new, acute damage was induced (Figure 3.3.6A). Control cells respond to this newly induced damage with a second pulse that is higher in amplitude than a normal second pulse (Figure 3.3.6A, left panel, compare also Figure 3.1.1G). After CHK2 inhibition, new damage leads to a second pulse with higher amplitude and normal timing (Figure 3.3.6A, right panel). However, after ATM inhibition, the

new damage does not amplify the second p53 pulse underlining the importance of ATM to mediate the response to acute damage (Figure 3.3.6A, middle panel).

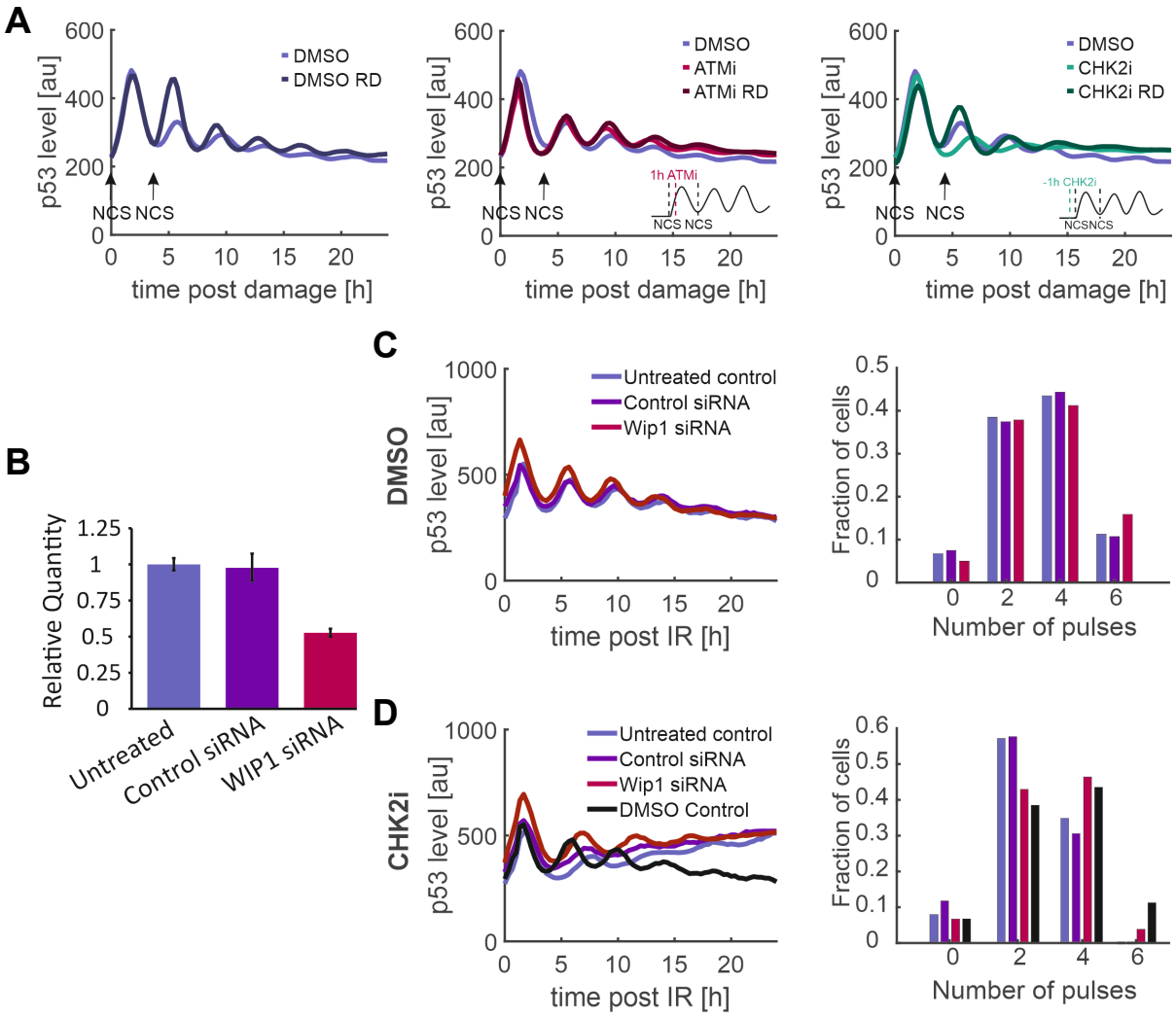

Figure 3.3.6: WIP1 limits the role of ATM to the response to acute damage.

A. A549 reporter cells were damaged with 0.2 µg/mL, Neocarcinostatin (NCS) and were re-damaged 4 h after an initial treatment with 0.2 µg/mL NCS. Cells were either treated with DMSO (left) or a CHK2 inhibitor (right) 1 h before the initial NCS addition or an ATM inhibitor (middle) 1 h after initial NCS addition and followed using live-cell time-lapse microscopy. Trajectories show the median nuclear fluorescence intensity of p53. **B.** A549 reporter cells were transfected with an siRNA targeting WIP1 or a control siRNA. Levels of WIP1 mRNA were measured via qRT-PCR. The ΔΔCt method was used to calculate relative gene expression, β-Actin was used as a housekeeping gene for the calculation of ΔCt. Error bars represent the RQmin and RQmax values obtained with three technical replicates. **C-D.** WIP1 depleted cells were tracked via live-cell time-lapse microscopy in response to 5 Gy IR. Trajectories show the median nuclear fluorescence intensity of p53 (left). Histograms show the fraction of cells with the indicated number of p53 pulses within 24 h (right, binning: 2). Cells were treated with DMSO (**C**) or a CHK2 inhibitor (**D**). The number of cells analyzed per condition as well as the threshold used for pulse analysis can be found in Table 7.4.1 and Table 7.4.2.

Why is the role of ATM limited to the response to acute damage? One possible mechanism would be dephosphorylation via the negative regulator WIP1 mediating the inactivation of ATM after the first pulse. Consequently, WIP1 depletion should allow a prolonged contribution of ATM to

the p53 response. An siRNA against WIP1 was used to deplete its cellular levels (Figure 3.3.6B). Consistent with previous publications, WIP1 depletion did not alter the features of p53 dynamics (Mönke *et al.*, 2017) (Figure 3.3.6C, left panel). With the given knock-down efficiency and applied damage dose, I observed no change towards a higher total number of pulses (Figure 3.3.6C, right panel). CHK2 inhibition led to a shift towards a lower total number of pulses in control cells (Figure 3.3.6D). In contrast, WIP1 depleted cells show a shift back to higher pulse numbers comparable to the control cells (Figure 3.3.6D), most likely through extended input of ATM compensating the loss of CHK2 activity.

The immediate p53 response is triggered via the ATM-p53/MDM2-WIP1 feedback. Upon IR, ATM is activated rapidly, allowing not only the stabilization of p53 but also inducing the fast degradation of MDM2 (Khosravi *et al.*, 1999; Stommel and Wahl, 2004). This network architecture conveys excitability to the immediate p53 response. Experimentally, this could be shown by limiting the input from the upstream kinases using an inhibitor (Batchelor *et al.*, 2008). To test whether also pulses of the sustained response arise from an excitable mechanism, CHK2 was inhibited after 5 h, when the second pulse has already started to rise (Figure 3.3.7A).

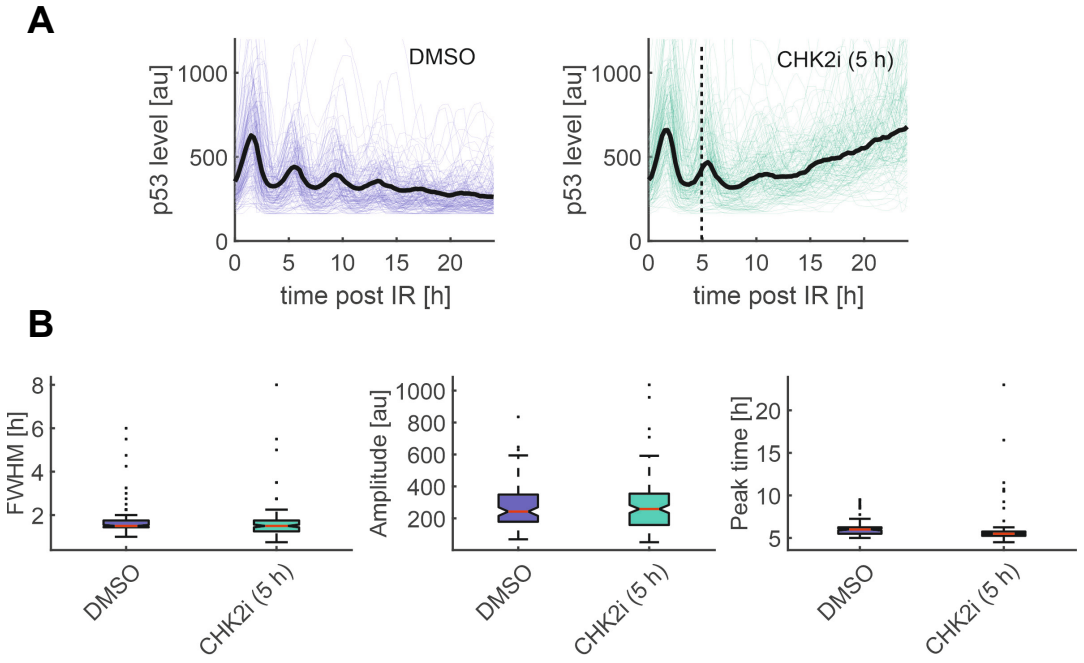

Figure 3.3.7: P53 pulses of the sustained response are excitable.

A. A549 reporter cells were treated with a CHK2 inhibitor 5 h after 5 Gy IR. Cells were followed using live-cell time-lapse microscopy. Thick black lines show the median nuclear fluorescence intensity of p53, thin lines represent a random subset of 100 single cells. The dashed line indicates the time point of inhibitor addition. **B.** Quantification of the timing, amplitude and duration (FWHM: full-width at half-maximum) of the second pulse. Only cells that had already passed the first trough at 5 h were included in the analysis. The number of cells analyzed per condition as well as the threshold used for pulse analysis can be found in Table 7.4.1 and Table 7.4.2.

This transient CHK2 activity induced a full second p53 pulse and led to a delay of the following third pulse (Figure 3.3.7A). As the p53 dynamics become more and more asynchronous over the course of the response, for the quantification of the features of the second pulse only cells that had already passed the first trough were taken into the analysis. No differences in the duration, amplitude or timing could be detected (Figure 3.3.7B), indicating that the CHK2 dependent stabilization of p53 results from an excitable mechanism.

3.4 CHK2 activity shows non-pulsatile dynamics post IR

Previous publications suggested a pulsatile activation of CHK2 based on its phosphorylation on T68 in MCF7 cells (Batchelor *et al.*, 2008). Indeed, an increase in phosphorylation on this residue was observed after IR in A549 cells as well followed by a steady decrease (Figure 3.4.1A). However, no second increase in phosphorylation could be observed. Note that even within a time frame of 11 h no second pulse of T68 phosphorylation was observed (data not shown). Moreover, inhibition of ATM after 1 h leads to an immediate loss of phosphorylation on this residue (Figure 3.4.1B). This is not surprising, considering that T68 is phosphorylated by ATM in response to damage (Figure 3.4.1C). Consequently, T68 phosphorylation might not be a suitable measure of CHK2 activity.

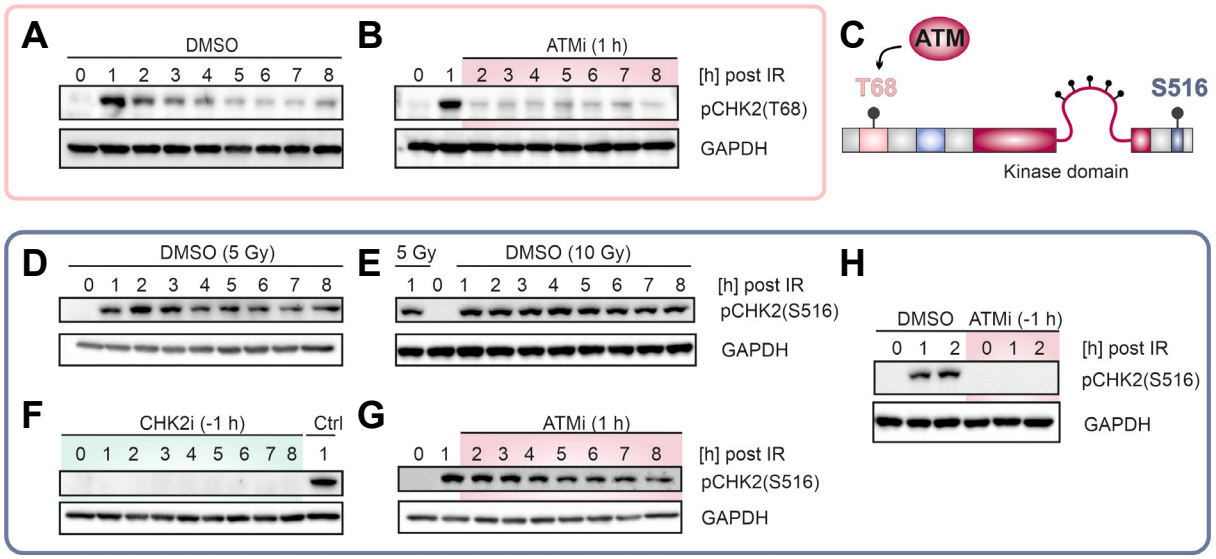

Figure 3.4.1: CHK2 activity shows non-pulsatile dynamics post IR.

A-B. A549 WT cells were treated with DMSO (**A**) 1 h before or an ATM inhibitor (**B**) 1 h post 5 Gy irradiation (IR). Cells were harvested at indicated time points after IR and pCHK2(T68) levels were assessed via western blotting. GAPDH was used as a loading control. **C.** Scheme of CHK2 domains with selected modifications. In response to genotoxic stress, CHK2 is phosphorylated on T68 via the kinase ATM. This and other modifications induce dimerization of CHK2, which subsequently facilitates auto-phosphorylation of several residues in the T-loop of the kinase domain as well as S516. **D-E.** Cells were irradiated with 5 Gy (**D**) or 10 Gy (**E**) and pCHK2(S516) levels were assessed via western blotting. GAPDH was used as a loading control. **F-H.** Cells were treated with the CHK2 inhibitor 1 h prior to 5 Gy IR (**F**), ATM inhibitor 1 h post IR (**G**) or 1 h before IR (**H**) and pCHK2(S516) levels were assessed via western blotting.

Instead, phosphorylation on S516 was used to assess CHK2 activity. Upon activation, CHK2 is auto-phosphorylated on several residues including S516 (see chapter 1.2) (Figure 3.4.1C). Studies have shown that phosphorylation on S516 in contrast to T68 depends on the kinase activity of CHK2 (Schwarz, Lovly and Piwnica-worms, 2003; Wu and Chen, 2003). With regard to its important role for maintaining the p53 response, how do the levels of active CHK2 change in the course of the DNA damage response? In response to 5 Gy IR, an increase of S516 phosphorylation was observed. Interestingly, in contrast to phosphorylation on T68, the signal remained relatively stable with only a slight decrease over time (Figure 3.4.1D). Irradiation with a higher dose of 10 Gy prolonged the time CHK2 was active (Figure 3.4.1E). Inhibition of CHK2 before IR led to a loss of phosphorylation on this residue underlining that auto-phosphorylation on this residue reflects CHK2 activity (Figure 3.4.1F). Inhibition of ATM after IR did not alter the dynamics of CHK2 activity showing that the latter is independent of continuous ATM activity (Figure 3.4.1G). However, inhibition of ATM before IR led to a loss of phosphorylation on S516 showing that initial CHK2 activation depends on ATM activity (Figure 3.4.1H).

3.5 A constant CHK2 input can trigger pulsatile p53 dynamics

My results provide evidence that sustained p53 oscillations are independent of upstream ATM activity. In contrast, previous approaches to model the p53 response suggested that sustained oscillations result from recurrent activation of ATM (Mönke *et al.*, 2017): The detection of DSB facilitates the switch-like activation of ATM via a positive feedback loop involving γH2AX and the MRN complex (see chapter 1.2). In turn, ATM mediates the destabilization of MDM2 and stabilization of p53. p53 induced expression of WIP1 interferes with the positive feedback and leads to dephosphorylation and inactivation of ATM. If after one completed pulse DSB remain, another pulse is triggered by the same mechanism. However, in this model, inhibition of ATM would terminate p53 oscillations (Supplementary Figure 7.5.2). Moreover, opposed to the pulsatile input from ATM suggested by Batchelor *et al.*, 2008 or Mönke *et al.*, 2017, I observe a stable, non-pulsatile input by CHK2 driving sustained oscillations. Consequently, my new results collide with the currently suggested network topologies and models. To elucidate how a constant CHK2 input can lead to sustained pulses of p53 accumulation and which negative feedbacks and regulators are involved in shaping the sustained p53 response, I combined my experimental data with mathematical modeling in cooperation with Raphael Löffler, Isabella Mendler and Barbara Drossel (TU Darmstadt).

As described in chapter 1.3, sustained oscillations can be generated by a delayed negative feedback (NF) on p53. In the model of recurrent initiation, ATM was direct part of a second

negative feedback coupled to the core NF between p53 and MDM2. Unlike ATM, CHK2 itself cannot be part of a NF as it does not show pulsatile dynamics of activity. Consequently, sustained p53 oscillations are not induced by repeated activation of upstream input signals. However, CHK2 can act as a bifurcation parameter on the NF. Which NF qualifies to drive sustained oscillations mediated by CHK2 activity? One option is the central p53-MDM2 feedback which can be influenced by CHK2 in two ways: The kinase could either stabilize p53 or destabilize MDM2. For both possibilities, a model was generated based on ordinary differential equations (Figure 3.5.1A and B) (for details see Löffler, 2021). In the models, either the degradation rate of MDM2 (D_M) or the degradation rate of p53 (D_P) are modulated by active CHK2 (CHK2*). In both models, D_M additionally depends on the levels of active ATM (ATM*).

How do p53 levels respond to changes in D_M or D_P? To approach this question, we examined the isolated p53-MDM2-NF independent of the other network players via bifurcation analysis and treated D_M or D_P as parameters that can be regulated directly. Under basal conditions, D_M is below the Hopf point H1 (Figure 3.5.1D) and the system remains in a stable steady state. When the cell encounters genotoxic stress, D_M increases and the system enters the limit cycle. Vice versa, D_P is high under non-stressed conditions and decreases upon IR. Even though the bifurcation analysis shows that modulation of D_M or D_P can lead to sustained oscillations, it also demonstrates that the amplitude of the resulting oscillations depends on the parameter value of D_M and D_P. In the complete model, the increase of D_M is mediated by activation of CHK2. To prevent variations in the amplitude of the pulses due to gradually increasing D_M, CHK2* is modeled as a bistable switch: During activation, CHK2 undergoes auto-phosphorylation which makes it independent of ATM* and formally builds a positive feedback leading to bistability. Accordingly, CHK2 exists in two discrete states: Under basal conditions, CHK2 is switched ‘off’. In response to genotoxic stress, CHK2 is switched ‘on’ by ATM and subsequently stays active even when ATM is inactivated. This explains why initially ATM activity is crucial to trigger p53 oscillations but is dispensable for the sustained response.

In the simulated time series, both models can equally reproduce most of the experimental results (Figure 3.5.1A and B). Both show that the p53 response is biphasic: The immediate response (first pulse) is mediated by ATM. Initial ATM activity is crucial to initiate the p53 response but alone does not lead to persisting oscillations. Activation of CHK2 via ATM pushes the system from a stable steady state to sustained oscillations mediated by the delayed negative feedback between p53 and MDM2.

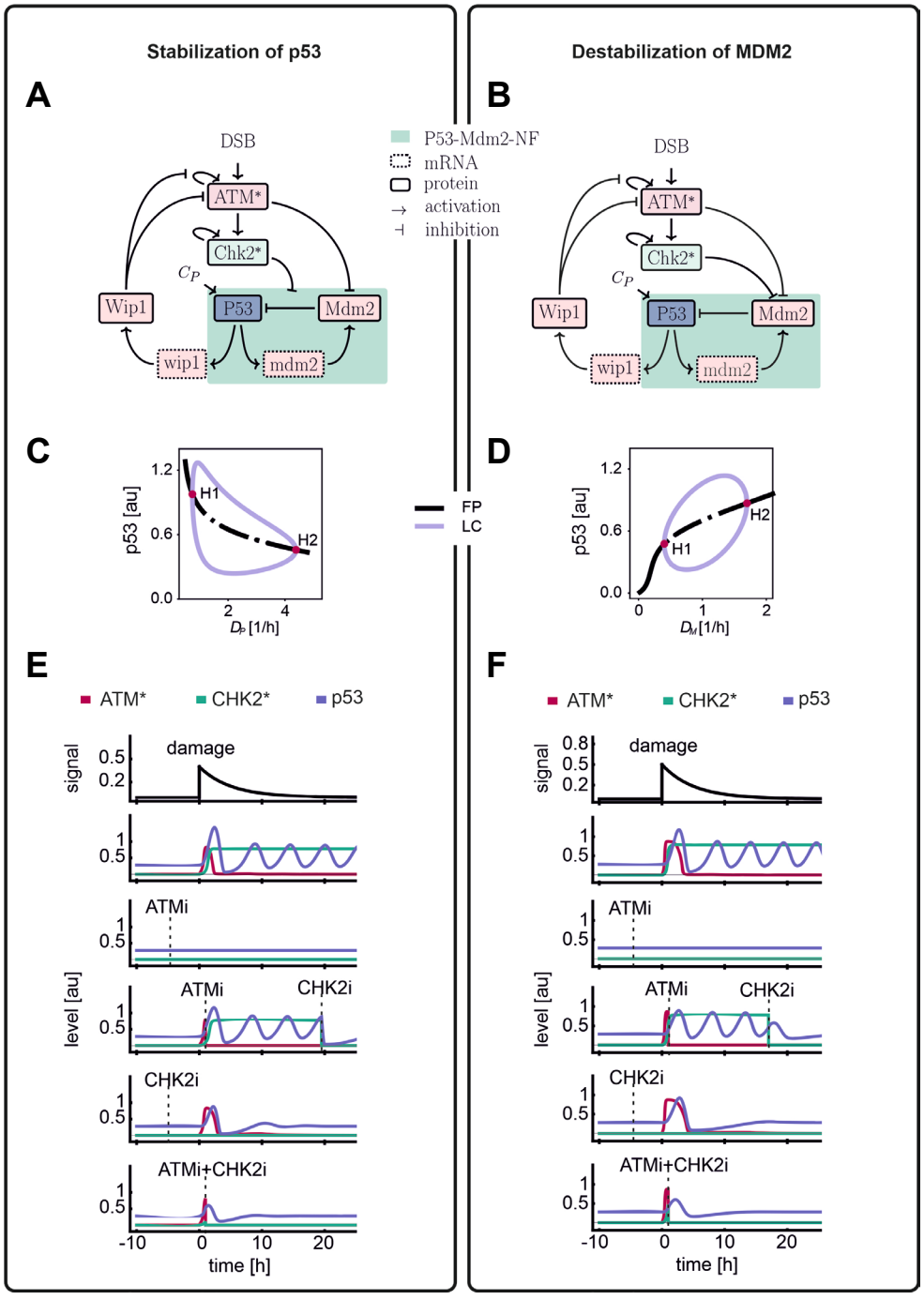

Figure 3.5.1: A constant input can trigger pulsatile p53 dynamics (Modelling by Raphael Löffler).

A-B. Network scheme for the model. ATM activation is induced by DNA DSB. Active ATM (ATM*) fosters the formation of more ATM*. Once activated, ATM activates CHK2. Moreover, active ATM destabilizes MDM2 and stabilizes p53 by phosphorylation. P53 activates transcription of WIP1 and MDM2. WIP1 dephosphorylates ATM and interferes with positive feedback on ATM. CHK2 stays active independent of the activation status of ATM and influences the p53-MDM2-NF by stabilization of p53 (**A**) or destabilization of MDM2 (**B**) **C-D.** Bifurcation analysis. D_P: degradation rate of p53. D_M: degradation rate of MDM2. For high D_M or low D_P, the system enters a limit cycle through two supercritical Hopf bifurcations. **E-F.** Simulated time series for the models based on CHK2 influencing the p53-MDM2 feedback by stabilization of p53 (**E**) or destabilization of MDM2 (**F**). The damage signal shows an exponential decay. ATM*: active ATM; CHK2* active CHK2. Dashed lines indicate the addition of inhibitors.

3.6 MDMX levels are stabilized after CHK2 inhibition

The results from modeling suggest that CHK2 can influence the p53-MDM2 feedback both via stabilization of p53 or by destabilizing MDM2. Studies propose that CHK2 stabilizes p53 by phosphorylation on S20 (Chehab *et al.*, 1999; Shieh, Taya and Prives, 1999) (Figure 3.6.1A). However, initial western blot experiments did not show any reduction of S20 phosphorylation after CHK2 inhibition in repeated experiments (data not shown). On the other hand, CHK2 indirectly destabilizes MDM2 via phosphorylation of MDMX on S367 (Chen *et al.*, 2005) (Figure 3.6.1A). MDMX forms heterodimers with MDM2 increasing the stability of MDM2 as well as its E3 ligase activity (see also section 1.2) (Sharp *et al.*, 1999; Tanimura *et al.*, 1999). Degradation of MDMX mediated via CHK2 dependent phosphorylation consequently decreases the stability of MDM2. Inhibition of CHK2 should therefore stabilize both MDMX and MDM2.

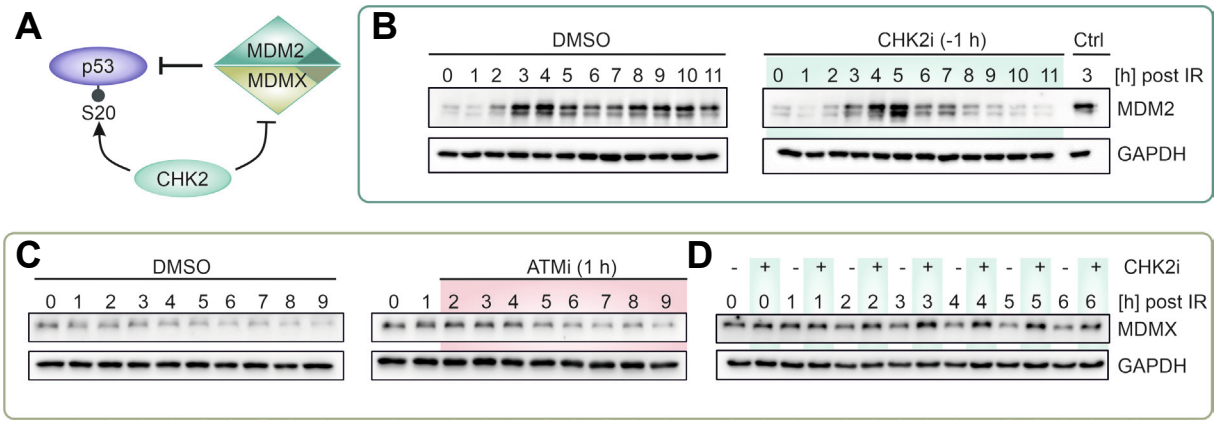

Figure 3.6.1: MDMX levels are stabilized upon CHK2 inhibition.

A. CHK2 could modulate p53 levels by stabilizing p53 via phosphorylation on S20 or by phosphorylating the negative regulator MDMX. Thereby, CHK2 mediates the degradation of MDMX and destabilizes MDM2. **B.** A549 WT cells were treated with DMSO or a CHK2 inhibitor 1 h prior to 5 Gy irradiation (IR). Cells were harvested at indicated time points after IR and MDM2 levels were assessed via western blotting. GAPDH was used as a loading control. **C-D.** Cells were treated with DMSO 1 h prior to 5 Gy IR (**C**), the ATM inhibitor 1 h post IR (**C**) or the CHK2 inhibitor 1 h before IR (**D**) and MDMX levels were assessed via western blotting.

To determine the effects of ATM or CHK2 inhibition on MDM2 and MDMX, the levels of the negative regulators were assessed via western blotting. In control cells, MDM2 levels decrease immediately after IR and then increase peaking around 3-4h. A second pulse was observed peaking after 9-10 h (Figure 3.6.1B). After CHK2 inhibition the first MDM2 accumulation was prolonged peaking around 5 h. No second MDM2 peak could be observed, most likely due to missing transcriptional activation by p53. Under basal conditions, MDMX levels were high in control cells and decreased in response to IR (Figure 3.6.1C and D). After inhibition of ATM after 1 h, the MDMX dynamics were similar to the control cells and showed a decrease post IR as well

(Figure 3.6.1C). In contrast, CHK2 inhibition led to a stabilization of MDMX (Figure 3.6.1D). Thus, MDMX destabilization via CHK2 is a possible mechanism to control the p53-MDM2 feedback.

3.7 How is the CHK2 activity maintained over time?

The previous model of recurrent initiation generated repeated p53 pulses via the ATM-p53/MDM2-WIP1 feedback. Through the MRN complex, the main kinase in this model, ATM, has a direct connection to the break sides and would therefore have the capacity to detect when damage is repaired. In contrast, CHK2 activity is not controlled by the repair status of the DNA aside from its activating stimulus by ATM. Previous studies have shown a clear correlation between the damage dose and the total number of p53 pulses. Furthermore, I also observed a prolonged CHK2 activity at a higher dose (Figure 3.4.1C). How is the duration of CHK2 activity connected to the degree of damage?

One option would be a third protein besides ATM whose activity is influenced by the repair status of the DNA and that can (re-)activate CHK2 in the absence of ATM activity. To test this possibility, I sequentially added first the ATMi and then the CHK2i leading to a loss of both ATM and CHK2 activity as shown via western blotting based on CHK2 phosphorylation on T68 or S516, respectively (Figure 3.7.1A). After washing off both inhibitors, both phosphorylation signals can be recovered. In the next step, again both the CHK2 and the ATM inhibitor were added sequentially. However, after inactivating both kinases, only the CHK2i was washed off, while keeping the cells under ATM inhibition. Also in the absence of ATM activity, a partial reactivation of CHK2 was possible. To see whether this partial reactivation would lead to restored p53 dynamics after CHK2 and ATM inhibition, a corresponding microscopy experiment was performed (Figure 3.7.1B). After ATM and CHK2 inhibition, I observed a strong delay in the second pulse and overall an impaired sustained p53 response. Wash-off of both ATMi and CHK2i led to a full recovery of the pulsatile dynamics. Wash-off of only the CHK2 inhibitor, however, only allowed partial recovery of the p53 response consistent with the partial recovery of the CHK2 activity. Based on these results, the involvement of a third protein can neither be completely proven nor denied and further experiments are necessary to shed light on this question.

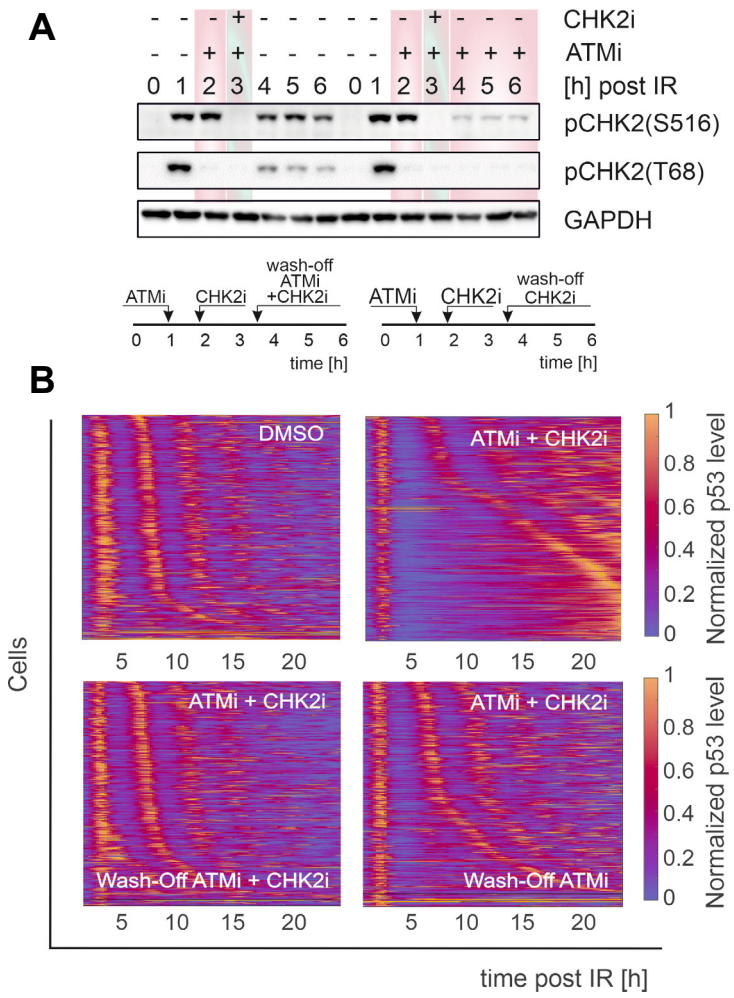

Figure 3.7.1: Wash-off of CHK2 inhibition allows partial recovery of CHK2 activity and pulsatile p53 dynamics in the absence of ATM activity.

A. After 5 Gy irradiation (IR), A549 WT cells were sequentially treated with an ATM (1h post IR) and CHK2 inhibitor (2 h post IR). After 3 h, either both inhibitor (left) or only the CHK2 inhibitor (right) were washed off. Cells were harvested at indicated time points post IR and pCHK2(T68) and pCHK2(S516) levels were assessed via western blotting. GAPDH was used as a loading control. The scheme shows the timing of inhibitor addition. **B.** Heatmap of p53 levels. Each trajectory was min-max-normalized. After 5 Gy irradiation (IR), A549 reporter cells were sequentially treated with an ATM (1 h post IR) and CHK2 inhibitor (1.5 h post IR) (upper panel, right) or DMSO (upper panel, left). After 3 h, either both inhibitor (lower panel, left) or only the CHK2 inhibitor (lower panel, right) were washed off. Cells are sorted by the timing of their second pulse. The number of cells analyzed per condition as well as the threshold used for pulse analysis can be found in Table 7.4.1 and Table 7.4.2.

Another option to connect the duration of the CHK2 activity with the degree of damage could be the strength and duration of the activating ATM input (Figure 3.7.2). Once ATM is inactivated by WIP1, CHK2 might be inactivated as well at a constant speed by phosphatases that keep CHK2 inactive under non-stressed conditions as for instance PP2A or PP1 (Zannini, Delia and Buscemi, 2014). The higher or longer the initial ATM input, the longer CHK2 would be active. The initial input signal by ATM would be comparable to a timer that is set depending on the degree of damage.

Figure 3.7.2: Duration of CHK2 activity increases with the strength and duration of the activating ATM input.

Scheme of CHK2 activity in the course of the damage response depending on the ATM activity. ATM activates CHK2 in response to damage. As long as ATM is active, CHK2 remains fully active. Once ATM is inactivated, CHK2 is inactivated as well at a constant speed by phosphatases like PP2A and PP1 that keep CHK2 inactive under non-stressed conditions. Alteration of the strength (left panel) or the duration (right panel) of the ATM activity upon different degrees of damage could therefore influence how long CHK2 is active.

This explanation would require that the CHK2 protein itself is stable over the time of the response to maintain an active conformation until inactivation. The stability of CHK2 was determined via a cycloheximide (CHX) chase. CHX inhibits protein biosynthesis by interfering with translational elongation (Kao *et al.*, 2015). To exclude that the stability of CHK2 is altered in response to IR, the CHX chase was performed in undamaged as well as in irradiated cells (Figure 3.7.3A).

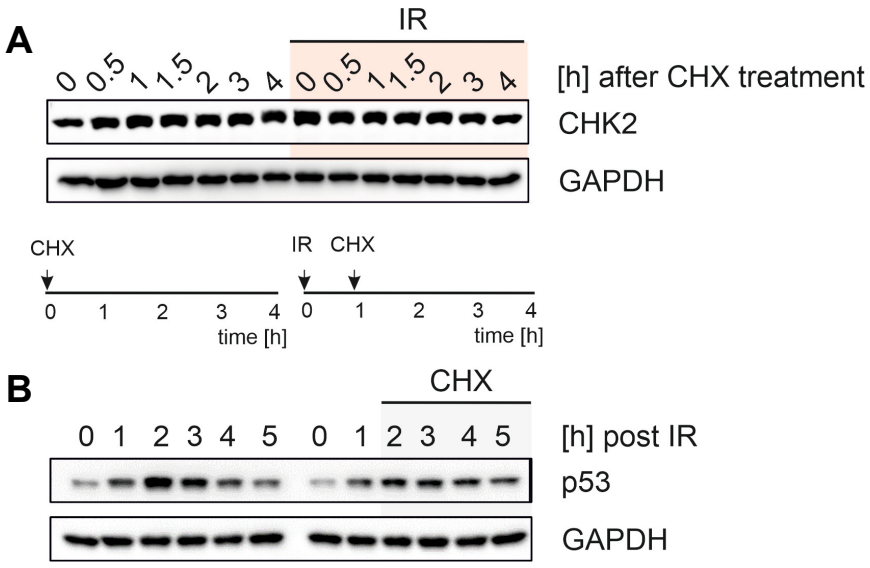

Figure 3.7.3: CHK2 protein levels are stable upon inhibition of protein synthesis.

A. A549 WT cells were treated with the inhibitor of protein synthesis cycloheximide (CHX) either in the absence of DNA damage or 1 h post 5 Gy irradiation (IR). Cells were harvested at indicated time points post IR and total CHK2 levels were assessed via western blotting. GAPDH was used as a loading control. The scheme indicates the timing of CHX addition and IR. **B.** Cells were irradiated with 5 Gy (left) or additionally treated with CHX after 1 h (right). P53 levels were measured via western blotting.

Both conditions indicate that CHK2 is stable over the time of the p53 response. As a control, cells were irradiated and treated with CHX 1 h post IR. Due to the inhibition of protein synthesis, p53 levels did not increase after 1 h and were stabilized due to missing expression of the negative regulators WIP1 and MDM2 (Figure 3.7.3B).

To test whether the duration and/or strength of the ATM input differs in response to different doses, ATM activity was determined upon 1 to 10 Gy IR based on CHK2 phosphorylation on T68 (Figure 3.7.4A). As hypothesized, ATM activity increased with the damage dose until it saturates at high doses. In a corresponding microscopy experiment, the total number of pulses at different degrees of damage was determined. Here, a saturation of the number of pulses at high doses was observed as well (Figure 3.7.4B and Supplementary Figure 7.5.3A).

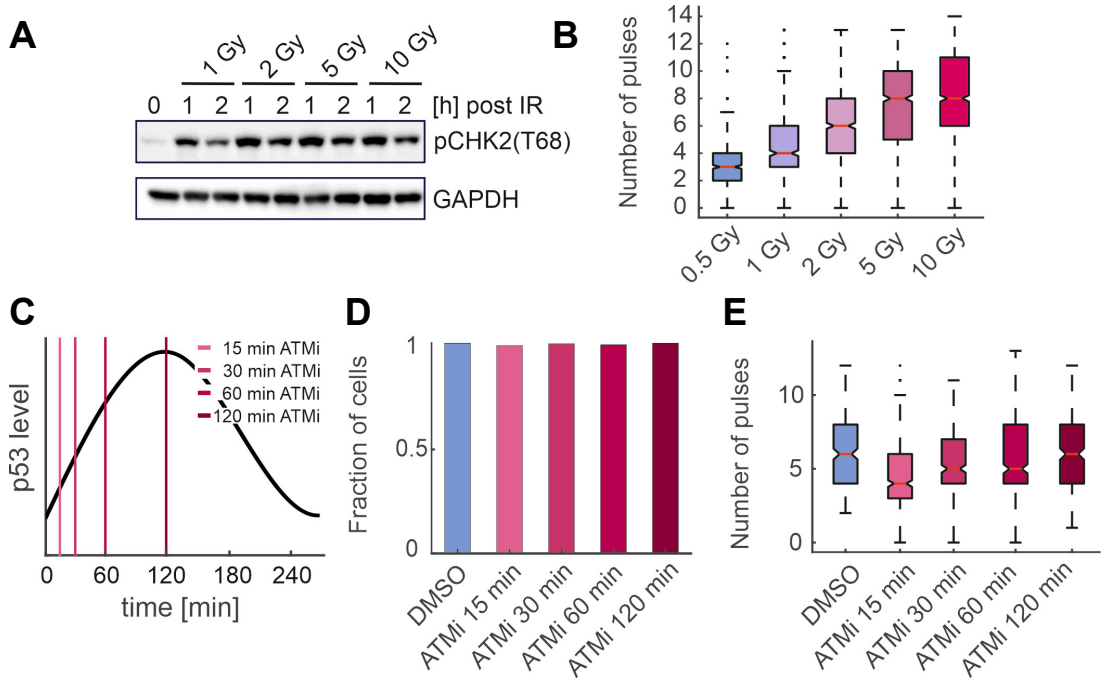

Figure 3.7.4: Shortened ATM activity leads to a decrease in the total number of p53 pulses.

A. A549 WT cells were irradiated with increasing doses (1 to 10 Gy). Cells were harvested at indicated time points post IR and pCHK2(T68) levels were assessed via western blotting. GAPDH was used as a loading control. **B.** A549 reporter cells were irradiated with increasing doses (0.5 to 10 Gy) and followed via time-lapse live-cell microscopy. The total number of pulses observed within 48h was assessed. The number of cells analyzed per condition as well as the threshold used for pulse analysis can be found in Table 7.4.1 and Table 7.4.2. **C-E.** A549 reporter cells were treated with an ATM inhibitor at different time points post 5 Gy IR (15-120 min) and tracked via time-lapse live-cell microscopy. The fraction of cells responding with a first pulse (**D**) and the total number of pulses observed within 48h (**E**) were calculated. The number of cells analyzed per condition as well as the threshold used for pulse analysis can be found in Table 7.4.1 and Table 7.4.2.

If the initial ATM input determines the total number of pulses, limiting the ATM input should consequently also limit the total number of pulses, even if the features of the pulses stay the same (Figure 3.7.4C). Again, a small molecule inhibitor was used and added to the cells at

different time points shortly after IR. For all chosen time points, almost all the cells initiated the p53 response (Figure 3.7.4D). Limiting the ATM input to 15 min clearly decreased the total number of pulses (Figure 3.7.4E and Supplementary Figure 7.5.3B). The longer the ATM input duration was, the more pulses were observed.

3.8 The transcriptional activity of p53 targets is gene-specific with changes between the first and the second pulse

My previous observations show that the immediate and sustained p53 response differ with regard to their underlying networks. What is the purpose of these different networks and are there differences in target gene expression during the immediate and sustained response? This chapter of my thesis has been conducted in collaboration with Dhana Friedrich and has already been published (Friedrich *et al.*, 2019). Contributions by Dhana Friedrich are marked in the respective sections.

Two representative targets were chosen: CDKN1A (involved in cell cycle arrest) and BAX (involved in apoptosis). In a first step, the transcription of these targets was measured via qRT-PCR. Both targets showed a clear reduction in the relative quantity after 16 h and 24 h when CHK2 was inhibited, showing that a single ATM-induced pulse is not sufficient to maintain full target gene expression (Figure 3.8.1).

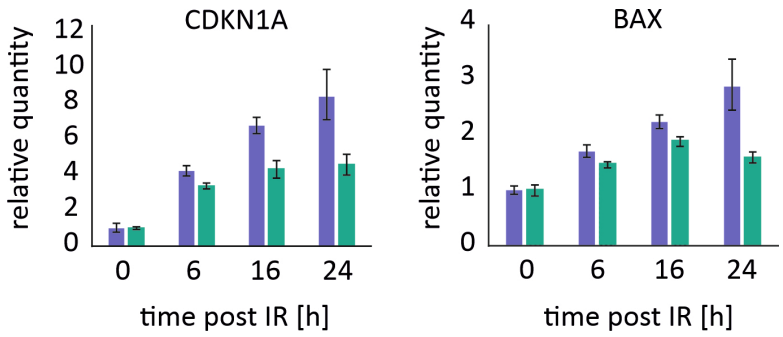

Figure 3.8.1: CHK2 inhibition causes a reduced induction of target gene expression.

A. A549 WT cells were treated with DMSO or CHK2 inhibitor 1 h prior to 5 Gy irradiation (IR) and harvested at indicated time points. Levels of CDKN1A and BAX mRNA were measured via qRT-PCR. The ΔΔCt method was used to calculate relative gene expression, β-Actin was used as a housekeeping gene for the calculation of ΔCt. Error bars represent the RQmin and RQmax values obtained with three technical replicates.

To get a better understanding of the differences in target gene expression for the immediate and the sustained response, we took a closer look at transcription comparing the first and the second pulse. Target gene mRNAs were quantified at four time points representing basal conditions (undamaged), 3 h post IR (peak of 1st pulse), 6 h (trough after 1st pulse) and 9 h (peak of 2nd pulse). Using smFISH, it could be shown that BAX and CDKN1A had a similar fold change (fc) of

expression during the first pulse, however, the later time points showed different patterns of transcription (Figure 3.8.2A and C). While CDKN1A showed a decrease in the number of RNA/cell, for BAX the number of RNA/cell was constantly increasing.

The transcription of a certain target can be either continuous or burst-like. In case of the latter, gene expression transitions between transcriptionally inactive and active states (Nicolas, Phillips and Naef, 2017). In this case, the number of RNA/cell can be influenced by different parameters: The promoter can be active more frequently, for a longer period or show a higher rate of transcription while it is active (Raj *et al.*, 2006; Lionnet and Singer, 2012). Using dual-color labeling of introns and exons by smFISH combined with mathematical modeling, transcription rates, promoter states and mRNA lifetime can be determined (Bahar Halpern *et al.*, 2015).

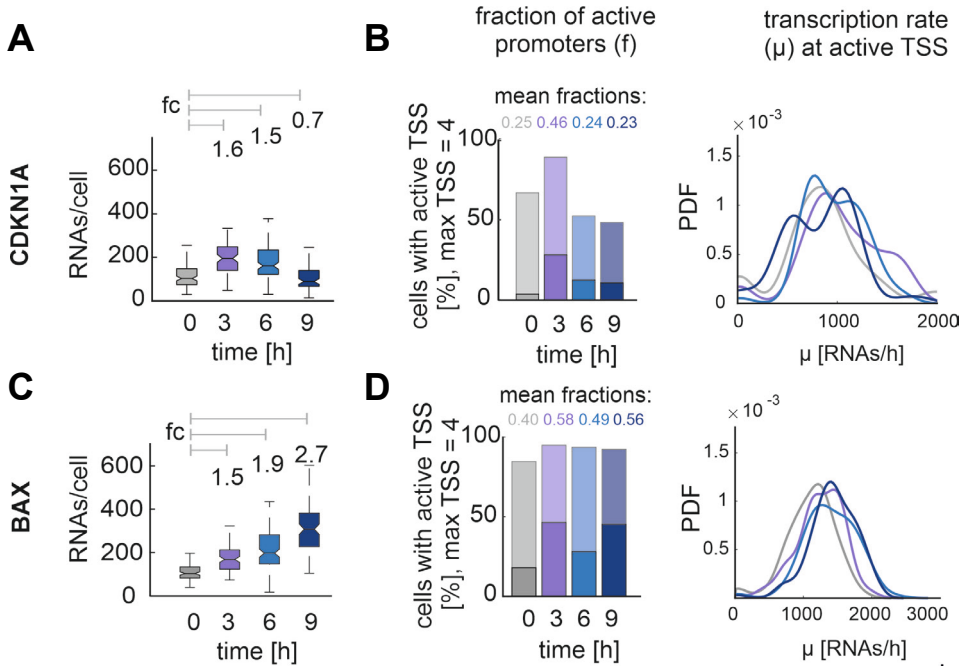

Figure 3.8.2: Targets show gene-specific patterns of expression in response to DNA damage (data from Dhana Friedrich).

A. A549 WT cells were irradiated with 10 Gy and RNA/cell for the target CDKN1A were quantified using smFISH. fc: median fold change of induction relative to basal values. **B.** The fraction of active promoters (f, left panel) and the transcription rate (μ, right panel) at active transcription start site (TSS) were calculated based on data obtained via smFISH for the target CDKN1A. Left panel: Solid colors indicate strong TSS activity (> 75% of TSS active), shaded colors show partial TSS activity (minimum one, but less than 75% of TSS active). The mean fraction of active promoters gives the ratio of all active TSS to the total number of genomic loci. Right panel: Distribution of transcription rate at active TSS as probability density estimate (PDF). **C.** A549 cells were irradiated with 10 Gy and RNAs per cell for the target BAX were quantified using smFISH. **D.** The fraction of active promoters (f, left panel) and the transcription rate (μ, right panel) at active transcription start site (TSS) were calculated based on data obtained via smFISH for the target BAX. Left panel: Solid colors indicate strong TSS activity (> 75% of TSS active), shaded colors show partial TSS activity (minimum one, but less than 75% of TSS active). The mean fraction of active promoters gives the ratio of all active TSS to the total number of genomic loci. Right panel: Distribution of transcription rate at active TSS as probability density estimate (PDF).

While the transcription rate (proxy for burst size) did not exhibit major changes, the fraction of active promoters (proxy for frequency of target gene promoter activation) increased for both targets in response to IR (Figure 3.8.2B and D). However, while CDKN1A showed a decrease at 6 and 9 h, for BAX the fraction of active promoters stayed high. According to their specific pattern of stochastic gene expression, the targets were grouped into different archetypes of expression with CDKN1A showing transient expression and BAX showing sustained expression (Figure 3.8.3A). Can the changes in gene expression be explained by different temporal changes in p53 binding to the promoters of the respective targets? Chromatin Immunoprecipitation (ChIP) experiments showed an increase in promoter binding for both targets in response to IR (Figure 3.8.3B). However, after 6 h levels decreased to intermediate levels and stayed at these levels until 9 h even though total p53 levels were increasing. No gene-specific differences in the promoter binding were determined.

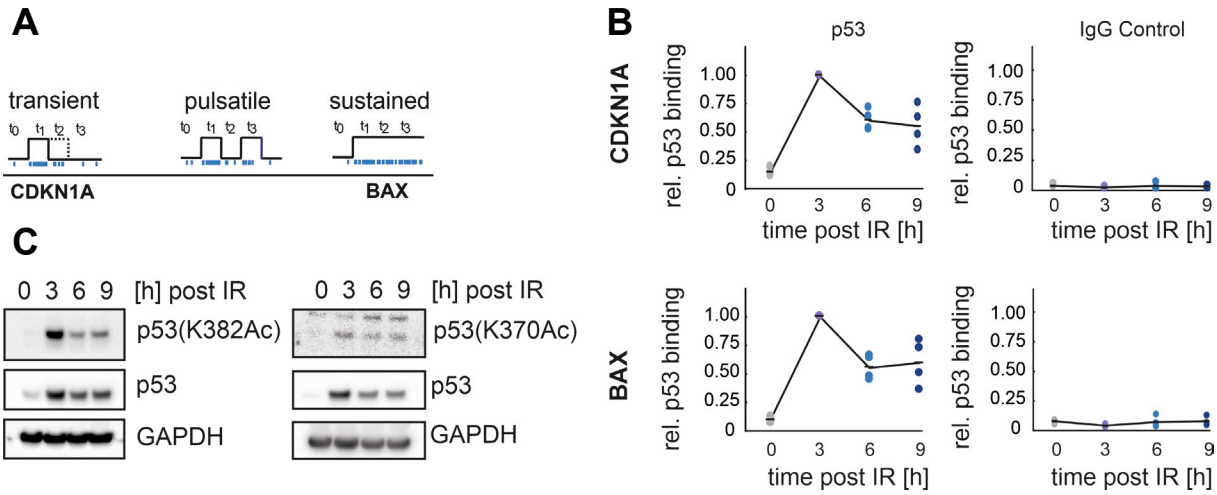

Figure 3.8.3: Fraction of acetylated p53 decreases between the first and the second pulse.

A. Targets were sorted according to their promoter activity into three archetypes of expression patterns. **B.** Binding of p53 to the promoter of CDKN1 and BAX. The percentage of the input was calculated and normalized to the 3 h time point. Individual measurements of 4 biological replicates are given as dots; mean values are shown as lines. **C.** A549 cells were irradiated with 10 Gy and harvested at indicated time points. The levels of p53(K382Ac) (left panel), p53(K370Ac) (right panel) and total p53 were measured via western blotting. GAPDH was used as a loading control.

We can conclude that the transcriptional activity is gene-specific with changes between the immediate response (first pulse) and the sustained response (second pulse). How can gene-specific target gene promoter activity be achieved despite uniform p53 dynamics? P53 is acetylated on several residues in the C-terminus including K370 and K382. Acetylation of p53 on these residues has been connected with transcriptional activation, while methylation had an inhibitory effect on transcription (see section 1.5.2). Do changes in the acetylation state explain differential expression of target genes during the first versus the second pulse? In response to IR, an increase both in the total p53 levels and in levels of acetylated p53 can be observed

(Figure 3.8.3C). However, while we see a clear increase at 3 h, no second increase in acetylation corresponding to the second total p53 pulse at 9 h can be found.

Previous studies associated a change of the dynamics of p53 with altered target gene expression and cell fate (see section 1.4). Therefore, we modulated the dynamics of p53 to determine how this would change stochastic transcription (Figure 3.8.4A).

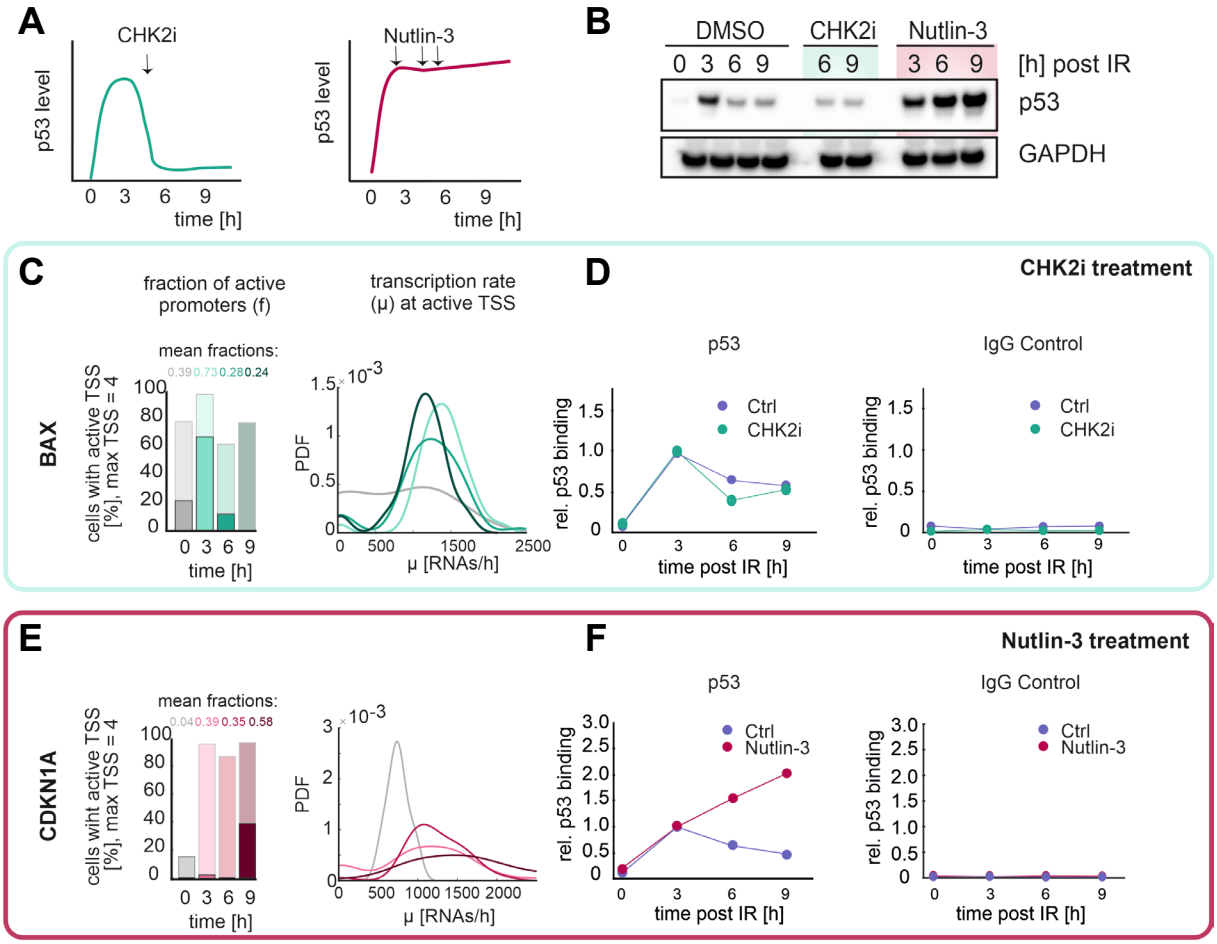

Figure 3.8.4: Patterns of expression in response to DNA damage upon modulation of p53 dynamics (smFISH data by Dhana Friedrich).

A. Treatment with CHK2 inhibitor impairs the sustained p53 response and induces transient dynamics. In contrast, sequential treatment with Nutlin-3 converts the dynamics to sustained high levels of p53. **B.** A549 WT cells were irradiated with 10 Gy, treated with CHK2i or Nutlin-3 and harvested at indicated time points. The levels of total p53 were measured via western blotting. GAPDH was used as a loading control. **C-F.** A549 WT cells were treated with a CHK2 inhibitor to induce transient p53 dynamics (**C-D**) or were sequentially treated with Nutlin-3 to induce sustained high p53 levels (**E-F**). The fraction of active promoters (f, **C** and **E** left panel) and the transcription rate (μ, **C** and **E** right panel) at active transcription start site (TSS) were calculated based on data obtained via smFISH for the target BAX. Left panel: Solid colors indicate strong TSS activity (> 75% of TSS active), shaded colors show partial TSS activity (minimum one, but less than 75% of TSS active). The mean fraction of active promoters gives the ratio of all active TSS to the total number of genomic loci. Right panel: Distribution of transcription rate at active TSS as probability density estimate (PDF). The Binding of p53 to the promoter of BAX in control cells and upon CHK2i treatment is shown in (**D**) and (**F**). The percentage of the input was calculated and normalized to the 3 h time point.

Firstly, we suppressed the sustained response using the CHK2 inhibitor. Secondly, we stabilized p53 at peak levels using the MDM2 inhibitor Nutlin-3 leading to sustained high levels of p53 (Figure 3.8.4A and B). Additionally, treatment with Nutlin-3 might preserve PTM modifications that were present during the first pulse. Upon suppression of the sustained p53 response, BAX, which was grouped as a sustained responder, showed a decrease in burst frequency from 56% at 9h to 24% (Figure 3.8.4C and Figure 3.8.2D). Interestingly, the level of promoter binding did not show major changes (Figure 3.8.4D) despite strongly decreased total p53 levels. Based on these observations we can conclude that the second pulse is needed to keep BAX transcription active after the first pulse. Upon Nutlin-3 treatment, CDKN1A, grouped as a transient responder, showed an increase in burst frequency from 23% at 9 h to 58% (Figure 3.8.4E and Figure 3.8.2B). Additionally, the promoter binding was increased under these conditions (Figure 3.8.4F).

3.9 C-terminal acetylation state of p53 mediates gene-specific regulation of transcriptional activity

Control cells showed higher level of acetylated p53 during the immediate p53 response compared to the sustained response (Figure 3.8.3C). To determine whether modulation of p53 dynamics was associated with alteration of its PTM, we took a closer look at the acetylation state of p53 after CHK2i and Nutlin-3 treatment. We observed low levels of acetylation after CHK2i and strongly increased levels of acetylation after Nutlin-3 addition (Figure 3.9.1A and B). This increase in acetylation might facilitate the expression of otherwise transiently expressed genes like CDKN1A.

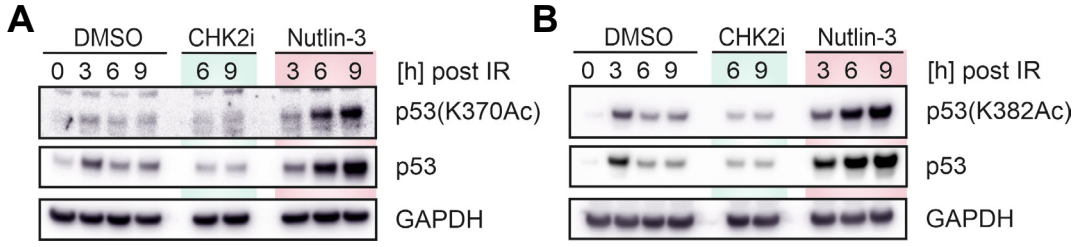

Figure 3.9.1: Nutlin-3 treatment leads to increased levels of acetylated p53.

A-B. A549 WT cells were treated with a CHK2 inhibitor to induce transient p53 dynamics or Nutlin-3 to induce sustained high p53 levels. Cells were irradiated with 10 Gy and harvested at indicated time points. The levels of p53(K370Ac) (**A**), p53(K382Ac) (**B**) and total p53 were measured via western blotting. GAPDH was used as a loading control.

To decrease inhibitory methylation and to increase acetylation while keeping the dynamics of p53 pulsatile, we used an shRNA to reduce the RNA levels of the methyl-transferases SMYD2 and

SET8 to 22% and 20% (for details see Friedrich *et al.*, 2019). Depletion of SMYD2 and SET8 led to an increase in acetylation at K370 (SMYD2 KD) and K382 (SET8 KD) (Figure 3.9.2A and B).

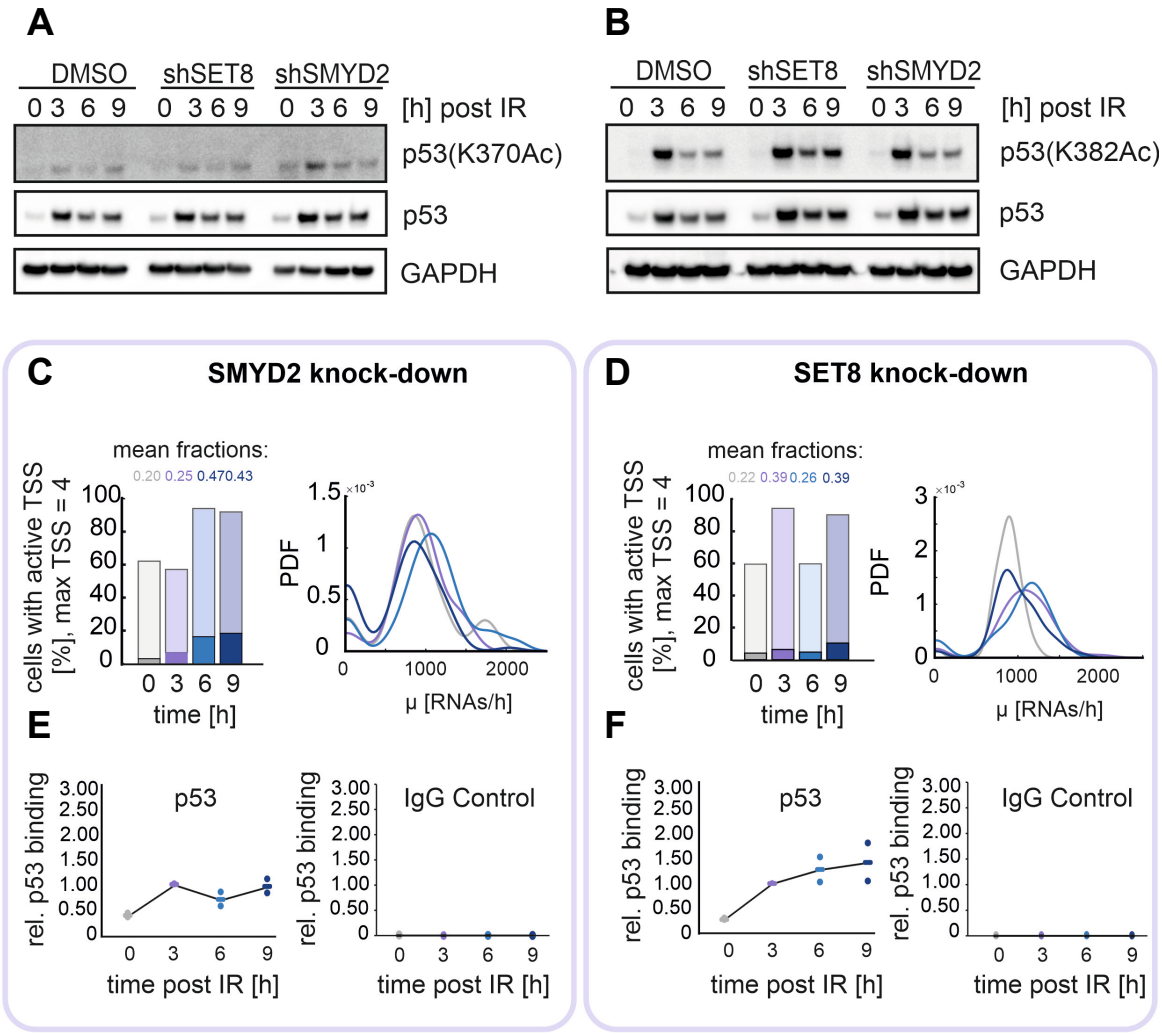

Figure 3.9.2: Switch between acetylation and methylation modulates the transcription of transiently expressed targets (smFISH data by Dhana Friedrich).

A-B. A549 WT, SMYD2 and SET8 knockdown cells were irradiated with 10 Gy and harvested at indicated time points. The levels of p53(K370Ac) (**A**), p53(K382Ac) (**B**) and total p53 were measured via western blotting. GAPDH was used as a loading control. **C-D.** SMYD2 and SET8 knockdown cells were irradiated with 10 Gy. The fraction of active promoters (f, left panel) and the transcription rate (μ, right panel) at active transcription start site (TSS) were calculated based on data obtained via smFISH for the target CDKN1A in SMYD2 knockdown (**C**) and SET8 knockdown cells (**D**). Left panel: Solid colors indicate strong TSS activity (> 75% of TSS active), shaded colors show partial TSS activity (minimum one, but less than 75% of TSS active). The mean fraction of active promoters gives the ratio of all active TSS to the total number of genomic loci. Right panel: Distribution of transcription rate at active TSS as probability density estimate (PDF). **E-F.** Binding of p53 to the promoter of CDKN1A in SMYD2 knockdown (**E**) and SET8 knockdown cells (**F**). The percentage of the input was calculated and normalized to the 3h time point. Individual measurements of 2 biological replicates are given as dots; mean values are shown as lines.

To see whether this change in the modification state of p53 alters the transient CDKN1A gene expression, we again determined burst frequency and burst size. While both values did not show major changes under basal conditions and after 3h, the frequency of active promoters was

increased after 9 h from 23% to 43% after SMYD2 depletion and from 23% to 39% after SET8 depletion compared to wild-type cells (Figure 3.9.2C and D and Figure 3.8.2B). Additionally, an increase in promoter binding was observed at 6 h and 9 h (Figure 3.9.2E and F). Together these results indicate that methylation via SMYD2 and SET8 might contribute to gene-specific changes in the expression profiles between the first and the second pulse.

4 DISCUSSION

4 DISCUSSION

In response to DNA DSB, p53 exhibits a series of pulses of accumulation in the nucleus. Based on experimental data as well as mathematical modeling, previous studies suggested that all of these pulses are triggered by the same underlying mechanism: The MRN complex senses the DNA DSB, promotes activation of ATM which in turn fosters its own activation by a feed-forward loop and stabilizes p53. In these studies, it was assumed that already low degrees of damage trigger full activation of ATM (Kastan and Bakkenist, 2003). Consequently, even though the number of breaks is decreasing due to repair throughout the DNA damage response, p53 pulses are induced with full amplitude and duration. Based on this mechanism, many subsequent studies focused their research on the first pulse and assumed similar mechanisms for the sustained response. However, across different cell lines, broad variation in the ATM activity was observed with some cell lines showing a dose-dependent increase in the levels of active ATM (Gately *et al.*, 1998; Buscemi *et al.*, 2004; Bhoumik *et al.*, 2005; Xue *et al.*, 2009; Stewart-Ornstein and Lahav, 2017). Together with the rapidly changing state of the genome, these observations cast doubt on whether the current hypothesis of recurrent activation of ATM is sufficient to explain the induction of sustained, undamped oscillations. Therefore, in my thesis, I investigated the mechanisms behind the immediate p53 response to acute damage and the sustained response to persisting damage.

4.1 Two interconnected networks drive the acute and the sustained p53 response

To investigate the characteristics of acute damage in the p53 response and how new breaks perturb the p53 dynamics, I repeatedly challenged the cells with acute DSB using NCS. I could show that new damage leads to immediate reactivation of ATM which is directly reflected in the p53 dynamics: Depending on the time of re-damaging, the p53 levels responded with an increased amplitude of the respective pulse (re-damaging before the peak) or with an immediate re-accumulation of p53 (re-damaging after the peak) (Figure 3.1.1). The latter was especially surprising as the levels of the negative regulators are high at this point of the response. However, based on my data it seems like reactivation of ATM due to newly sensed breaks can mediate p53 stabilization despite high WIP1 and MDM2 levels. In line with this observation, previous studies have shown that the first p53 pulse can be triggered despite overexpression of WIP1 (Batchelor *et al.*, 2008; Mönke *et al.*, 2017). Still, the precise interplay of negative and positive players upon re-damaging remains to be elucidated. For instance, it would be crucial to understand via which mechanism reactivation of ATM facilitates the accumulation of p53. This would require a detailed analysis of protein levels of the negative regulators MDM2 and WIP1.

Interestingly, the amplitude of the first pulse varied upon different damage doses, while the amplitude of the second pulse was fixed (Figure 3.1.1B). Only the detection of new breaks altered the amplitude of the second pulse, which already hinted towards differential regulation of the first pulse compared to the following pulses. Indeed, further investigations on the role of ATM in the course of the response showed that ATM is crucial to initially trigger the p53 response. However, continuous ATM activity was dispensable to sustain the oscillations. In line with this finding, I only observed one pulse of ATM activity upon 5 Gy IR corresponding to the first p53 pulse. Additionally, I found an increase in ATM activity upon increase of the damage strength (Figure 3.7.4A), which might explain the dose-dependent variation in the amplitude of the first pulse I detected. However, if variations in the levels of ATM activity result in altered amplitudes of the p53 pulses, then very low levels of active ATM, as I detected via western blotting, are unlikely to drive undamped p53 oscillations for several more hours. Still, western blotting is a relatively insensitive method not providing any detail on single-cell level not to mention information on the past and the future of a specific cell. In this context, a live cell reporter could provide details on the kinetics of ATM activity in single cells and would allow a final correlation between ATM activity and the probability to trigger a p53 pulse (Johnson, You and Hunter, 2007; Jaiswal *et al.*, 2017; Nyati *et al.*, 2018). In contrast to the observations in A549 cells, MCF7 cells were reported to show two pulses of ATM activity (Batchelor *et al.*, 2008). This might be rooted in the higher damage dose used between the experiments (5 Gy vs. 10 Gy). However, cell line-specific differences in the levels of active ATM and/or WIP1, as well as the respective DNA-repair efficiency, might also influence the number of pulses of ATM activity post IR. In this context, a study comparing p53 dynamics in different cell lines showed varying levels of active ATM and different repair proficiencies comparing A549 and MCF7 cells (Stewart-Ornstein and Lahav, 2017).

As ATM activity was not crucial for sustaining the p53 response, I examined whether another kinase replaces ATM in the course of the p53 response. Eventually, I could determine the kinase crucial for sustaining the p53 response as the checkpoint kinase CHK2. Both, inhibitor treatment or depletion using an siRNA did not alter the first pulse but led to a strongly impaired sustained p53 response. For the immediate p53 response it was suggested that the rapid, switch-like activation of ATM and the fast degradation of MDM2 convey excitability for the first pulse. Experimentally, this could be shown by addition of the PIKK-inhibitor wortmannin 1h post IR. The resulting transient input by ATM still triggered a full p53 pulse (Batchelor *et al.*, 2008, 2011). Similarly, I could show for the sustained response that a transient CHK2 input was enough to drive a full second pulse with normal timing, duration and amplitude. Accordingly, also the sustained p53 response arises from an excitable mechanism. Based on these results I

can conclude that the immediate response to acute damage depends on the activity of ATM while the sustained response is mediated via CHK2 independent of ATM (Figure 4.1.1). It would be interesting to test whether CHK2 - activated independently of ATM as for instance via mutation of inhibitory residues- would show oscillations of p53 in the absence of damage or if the initial induction of oscillations essentially needs activation via ATM.

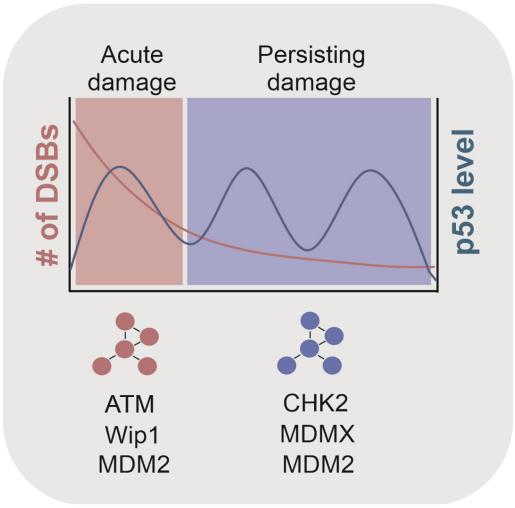

Figure 4.1.1: The p53 response is mediated by two interconnected networks.

The immediate response to acute damage is mediated by ATM. The sustained response to persisting damage is mediated by CHK2.

In addition to CHK2, I also tested, whether ATR or DNA-PK, which belong to the same kinase family as ATM, contribute to sustaining p53 response. However, neither inhibition of ATR or DNA-PK alone nor combined with inhibition of ATM impaired the sustained p53 response. The contribution of ATR is limited to S/G2-phase cells as only in these cell cycle phases the necessary sister chromatid for HR is present. Still, even in G2 cells only 20–30% of the breaks induced upon 2 Gy IR show RAD51 foci indicating repair via HR (Beucher *et al.*, 2009; Shibata *et al.*, 2011). Consequently, it is not surprising that no major contribution of ATR was detected in a set-up where the response of cells in different cell cycle phases was averaged. Moreover, considering CHK2's important role in sustaining the p53 response, it is likely that the contribution of ATR to the p53 response is concealed by the dominating input via CHK2. Specific inhibition of ATR in S/G2-phase cells also in combination with CHK2 inhibition might provide a better understanding of the contribution of ATR to the p53 response upon IR. One possible hint can be found in the p53 response in G1 vs G2/S-phase cells upon combined inhibition of ATM and CHK2. Inhibition of both kinases led in G1-phase cells to an almost complete abolishment of sustained p53 oscillations. In contrast, G2/S-phase cells still exhibited residual dynamical though not regular pulsatile behavior (Figure 3.3.5). This may reflect a contribution of ATR. Regarding the role of DNA-PKcs, previous studies support a minor contribution to the

stabilization of p53 as even in the absence of DNA-PKcs activity, the p53 response remained intact and showed normal activation of target gene expression and cell cycle arrest (Jimenez *et al.*, 1999).

The surprising role of CHK2 in regulating the sustained p53 response contradicted currently postulated models of the network (Batchelor *et al.*, 2008; Mönke *et al.*, 2017). As in these models, the main driver of p53 accumulation was ATM, inhibition of the kinase at any time during the response was predicted to terminate p53 oscillations. Additionally, the models relied on upstream signals showing pulsatile dynamics due to the Wip1-mediated negative feedback. In contrast, the kinase activity of CHK2 appeared rather constant and not pulsatile over the course of the response in my experimental data. To explore which network architectures could give rise to pulsatile dynamics despite continuous input from the upstream signaling, we designed a new model in cooperation with Raphael Löffler, Isabella Mendler and Barbara Drossel (TU Darmstadt). In the newly suggested model, immediate and sustained p53 dynamics are induced by interaction of different network players. The first pulse is triggered via ATM: The kinase is rapidly activated via the mechanisms described in section 1.2 and influences the negative feedback between p53 and MDM2 by degrading MDM2 and stabilizing p53. The contribution of ATM is counteracted by the second negative feedback involving WIP1. Sustained p53 oscillations are generated via the p53-MDM2-negative feedback loop regulated by CHK2. To prevent variations in the amplitude of the pulses upon variation of the input signal, CHK2's activity is modeled as a bistable switch. When no breaks are sensed by the cell, CHK2 activity is switched off. Upon detection of DSB, CHK2 is switched on by ATM and once activated is independent of ATM. Consequently, CHK2 activity stays high and p53 oscillations continue despite decreasing ATM activity. All in all, with this model we were able to show that sustained p53 oscillations can be generated by a constant CHK2 input independent of continuous ATM activity. Nevertheless, the model as shown in this thesis had some limitations and was not able to describe all experimental observations. For instance, the modeling of the CHK2 activity as a bistable switch has some drawbacks. On western blot level, I observed a continuous decrease over time. This can have two reasons: On the one hand, averaging the response of a population of cells showing discrete activity levels could lead to these kinetics. On the other hand, CHK2 may show a gradual decrease on single-cell level, which would contradict the suggested bistability. Furthermore, data by Buscemi *et al.* indicates that the maximal levels of CHK2 activity might depend on the degree of damage (Buscemi *et al.*, 2004). This would lead to dose-dependent changes in the amplitude of the sustained response. Furthermore, I observed excitability for all pulses including the sustained response. In the current model, inhibition of ATM and CHK2 shortly after the pulse was generated leads to a decrease in the amplitude. To reconcile the model with these

experimental observations, the delayed negative feedback between MDM2 and p53 was supplemented with a positive feedback on p53 via the process of ubiquitination and deubiquitination, thereby introducing another source of bistability into the system (Löffler, 2021). This model was able to reproduce excitatory dynamics as experimentally observed and could generate oscillations with a fixed amplitude even upon low degrees of damage or decreasing CHK2 input.

4.2 How does CHK2 control the p53-MDM2 feedback?

The feedback between p53 and MDM2 can be influenced by two mechanisms: stabilization of p53 and/or destabilization of MDM2. According to our model, both options are possible. To stabilize p53, the interaction with its negative regulator MDM2 has to be disturbed, for instance by phosphorylating residues in TAD, the domain that interacts with MDM2. Early studies in U-2 OS cells reported that CHK2 phosphorylates p53 on S20 (Chehab *et al.*, 1999). However, I could not find any reduction of S20 levels upon CHK2 inhibition. The literature regarding CHK2 mediated phosphorylation of S20 is conflicting. In accordance with my results, previous studies already indicated that S20 phosphorylation stays intact despite CHK2 depletion (Ahn, Urist and Prives, 2003; Jallepalli *et al.*, 2003). In addition to S20, CHK2 has also been associated with the modification of T18, a residue located in the TAD as well (Shieh *et al.*, 2000). Phosphorylation of T18 was suggested to play an important role in regulating the binding between p53 and MDM2 and was proposed to act as an 'on-off' switch (Sakaguchi *et al.*, 2000; Teufel, Bycroft and Fersht, 2009; Gu and Zhu, 2012). Additionally, T18 fosters binding of p300 (Teufel, Bycroft and Fersht, 2009). Yet, details are missing about the relationship between phosphorylation of T18 and CHK2 and further investigations are needed to determine the connection between T18 modification and CHK2 as well as the kinetics of phosphorylation.

Regarding a destabilizing effect of CHK2 on MDM2, no direct modification of the E3 ubiquitin ligase mediated by CHK2 was reported so far. Still, CHK2 modifies and destabilizes MDMX. MDMX, in turn, was shown to interact with MDM2 thereby enhancing its stability and ligase activity. Consequently, MDMX destabilization also destabilizes MDM2. In response to IR, CHK2 mediates phosphorylation of MDMX on S367 which promotes its degradation and consequently results in a decrease of cellular MDMX levels (Chen *et al.*, 2005). In line, I could show that CHK2 inhibition leads to the stabilization of MDMX even in the presence of genotoxic stress. In contrast, ATM inhibition after IR still allowed degradation of MDMX post IR. Opposed to this finding, previous studies indicated that ATM-deficient cells failed to mediate IR-dependent degradation of MDMX (Chen *et al.*, 2005). Still, mutation of S403, the residue that is

phosphorylated by ATM, only had minor effects on polyubiquitination and degradation of MDMX compared to mutation of S367 which is uniquely modified by CHK2. This indicates that here again ATM and CHK2 may have time-varying contributions and the effects observed after ATM depletion might reflect impaired CHK2 activation.

The stabilization of MDMX most likely contributed to the prolonged MDM2 accumulation I observed upon CHK2 inhibition (Figure 3.6.1). Additionally, MDMX is necessary for complete induction of the MDM2 promoter (Biderman *et al.*, 2012). Enhanced MDMX levels could therefore facilitate transcriptional activation of MDM2. To differentiate between these two possibilities, an increase of mRNA levels assessed via qRT-PCR could indicate regulation on transcription level. Supporting the role of MDMX in the sustained response, recent studies have shown that overexpression of MDMX induced p53 dynamics similar to CHK2i: The first pulse remains unchanged with normal features, while the sustained response was strongly impaired showing that MDMX overexpression alone was able to suppress p53 oscillations (Chen, Forrester and Lahav, 2016). Moreover, MDMX depletion led to sustained oscillations upon UV radiation or in response to a post-mitotic pulse (Heltberg *et al.*, 2019). Together these results indicate an important role of MDMX for sustaining p53 oscillations and consequently, a stronger role of destabilization of MDM2 compared to direct stabilization of p53 via phosphorylation of its TAD. In line, many studies suggested that N-terminal phosphorylations of p53 provide no major contribution to the accumulation of p53: Mutation of the residues analog to S15 and S20 in mice did not impair p53 accumulation or show any severe defects and hence, it was concluded that p53 accumulation is mainly facilitated via anti-repression of MDM2/MDMX (Kruse and Gu, 2009). Mutations of the respective residues via the CRISPR/Cas-system might allow further insights into the role of TAD phosphorylations on the stabilization of p53 and the resulting dynamics.

Putting all my observations in a nutshell, I propose that the p53 dynamics in response to IR are induced by the following mechanism: ATM initially stabilizes p53 and destabilizes MDM2 mediating the first pulse of p53 accumulation (Figure 4.2.1). Additionally, ATM activates CHK2. Increasing levels of WIP1 facilitate the dephosphorylation of ATM and its targets thereby limiting ATM's influence on the first pulse. In combination with increased levels of MDM2 due to transcriptional activation via p53, this leads to a decrease of p53 levels in the cell.

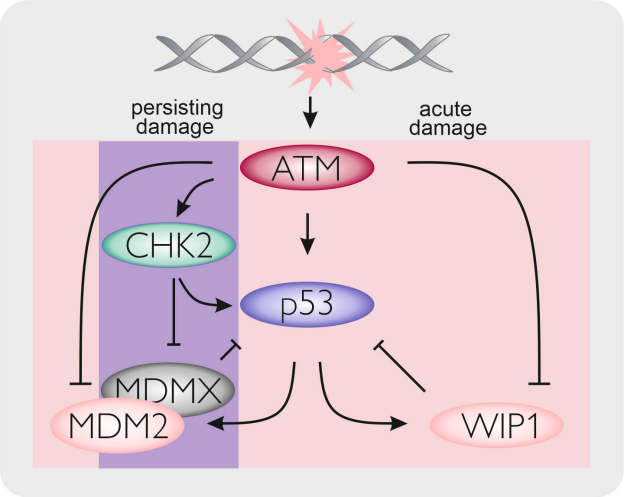

Figure 4.2.1: Schematic overview of the proposed p53 network in response to IR.

Upon detection of new breaks (acute damage), the kinase ATM activates CHK2 and mediates the stabilization of p53 and destabilization of MDM2. P53 can then induce the expression of its target genes including the negative regulators WIP1 and MDM2. WIP1 dephosphorylates p53 and ATM limiting the role of ATM to the immediate response. CHK2 can phosphorylate p53 and the negative regulator MDMX, thereby stabilizing p53 and destabilizing MDM2.

Active CHK2 is independent of sustained ATM activity and destabilizes MDMX. Thereby, CHK2 also destabilizes MDM2 leading to oscillations of p53. When CHK2 is inactivated, MDMX levels increase and p53 oscillations stop. To verify that MDMX levels determine whether a subsequent p53 pulse can be triggered, further experiments that correlate the probability to induce a pulse with cellular MDMX levels are necessary. Additionally, mutation of S367 to alanine should impair degradation and consequently, expression of the respective mutant should lead to similar dynamics as CHK2 inhibition.

4.3 Which factors control the CHK2 activity in response to IR?

As the main factor regulating MDMX levels in response to IR, the duration of CHK2 activity determines how long p53 oscillations continue. Thus, it is important to understand how the cellular CHK2 activity is controlled. In my thesis, I could show that CHK2 activity relies on activation via ATM. Remarkably, no sustained ATM activity was needed to maintain CHK2's activity. Moreover, I observed a prolonged CHK2 activity with increasing doses (Figure 3.4.1), which in turn would allow sustaining the p53 oscillations for a longer time period. This could explain the correlation between the degree of damage and the total number of p53 pulses that was observed here in this thesis and previous studies. But if not by ATM, how is the duration of CHK2 activation controlled and is there a connection to the repair status of the cell?

One way to modulate the activity of CHK2 are distinct time-dependent phosphorylations of residues in the kinase domain which also control the localization of the kinase (Guo *et al.*, 2010). Phosphorylation of T383 in the T-loop mediates recruitment to the chromatin. Subsequent

phosphorylation of T389 has an inhibitory effect on the kinase and is required for T387 phosphorylation. Eventually, phosphorylation on all three residues (T383, T389, T387) facilitates chromatin egress. This change in localization from damage site to nucleoplasm might provide an additional layer of regulation and allow modification of targets that are not concentrated at the break site. Moreover, phosphorylation on Y390 is decreased in response to damage and might serve as a signal for the inactivation of CHK2. Interestingly, Y390 mutation was found in high-risk breast cancer patients and was associated with impaired p21 expression (Wang *et al.*, 2015). Additionally, phosphorylation of residues in the FHA might mediate the inactivation of CHK2: PLK1 phosphorylates CHK2 in this domain which was suggested to impair dimerization and kinase activity (Vugt *et al.*, 2010). Interestingly, PLK1 activity itself is regulated by ATM (Jaiswal *et al.*, 2017). Initial experiments using a PLK1/PLK3 inhibitor, however, did not show any effect on the sustained p53 response (data not shown).

Another possibility would be a third protein besides ATM that maintains CHK2 activity. The previous experiments shown in this thesis could neither prove nor exclude this possibility. The observed reactivation of CHK2 even in the absence of ATM activity hints towards the possibility of an ATM-independent CHK2 activation when the DNA damage response has started. However, the levels of reactivated CHK2 were clearly smaller compared to reactivation in the presence of ATM activity (Figure 3.7.1). To exclude that CHK2 simply maintains an active conformation, active CHK2 has to be detected in the pool of newly synthesized protein that never existed in the presence of ATM activity. In this context, nascent proteins can be labeled using the methionine surrogate AHA (L-Azidohomoalanine) in combination with click chemistry (Landgraf *et al.*, 2014). Simultaneous inhibition of ATM allows determining whether CHK2 can be activated *de novo* in the absence of ATM activity by third protein. If a third protein is involved in the reactivation of CHK2, which kinase would be good candidates? A recent study could exclude that ATR or DNA-PKcs are involved in preserving CHK2 activity in G1 arrested cells (García-santisteban *et al.*, 2021). For another promising candidate, polo-like kinase 3 (PLK3) which was reported to phosphorylate CHK2 and to promote its activation, I did not observe any effect on the sustained p53 response upon inhibition of PLK3 (data not shown) (Bahassi *et al.*, 2002, 2006). An siRNA screen would be a more systematic possibility to identify proteins that both, modify CHK2 and alter the sustained p53 response.

Besides activating or inhibitory phosphorylations, CHK2's activity might also be regulated by dephosphorylation. WIP1 dephosphorylates T68 of CHK2, however, it does not remove autophosphorylations in the T-loop like pT387 (Fujimoto *et al.*, 2006; Fuku *et al.*, 2007; Oliva-Trastoy *et al.*, 2007). Remarkably, reduction of pT68 to 10% still showed 80% of the CHK2

activity and intact T387 phosphorylation (Oliva-Trastoy *et al.*, 2007). In line, I could show that CHK2 is significantly contributing to sustained p53 oscillations even in the absence of ATM activity or phosphorylation on T68. Moreover, it was shown that CHK2 can phosphorylate CDC25 irrespective of its T68 phosphorylation status (Ahn and Prives, 2002). Based on these studies and my data, one can conclude that loss of T68 phosphorylation does not lead to a loss of CHK2 activity. Another phosphatase that was shown to interact with CHK2 is PP2A. PP2A consists of 3 subunits: The scaffold subunit A , a catalytic C subunit and a regulatory B subunit, while the B subunit determines its substrate specificity (Virshup and Shenolikar, 2009; Freeman *et al.*, 2010; Seshacharyulu *et al.*, 2013). There are four major families: B, B', B'', B''' with each family having several sub members. PP2A B'α and other B' family members bind to CHK2 (Dozier *et al.*, 2004; Freeman *et al.*, 2010). In response to DNA damage, PP2A and CHK2 dissociate in a dose and ATM-dependent manner (Freeman *et al.*, 2010). This dissociation allows CHK2 to be activated. Interestingly, 4h post IR re-association of CHK2 and PP2A is observed which correlates with the dephosphorylation of the SQ/TQ cluster. This reassociation could mediate a gradual inactivation of CHK2 as observed on western blot level: As long as ATM is active in the cell, CHK2 does not associate with PP2A. When ATM is inactivated, CHK2 and PP2A associate leading to the inactivation of CHK2. The strength and duration of ATM activity would determine how long CHK2 is active and encode the degree of damage, comparable to a timer that is set at the beginning of the response ('timer-hypothesis'). It has to be noted, that in the case of the 'timer-hypothesis', the duration of p53 would not be directly linked to the repair status of the genome. I could show that upon different doses the strength of the ATM activity differs. Moreover, timely limiting the ATM input also led to a decrease in the number of pulses suggesting that the initial strength and/or duration of the ATM input determine how long p53 oscillates (Figure 3.7.4). However, I showed variation of the duration of CHK2 activity only for two doses and a systematic assessment of CHK2's activity in response to different doses as well as to different input durations of ATM activity is needed to support the 'timer-hypothesis'. Early studies investigating the activation of CHK2 in response to different doses indicated that not only the duration of CHK2 activity might be altered by different doses but also the maximal levels of CHK2 activity depend on the degree of damage (Buscemi *et al.*, 2004, 2006). In this context, it might be interesting that higher degrees of damages are necessary to activate CHK2 compared to ATM (Buscemi *et al.*, 2004). While T68 was phosphorylated by ATM even upon 0.25 Gy, doses above 1 Gy were necessary to induce autophosphorylation of CHK2. Sufficiently high levels of active ATM might be necessary to counteract the basal levels of WIP1 (Mönke *et al.*, 2017). This might explain why no sustained pulses are observed upon low levels of damage. Moreover, phosphorylation of the SCD and autophosphorylation of the kinase domain happen on

different time scales: While the SCD is phosphorylated within minutes, phosphorylations of the kinase domain reach their highest levels around 1h post damage (Buscemi *et al.*, 2006).

4.4 The role of WIP1 in the p53 response

The phosphatase WIP1 is overexpressed and mutated in different types of cancer, for instance, medulloblastoma and breast tumors (Castellino *et al.*, 2008; Deng *et al.*, 2020). In the context of the p53 response, WIP1 dephosphorylates ATM-mediated phosphorylations on p53 and ATM itself (Lu, Nannenga and Donehower, 2005; Lu, Nguyen and Donehower, 2005; Shreeram *et al.*, 2006). I could show that WIP1 mediated inactivation limits the role of ATM to the first pulse, while depletion allows for a longer contribution of the kinase (Figure 3.3.6). In my experiments, WIP1 depletion did not alter the features of the dynamics, in line with a previous publication (Mönke *et al.*, 2017). However, earlier studies found an increase in the number of pulses upon WIP1 depletion. As WIP1 dephosphorylates T68 of CHK2 (Fujimoto *et al.*, 2006; Fuku *et al.*, 2007; Oliva-Trastoy *et al.*, 2007), WIP1 depletion might preserve to some extent modifications in the SCD. Thereby, the decrease in WIP1 levels could prolong the duration of CHK2 activity as also seen in previous studies (Fujimoto *et al.*, 2006). The significantly higher dose and intermediate knock-down efficiency in the experiment in this study might affect the extent of this effect. Further experiments are necessary to systematically address the relationship between WIP1 and CHK2 activity in the context of the p53 response. For instance, to support the 'timer-hypothesis' it would be crucial to determine how depletion or overexpression of the phosphatase impact pCHK2(T68) phosphorylation and how modulation of WIP1 levels affect the duration of CHK2 activity.

As my data indicates that WIP1 mainly controls the immediate response, intuitively, one would assume that overexpression of WIP1 also affects primarily the first pulse. In contrast, previous studies have shown that overexpression results in only one pulse and then strongly impairs the sustained response (Batchelor *et al.*, 2008; Mönke *et al.*, 2017), implying a role for WIP1 in the sustained response. However, a deeper look at the processes controlled by WIP1 sheds a different light on these observations. As mentioned before, WIP1 also contributes to the dephosphorylation of CHK2's SCD, though it does not dephosphorylate autophosphorylation sites like T387 (Fujimoto *et al.*, 2006; Oliva-Trastoy *et al.*, 2007). How can we then explain the effect of WIP1 overexpression on the p53 response? Studies have shown that WIP1 overexpression prevents phosphorylation on T68 and autophosphorylation on T387 or S516 even though autophosphorylation of ATM stays intact (Fujimoto *et al.*, 2006; Batchelor *et al.*, 2008). Consequently, these cells show the same dynamics as cells upon CHK2 inhibition or

depletion. While WIP1 seems to be able to effectively counteract ATM-mediated activation of CHK2, even high WIP1 levels seem not to be able to prevent the first ATM-mediated pulse. In accordance with this hypothesis, I could show in my re-damaging experiments that reactivation of ATM after the peak of p53 accumulation could induce an immediate re-accumulation despite high levels of the negative regulators. In this context, more recent studies suggest that ATM located in different compartments shows different kinetics of activity (Jaiswal *et al.*, 2017): ATM directly at the lesions is continuously active due to persisting damage. WIP1 activity seems not to be able to contain ATM activity directly at the break sites. However, active ATM that is spread over the undamaged chromatin distal to break sites can be inactivated via WIP1 before all lesions are repaired (Jaiswal *et al.*, 2017). This spatial separation allows uncoupling ATM's role in DNA repair and its role in other signaling pathways like the p53 response. As we can draw from these insights that the role of WIP1 might vary depending on the time of the response, it is crucial to study its impact on the p53 response in a timely controlled manner. As we are currently lacking suitable inhibitors to control the activity of the phosphatase at different times throughout the response, one possibility would be the timely regulated overexpression of WIP1 by coupling the protein to a degron system as SMASh- or mAID –tags (Kao *et al.*, 2015; Natsume and Kanemaki, 2017).

4.5 Change in upstream networks modulates target gene expression

To investigate the impact of these different regulatory networks, we took a closer look at target gene expression comparing the first and the second pulse. Remarkably, while the 1st pulse was accompanied by an increase in transcription for both the arrest-associated target CDKN1A and the pro-apoptotic target BAX, the patterns of transcription varied for the 2nd pulse. CDKN1A was only transiently expressed and showed a decrease in RNA numbers for the 2nd pulse despite high p53 levels (Figure 3.8.2). In contrast, BAX exhibited sustained transcription with RNA numbers being high even during the trough. To check whether these distinct patterns of transcription are mediated by different promoter binding to the respective targets, we performed ChIP experiments. However, we observed no gene-specific changes in promoter binding (Figure 3.8.3). Similar to our observations also other groups observed different patterns of transcription despite similar promoter binding (Joshua R. Porter, Fisher and Batchelor, 2016; Hafner *et al.*, 2017). They proposed that RNA and protein stability define the final expression patterns (Joshua R Porter, Fisher and Batchelor, 2016; Hafner *et al.*, 2017; Hanson, Porter and Batchelor, 2019). The data shown here additionally implies a strong contribution via stochastic bursting: In response to IR, target gene promoters are controlled by modulation of burst frequency. The indication that the transcription process itself is regulated target gene specifically while the

binding of p53 to its target promoters is uniform across different loci supports the so-called 'selective context model'. The model suggests that binding of p53 to its RE alone does not lead to changes in gene expression (Espinosa, 2008; Smeenk *et al.*, 2011). Different p53 target loci exhibit for instance different *cis*-regulatory elements or histone modifications. Consequently, different loci need distinct co-regulators or modifications of the gene-specific TF (Espinosa, 2008).

Interestingly, while I observe an increase in promoter binding upon IR, the level of promoter binding subsequently decreased to intermediate levels and stayed at these levels even when total p53 increased during the second pulse of accumulation. In contrast, other studies find an increase in promoter binding during the 2nd pulse for all targets correlating with the p53 dynamics (Hafner *et al.*, 2017). Different reasons could account for the difference in promoter binding in my experiments. Firstly, the p53 response becomes more and more heterogeneous in the course of the response. Consequently averaging the response of a population of cells, as it is the case in ChIP experiments, could mask the true dynamics. Therefore, assessing p53's recruitment to chromatin on single-cell level could reveal so far hidden regulatory mechanisms (Loffreda *et al.*, 2017). Another possible reason could be differences between cell lines (Stewart-Ornstein and Lahav, 2017). For instance, ChIP experiments in MCF7 cells showed a second increase in promoter binding corresponding to the second pulse. These cells also show a second pulse of ATM activity which might change PTM patterns of p53 as the acetylation status and therefore modulate promoter binding.

To explain the differences in target gene expression between the first and the second pulse, I took a closer look at the modification state of p53. I could show that the first p53 pulse is accompanied by an increase in acetylation of p53. However, during the 2nd pulse, I did not observe such a strong increase, especially for K382. Interestingly, stabilization of the PTM of the first response including p53's acetylation using Nutlin-3 or increase in acetylation due to depletion of the methyltransferases SMYD2 and SET8 led to an increase in promoter binding as well (Figure 3.8.4). Moreover, increase in acetylation turned the transient response of CDKN1A into a sustained response. Consequently, we can conclude that the balance between acetylation and methylation of p53's CTD modulates both transcription and promoter binding. At this point, two major questions arise: How is this change in acetylation facilitated and how can acetylation change the promoter binding and transcription of specific targets?

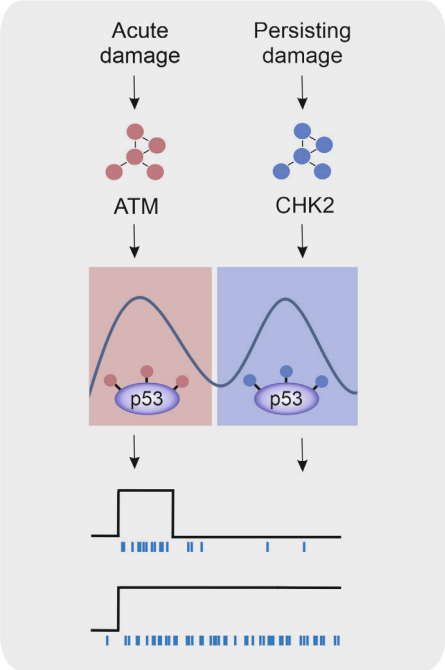

Figure 4.5.1: Upstream networks modulate p53's PTM patterns and target gene expression.

ATM and CHK2 mediated stabilization of p53 is accompanied by different PTM of the TF. Therefore, the PTM patterns change between the first and the second pulse resulting in altered target gene expression.

4.5.1 How is this change in acetylation facilitated?

p300 is an acetyltransferase involved in the modification of histones, however, it also directly acetylates the TF p53, especially in its CTD (Gu and Roeder, 1997; Miller Jenkins *et al.*, 2012). How can we explain the higher levels of acetylated p53 present during the 1st pulse? In this thesis, I showed that the immediate and the sustained response are mediated by different underlying networks. While the first pulse is mediated via a network induced by ATM, the sustained response is triggered based on CHK2. Interestingly, p300 itself was shown to be phosphorylated by ATM upon genotoxic stress (Jang *et al.*, 2010; Jang, Duk and Lee, 2011). This modification has a stabilizing effect on the acetyltransferase (Figure 4.5.2). In response to genotoxic stress, p300 forms a complex with JMY (junction-mediating and regulatory protein) and STRAP (stress-responsive activator of p300) (Smith and Thangue, 2005; Adighibe and Pezzella, 2018). Interestingly, JMY exists in different splicing variants which show selective activation of p53 targets (Shikama *et al.*, 1999; Smith and Thangue, 2005). The formation of the p300/JMY complex is controlled by STRAP (Demonacos, Krstic-Demonacos and Thangue, 2001). In turn, the nuclear accumulation of STRAP is mediated by ATM-dependent phosphorylation (Demonacos *et al.*, 2004; Adams *et al.*, 2008). Remarkably, ATM can influence acetylation of p53 not only by directly modulating the formation of the p300 co-activator complex. Additionally, binding of p300 to p53's N-terminus is increased by phosphorylation of the TAD which is

mediated partly by ATM (Miller Jenkins *et al.*, 2012; Liu, Tavana and Gu, 2019). Less N-terminal phosphorylation via ATM could therefore alter the acetylation status of p53 by impairing p300 binding.

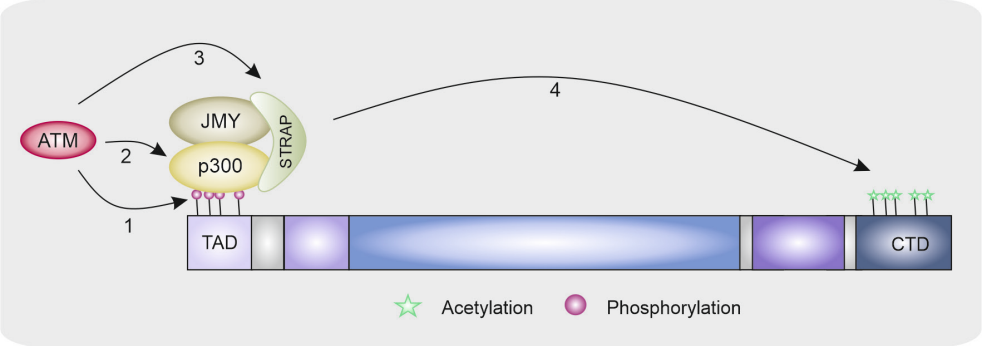

Figure 4.5.2: ATM modulates acetylation of p53.

(1) ATM mediates phosphorylation of S15 in the TAD which increases the affinity to p300. (2) ATM directly phosphorylates p300 thereby stabilizing the acetyltransferase. (3) ATM phosphorylates STRAP which induces nuclear accumulation of the protein. In turn, STRAP assembles with p300 and JMY to the co-activator complex. (4) The co-activator complex can mediate acetylation of p53's CTD.

4.5.2 How does acetylation affect stochastic bursting and promoter binding?

p53 has to find its target sites in the genome among the vast amount of sequences. For this purpose, p53 slides along nonspecific DNA via its short and unstructured CTD using linear diffusion (McKinney *et al.*, 2004; Terakawa, Kenzaki and Takada, 2012). The non-specific binding is facilitated via electrostatic interactions between positively charged lysine and arginine residues and the phosphate backbone (Friedler *et al.*, 2005; Laptenko *et al.*, 2015, 2016). This sliding together with three-dimensional hopping via the DBD allows scanning for its cognate RE (Laptenko *et al.*, 2016). The dwell time of p53 to non-specific DNA hereby is shorter than the dwell time at its RE (Schlereth *et al.*, 2010; Loffreda *et al.*, 2017). In response to DNA damage, the stability of the interaction between the RE and p53 is enhanced, which leads to an increased residence time at its cognate site. It could be shown that this was mediated by acetylation of the CTD (Loffreda *et al.*, 2017). A recent study suggested that the residence time of a TF can modulate burst frequency (Popp, Hettich and Gebhardt, 2021). Thereby, the acetylation state of the CTD is able to modulate stochastic bursting. The longer residence time can facilitate cofactor recruitment for transcription, a process that has additionally been connected to acetylation of the CTD. Here again, many studies focus on early time points post IR reflecting the immediate p53 response. To elucidate how target gene expression is regulated in the sustained response, it would be useful to investigate how for instance residence times of p53 on its RE change comparing the first and the second pulse.

4.6 Purpose of pulsatile dynamics

One major open question is the function of p53's pulsatile dynamics. A current hypothesis suggests that p53 pulses facilitate more diverse gene expression patterns. P53 target genes act as filters for the p53 pulses and their final expression pattern is modulated by their mRNA and protein half-life (Joshua R Porter, Fisher and Batchelor, 2016; Hanson, Porter and Batchelor, 2019). Additionally, p53's dynamical behavior prevents excessive accumulation of target proteins (Hafner *et al.*, 2020). For instance, strong accumulation of CDKN1A is associated with the induction of senescence instead of cell cycle arrest (te Poele *et al.*, 2002; Campisi and d'Adda di Fagagna, 2007). I observed changes in the upstream networks, altered modification states and differences in p53's transcriptional activity between the first pulse and second pulse. Together, these findings point towards another function of the pulses: Pulsatile dynamics facilitate an effective exchange of p53's modification patterns. These PTM in turn modulate target gene transcription. During the first pulse, we observe increased acetylation at K382 and partly at K370, most likely induced via the ATM signaling as described above. Are there characteristic PTM induced via the CHK2 signaling cascade marking the pulses of the sustained response? Post IR, several S/T residues in p53s CTD are phosphorylated by CHK2 as S366 and S378 (Ou *et al.*, 2005). Additionally, even though T387 was predicted to be a CHK1 target, CHK2 depletion leads to decreased phosphorylation on this residue implying a role of CHK2 in its modification (Ou *et al.*, 2005). Interestingly, the distinct phosphorylations of p53's TAD and CTD showed different kinetics post damage: While N-terminal phosphorylations and an increase in pS378 were detected rapidly in response to genotoxic stress, pS366 and pT387 were detected later, around 3h post IR. Remarkably, mutation studies indicated that modification of these residues might favor the expression of distinct targets (Ou *et al.*, 2005). Consequently, it would be worthwhile to take a deeper look into CHK2 mediated phosphorylations of p53's CTD comparing the immediate and the sustained response.

What could be the purpose for time-varying upstream networks inducing different PTM? In the course of the DNA damage response, the state of the genome is continuously changing: When the first pulse is induced, the cell has just sensed newly formed breaks and accordingly, the majority of the lesions remains unrepaired. In contrast, when the pulses of the sustained response are triggered, the breaks have already been marked and many of them have even been repaired. Only a subset of more complex breaks or lesions in heterochromatic regions remain. While breaks in euchromatin are usually repaired within 2-3 h, repair of breaks in heterochromatic regions takes more time (Jeggo, Geuting and Löbrich, 2011). Due to the dense packing of the DNA, the chromatin has to be remodeled to allow repair. Through distinct

molecular barcodes, the cell differentiates between a situation where new breaks are emerging and breaks that simply take longer time to repair (Batchelor, Loewer and Lahav, 2010). In turn, the resulting PTM allow the modulation of several processes of the p53 response as oligomerization, DNA binding and interaction with cofactors.

How do specific PTM patterns and p53's dynamics synergize to mediate the correct decision about life and death? In our experiments, prolonging PTM of the first pulse by Nutlin-3 treatment led to sustained accumulation of CDKN1A. Interestingly, strong accumulation of CDKN1A was connected to the induction of senescence (te Poele *et al.*, 2002; Campisi and d'Adda di Fagagna, 2007). In line, modulation of pulsatile dynamics into a sustained accumulation of p53 in response to IR was associated with the induction of apoptosis as well (Purvis *et al.*, 2012). Consequently, by exchanging PTM that were present during the first pulse the cell might prevent the induction of senescence or apoptosis. Impairment of sustained oscillations by inhibition of CHK2 led to changes in target gene expression both in smFISH and qRT-PCR experiments already indicating that the input of CHK2 and the sustained p53 response are crucial for p53 mediated cell fates upon IR. In this context, a recent study has shown that sustained CHK2 activity was essential to maintain G1 arrest upon genotoxic stress (García-santisteban *et al.*, 2021). Remarkably, similar to my observations, they saw as well, that after initially activating CHK2, ATM activity was no longer needed to maintain G1 arrest. Building on this finding, it would be crucial to systematically assess which cell fates are induced by ATM vs. CHK2 mediated networks and how inhibition of the kinases while keeping the shape of p53 dynamics alters the decision between life and death.

4.7 Conclusion & Outlook

P53 is a crucial player in the cellular response to genotoxic stress orchestrating the expression of targets involved in a variety of cellular outcomes. Consequently, huge responsibility lies on the guardian of the genome, as a mistake in cell fate decision could lead to the formation of cancer. In view of this, it is quite surprising that one protein is in charge of such vital decisions. Accordingly, more and more mechanisms regulating the p53 response have emerged over the years. In my work, I could show that p53 oscillation in response to severe damage doses are mediated by two interconnected networks with time-varying contributions. While the immediate response was mediated by ATM, the sustained response was controlled by CHK2. This allows the cell to differentiate between new, acute damage and breaks that persist in the cell, thereby adding another layer of regulation and fine-tuning to the p53 response. With my work, I could show that we have not only to pinpoint regulating interactions but also have to

characterize their temporal contributions to truly understand how the p53 response is shaped towards a specific cell fate. This requires sophisticated tools to control the levels or activity of certain players while monitoring the response of the protein of interest. Time-lapse live-cell microscopy and the usage of specific small molecule inhibitors or degron-tags allow to observe and manipulate protein levels in a timely precise manner and could provide valuable information on the time-dependent role of network members.

However, despite a better understanding of ATM's time-varying contribution to the p53 response, many open questions remain regarding the role of ATM. For instance, at least in some cell lines, pulsatile dynamics of activity are observed on western blot level or via immunofluorescence staining based on pCHK2(T68) (Batchelor *et al.*, 2008). In contrast, no such oscillations were reported for ATM foci at the break sites. Moreover, while ATM seems to be inactivated by WIP1 in the course of the response, ATM can be reactivated despite high WIP1 levels for instance upon re-damaging as shown here in this thesis or upon overexpression of the phosphatase (Batchelor *et al.*, 2008; Mönke *et al.*, 2017). One possible explanation might be distinct kinetics of ATM activity in different compartments underlining the importance to study protein activity not only in time but also in space (Jaiswal *et al.*, 2017). In the past years, spatial regulation of cellular processes has been subject to intensive research. One way to modulate cellular signaling is the formation of membraneless compartments through liquid-liquid phase separation (LLPS): Multivalent, weak interactions for instance via intrinsically disordered protein regions facilitate the formation of liquid-like droplets (Shin and Brangwynne, 2017; Lu *et al.*, 2021; Wang and Zhang, 2021). Recently, 53BP1 foci were shown to have characteristics of phase-separated compartments (Kilic *et al.*, 2019). The formation of these droplet-like compartments might facilitate the assembly of p53 and proteins involved in the activation the TF.

Another field that currently lacks systematic understanding is the variety of PTM found on players of the p53 response and their temporal contributions. For instance, CHK2 is modified early on at several other residues of the SCD in addition T68. Interestingly, studies suggested that the affinity of ATM to these other residues is lower leading to phosphorylation only upon higher degrees of damage (Buscemi *et al.*, 2006). Consequently, these modifications could serve as additional filters for the induction of sustained oscillations as they are a prerequisite for CHK2 activation. Detailed information on how these phosphorylations control CHK2 activity and how they contribute to the p53 response remains to be elucidated. Remarkably, while the SCD is modified rapidly within minutes, autophosphorylations in the kinase domain reach their highest level significantly later. Similarly, phosphorylations of the TAD of p53 are also detected earlier

than phosphorylations of the CTD. The mechanism and purpose of these time-varying phosphorylations are not fully clear yet. However, one can assume that they provide another layer of regulation to the p53 response joining the already known tools that enable p53 to faithfully decide whether a cell should live or die.

5 MATERIAL & METHODS

5 MATERIAL & METHODS

5.1 Cell lines

A549 (ATCC: CCL-185) is a human lung carcinoma cell line expressing wild-type p53 (Giard *et al.*, 1973; Lehman *et al.*, 1991). A549 reporter cells were described in Chen *et al.*, 2013; Finzel *et al.*, 2016. In brief, stable expression of p53-Venus and H2B-CFP under the control of the rat metallothionein promoter (MTp) and human ubiquitin C promoter (UbCp), respectively was achieved using lentiviral transduction. A549 SMYD2 and SET8 knockdown cell lines were described in Friedrich *et al.*, 2019. In brief, shRNAs were expressed using pRetroSuper.puro vectors that were modified accordingly (Loewer *et al.*, 2010; Brummelkamp, Bernards and Agami, 2016). A polyclonal population of cells was used.

As a second cell line, a non-transformed human breast epithelial cell line (MCF10A, ATTC: CRL-10317) was used. Importantly, also MCF10A cells express wild-type p53 (Soule *et al.*, 1990; Diella *et al.*, 1993). MCF10A reporter cells were described in Sheng, 2017; Sheng *et al.*, 2019. P53 and CBX5 were tagged with YFP and CFP, respectively on their endogenous loci which allowed expression from the endogenous promoter.

5.2 Cell culture

A549 WT cells were maintained at 37°C and 5% CO_2 in McCoy's 5A medium (GE Healthcare Life Sciences) supplemented with fetal calf serum (10%, (v/v), Thermo Fisher Scientific), GlutaMAX (2 mM, Thermo Fisher Scientific), penicillin and streptomycin (100 U/mL and 100 µg/mL, respectively, Thermo Fisher Scientific). Growth medium for A549 reporter cells was additionally supplemented with hygromycin (25 µg/mL, Thermo Fisher Scientific) and G418 (200 µg/mL, Carl Roth).

MCF10A reporter cells were maintained at 37°C and 5% CO_2 in Dulbecco's Modified Eagle Medium/ Nutrient Mixture F-12 (DMEM-F12) (Thermo Fisher Scientific) supplemented with horse serum (5% (v/v), Thermo Fisher Scientific), GlutaMAX (2 mM, Thermo Fisher Scientific), penicillin and streptomycin (100 U/mL and 100 µg/mL, respectively, Thermo Fisher Scientific) as well as EGF (20 ng/mL, PeptroTech), hydrocortisone (0.5 µg/mL, Sigma Aldrich), cholera toxin (100 ng/mL, Sigma Aldrich) and insulin (10 µg/mL, Sigma Aldrich).

For passaging, cells were rinsed with 1x PBS and incubated with 1x trypsin/EDTA in PBS for 5 min (A549 cells) or 20 min (MCF10A cells) at 37°C. The process was stopped by addition of growth medium and cells were pelleted by centrifugation. Subsequently, cells were resuspended in growth medium in the desired concentration.

5.3 Irradiation and treatment with inhibitors

Inhibitors were added 1 h before 5 Gy irradiation (dose rate of 1 Gy/26 s, 250 keV, 10 mA) or at time points as indicated in the respective section. The inhibitors used in this thesis and the concentrations used for experiments are given in Table 5.3.1. Nutlin-3 was sequentially added at distinct time points post IR in different final concentrations: 0.75 µM, 2.25 µM and 4 µM were added at 2.5 h, 3.5 h and 5.5 h, respectively.

Table 5.3.1: Inhibitors used in this thesis with the concentrations used during experiments.

Target	Inhibitor	Used concentration	Manufacturer
DNA-PK	NU7026	10 µM	MedChemExpress
ATR	AZD6738	2 µM	MedChemExpress
ATM	KU-55933	10 µM	MedChemExpress
ATM	KU-60019	3 µM	MedChemExpress
CHK2	BML-277	10 µM	MedChemExpress
MDM2	Nutlin-3	0.75-4 µM	Sigma-Aldrich
Protein synthesis	Cycloheximide	10 µg/mL	New England Biolabs

5.4 Time-lapse microscopy

Two days prior to experiments, 0.3×10^5 reporter cells/well were seeded in 24-well ibiTreat polymer-bottom plates (ibidi). One hour before the start of the experiment, media was exchanged for phenol red-free FluoroBrite medium (Thermo Fisher Scientific) supplemented with FCS (5%, (v/v), Thermo Fisher Scientific), GlutaMAX (2 mM, Thermo Fisher Scientific), penicillin and streptomycin (100 U/mL and 100 µg/mL, respectively, Thermo Fisher Scientific) and HEPES (10 mM, Carl Roth) when using A549 reporter cells. For MCF10A reporter cells, FluoroBrite medium was supplemented with HS (0.5%, (v/v), Thermo Fisher Scientific) instead of FCS and additionally, EGF (20 ng/mL, PeptroTech), hydrocortisone (0.5 µg/mL, Sigma Aldrich), cholera toxin (100 ng/mL, Sigma Aldrich) and insulin (10 µg/mL, Sigma Aldrich) were added to the medium. Cells were imaged every 15 min using a Nikon Eclipse Ti-E inverted microscope and a 20x plan apo objective (NA 0.75) enclosed by an incubator maintaining 37°C, 5% CO_2 and humidity. Imaging was controlled via the Nikon Elements software. The following filter sets were used: CFP: 438/24 nm excitation (EX), 458 nm dichroic beam splitter (BS), 483/32 nm emission (EM); YFP: 500/24 nm EX, 520 nm BS, 542/27 nm EM; Cy5: 628/40 nm EX, 692/40 nm EM; DAPI: 387/11 nm EX, 409 nm BS, 447/60 nm EM.

5.5 Image analysis and cell tracking

Cells were tracked based on the signal of the respective nuclear marker (H2B-CFP or CBX-CFP in A549 reporter or MCF10A reporter cells, respectively) using custom-written MATLAB (MathWorks) scripts as described in Finzel *et al.*, 2016; Strasen *et al.*, 2018. The code was based on work by the Alon lab (Cohen *et al.*, 2008) and the CellProfiler project (Carpenter *et al.*, 2006). To this end, raw images were subjected to flat field correction and background subtraction. Subsequently, segmentation of individual nuclei was accomplished using thresholding and seeded watershed algorithms based on the nuclear marker. To allow the assignment of cells from time frame to time frame, a greedy match algorithm was used. Cells that could not be tracked throughout all time frames were excluded from the analysis. Cells were tracked in forward direction starting from the first to the last time frame. The integrated nuclear fluorescence intensity of p53-YFP was determined for every cell in every time frame.

To detect pulses in the p53-YFP trajectories, nuclear fluorescence intensity of a single cell was normalized to the median nuclear fluorescence intensity of the distinct single cell. A threshold was set to avoid detection of local minima or maxima. The threshold was chosen based on the features to be quantified: Detection and quantification of features of the first two pulses were performed with a threshold between 0.15-0.2 also allowing the detection of low amplitude pulses. Depending on the microscope, the respective exposure time used and the resulting dynamic range, the threshold was set to 0.2 or 0.15. Reproducibility of features of the control samples was used as a quality standard. Quantification of the total number of pulses within 48h was performed with a higher threshold of 0.3 to avoid the detection of non-specific fluctuation in p53 levels, especially at later time points when regular pulsatile dynamics stop. Subsequently, the script used a watershed algorithm to find pulses above this threshold. For the distinct pulses, the absolute amplitude, the timing and the duration were calculated as well as the fraction of cells showing the respective pulse.

To visualize the response of all single cells, the nuclear fluorescence intensity was plotted as heatmaps. As different single cells show a broad variability in their fluorescence intensities (I), the data was min-max-normalized according to equation (1) to improve visualization.

$$I' = \frac{I - \min(I)}{\max(I) - \min(I)} \quad (1)$$

Subsequently, cells were sorted according to the timing of the second pulse.

5.6 Cell cycle analysis

To sort the cells according to their cell cycle phase at the time of the experiment, the latter was determined by combining labeling with the thymidine analog 5- ethynyl-2'-deoxyuridine (EdU)

with the detection of cell division. Cells were seeded as described in section 5.4. 24 h before treatment, media was exchanged for phenol red-free FluoroBrite medium (Thermo Fisher Scientific) supplemented with FCS (5%, (v/v), Thermo Fisher Scientific), GlutaMAX (2 mM, Thermo Fisher Scientific), penicillin and streptomycin (100 U/mL and 100 µg/mL, respectively, Thermo Fisher Scientific) and HEPES (10 mM, Carl Roth). To monitor cell division, images of the cells were acquired for 24h. 30 min before treatment, EdU (10mM, EdU Click-647, Carl Roth) was carefully added to the cells. After 30 min, EdU was washed off with PBS and fresh FluoroBrite Media was added. Cells were treated as indicated and imaging was restarted for 24h. Afterwards, cells were fixed immediately using paraformaldehyde (PFA, 2% in PBS) for 10 min at RT. Cells were washed twice with PBS and permeabilized using Triton X-100 (0.1% in PBS). Subsequently, goat serum (10% in PBS) was used to block the cells. Cells were washed again 3x using 0.1% Triton X-100 in PBS. To perform the Click-reaction, the reaction mix was prepared according to the manufacturer's protocol and added to the cells for 30 min in the dark. Cells were washed 3x with 0.1% Triton X-100 in PBS and counterstained with 2 µg/ml Hoechst in 0.1% Triton X-100 in PBS for 5 min in the dark. Cells were washed twice with PBS and subsequently, images were taken. Cells were sorted according to their EdU signal intensity and S-phase cells were determined using an edge detection algorithm (Sheng, 2017). To distinguish between G1- and G2 phase cells, cell division was detected based on a saw-tooth-like decrease in integrated intensity of the nuclear marker as well as the area of the nucleus. Based on the timing of their last division before the start of the experiment, cells were grouped into G1-or G2-phase cells. As the number of cells in G2 was significantly smaller compared to the group of G1-or S-phase cells, G2- phase cells were combined with the pool of S-phase cells.

5.7 Western blotting

Two days prior to experiments, 5×10^5 A549 WT cells were seeded in a 6 cm plate. After IR, cells were washed once with PBS and harvested in PBS supplemented with NaF (50 mM) at indicated time points. For detection of acetylated proteins, harvesting and all upcoming steps were performed in the presence of Trichostatin A (APExBio). The cell pellet was resuspended in RIPA Lysis buffer (50 mM Tris, 100 mM NaCl, 1% Triton X-100, 0.5% Na-Deoxycholate and 0.1% SDS) supplemented with NaF (50 mM), sodium orthovanadate (1 mM), protease inhibitor cocktail plus (1/100, Carl Roth) and phosphatase inhibitor cocktail (1/100, Sigma-Aldrich) and lysed on ice for 20 min. If acetylated protein ought to be detected, additionally deacetylase inhibitor cocktail (1/100, MedChemExpress) was added. Subsequent centrifugation allowed the removal of cell debris. Protein concentrations were measured via Bradford assay (Roti-Nanoquant, Carl Roth). Equal amounts of protein were denatured using NuPAGE Sample buffer (Invitrogen) and DTT (50 mM, Sigma) for 10 min at 70°C. Proteins with a size below 100 kDa were separated

using self-made 10% acrylamide gels for 1.5 h at 150 V via the Mini Trans-Blot® Cell System (Biorad) in electrophoresis running buffer (25 mM Tris/HCl, 0.2 M Glycin and 0.5% SDS). Proteins with a size above 100 kDa were separated using NuPAGE 3 to 8% Tris-Acetate gels (Invitrogen) in NuPAGE Tris-Acetate SDS Running Buffer (Invitrogen) for 1 h at 150 V. To estimate the molecular mass, Precision Plus Protein Dual Color Standards (Bio-Rad) was used. Proteins with a size below 100 kDa were transferred to PVDF membranes (Carl Roth) by electroblotting (Bio-Rad) for 1.5 h at 200 mA using transfer buffer (25 mM Tris, 192 mM glycine and 10 % Ethanol). For proteins with a size above 100 kDa, the transfer was performed overnight at 4°C using CAPS buffer (10 mM CAPS pH 11, 15% Methanol). Membranes were blocked with bovine serum albumin (5%, BSA, Carl Roth) or nonfat-dried milk (5%, NFDM, Carl Roth) in TBS-T for 1 h and incubated overnight with primary antibody at 4°C (see Table 5.7.1 for concentration).

Table 5.7.1:Antibodies used with their respective concentration.
NFDM: Non-fat dried milk. BSA: Bovine serum albumin.

Antibody	Identifier	Dilution	Buffer	Manufacturer
GAPDH	Cat #G9545	1:10,000	5% NFDM	Sigma-Aldrich
CHK2 total	Cat #3440	1:1000	5% NFDM	Cell signalling
pCHK2(T68)	Cat #2661	1:1000	5% BSA	Cell signalling
pCHK2(S516)	Cat #2669	1:1000	5% BSA	Cell signalling
p53 total	Cat #sc-126	1:5000	5% NFDM	Santa Cruz Biotechnology
p53 total	Cat #9282	1:1000	5% NFDM	Cell signalling
P53(K382Ac)	Cat #ab75754	1:2500	5% NFDM	Abcam
P53(K370Ac)	Cat #ab183544	1:1000	5% NFDM	Abcam
MDM2	Cat #sc-965	1:200	5% NFDM	Santa Cruz Biotechnology
MDMX	Cat #04-1555	1:1000	5% NFDM	Millipore
pATM(S1981)	Cat #ab36810	1:1000	5% BSA	Abcam
α-rabbit IgG, HRP	Cat #31410	1:10,000	5% NFDM	Thermo Fisher Scientific
α-mouse IgG, HRP	Cat #31460	1:10,000	5% NFDM	Thermo Fisher Scientific

For the detection of acetylated proteins, blocking and all upcoming steps were performed at 4°C. The following day the membrane was washed 4x with TBS-T and subsequently incubated with the secondary antibody (1:10,000, 5% NFDM in TBS-T) for 1h at RT. Membranes were washed again 4x with TBS-T and chemiluminescence was used to determine protein levels (Western Bright Quantum, Advansta). Chemiluminescence was detected via the Fusion Fx documentation system (Vilber Lourmat).

5.8 qRT-PCR

5.8.1 RNA isolation and cDNA Synthesis

Two days prior to experiments, 5×10^5 A549 WT cells were seeded in a 6 cm plate. After IR, cells were washed once with PBS and harvested in PBS at indicated time points. For RNA isolation, High Pure RNA Isolation kit (Roche) was used according to the manufacturer's protocol. RNA was eluted in Elution Buffer (30 µL) and the concentration was measured via a UV-Vis spectrophotometer (NanoDrop 2000c, Thermo Fisher Scientific). For the generation of cDNA, 1 µg RNA was mixed with components in Table 5.8.1 (Step 1) and incubated at 70°C for 5 min. Subsequently, the components of Table 5.8.1 (Step 2) were added and the reaction mix was incubated at 42°C for 1 h. cDNA synthesis was finalized by inactivation of the enzymes for 5 min at 80°C. cDNA was diluted 1:10 with DEPC treated water.

Table 5.8.1: Reagents for cDNA-Synthesis.

	Reagent	Amount	Manufacturer
STEP 1	RNA	1 µg	
	dNTP mix (10 mM)	2 µL	New England Biolabs
	Oligo dT (50 µM)	1 µL	New England Biolabs
	DEPC treated H_2O	Ad 12 µL	Carl Roth
STEP 2	5x ProtoScript II Buffer	4 µL	New England Biolabs
	DTT (0.1 M)	2 µL	New England Biolabs
	ProtoScript II Reverse Transcriptase	1 µL	New England Biolabs
	Murine RNase inhibitor	1 µL	New England Biolabs

5.8.2 Real-Time PCR

Quantitative real-time PCR was conducted in triplicates using the reaction mix in Table 5.8.2 in a 96-well plate (Applied Biosystems) sealed with adhesive foil (Biozym).

Table 5.8.2: Reaction mix for RT-PCR.

Reagent	Volume [µL]	Manufacturer
cDNA	3	
Primer mix	9.5	
Power Up SYBR Green Master Mix	12.5	Thermo Fisher Scientific

The StepOnePlus™ Real-Time PCR system (Thermo Fisher Scientific) was used with the program shown in Table 5.8.3.

Table 5.8.3: Thermal profile of the qPCR run.

Step	Temperature	Time	Cycles
Holding stage	95	10 min	1
Cycling stage	95	15s	40
	60	1 min	
Melt Curve stage	95	15 s	1
	60	1 min	1
	60-95°C, +0.3°C	15s	1

The sequence of the primers used in this thesis can be found in Table 5.8.4. Relative expression levels were determined using the ΔΔCt method. In brief, the difference between the Ct value of the gene of interest and a housekeeping gene was determined (ΔCt) as seen in equation (2). In the second step, the difference between the ΔCt of the sample of interest (SOI) and a control sample was calculated (ΔΔCt)(eq. 3). This value can then be used to determine the relative quantity (RQ) of target gene expression (eq. 4). Error bars correspond to the RQ_{min} and RQ_{max} values which characterize the variability of the respective RQ value using the standard error of the mean.

$$\Delta Ct = Ct_{gene\ of\ interest} - Ct_{housekeeping\ gene} \quad (2)$$

$$\Delta\Delta Ct = \Delta Ct_{SOI} - \Delta Ct_{Control} \quad (3)$$

$$RQ = 2^{-\Delta\Delta Ct} \quad (4)$$

Table 5.8.4: Primers used for determining mRNA levels via RT-PCR.

Primer	Sequence (5'-3')
CHK2 forward	GCA GCA GTG CCT GTT CAC A
CHK2 reverse	TGG ATA TGC CCT GGG ACT GT
WIP1 forward	ATA AGC CAG AAC TTC CCA AGG
WIP1 reverse	TGG TCA ATA ACT GTG CTC CTT C
BAX forward	CTG ACG GCA ACT TCA ACT GG
BAX reverse	GAT CAG TTC CGG CAC CTT GG
CDKN1A forward	TCC TGT GGG CGG ATT AG
CDKN1A reverse	TGG ACC TGT CAC TGT CTT GT

5.9 siRNA mediated knockdown

Depending on the target, different protocols were used: For WIP1 depletion, 2.5 × 10^5 A549 reporter cells were seeded using A549 WT media in 6 well plates. Following seeding, 25 nM WIP1 targeting siRNA (Ambion, Thermo Fisher Scientific) or control siRNA were transfected using the TransIT-X2 Dynamic Delivery System (Mirus Bio LLC). To this end, the indicated amount of siRNA was added to 250 µL Opti-MEM Reduced-Serum Medium (Thermo Fisher Scientific) and mixed by pipetting. Subsequently, 7.5 µL TransIT-X2 were added and again mixed by pipetting. The mixture was incubated for 25 min at RT to facilitate the formation of complexes and afterwards given drop-wise to different parts of the well. Two days after transfection, cells were seeded for live-cell microscopy as described in section 5.4 or seeded for qRT-PCR as in section 5.8.

For CHK2 depletion, 1.5 × 10^5 A549 reporter cells were seeded using A549 WT media in 6 well plates. 24 h and 72 h after seeding, 25 nM CHK2 targeting siRNA (Thermo Fisher Scientific) or control siRNA were transfected as described above. One day after the second transfection, cells were seeded for live-cell microscopy or qRT-PCR.

5.10 Chromatin Immuno-Precipitation (ChIP) assay

A total of 1.6 × 10^7 cells per condition were rinsed with PBS and proteins were cross-linked to the DNA using paraformaldehyde (PFA, 1% in PBS) for 10 min. Cells were washed again with cold PBS, incubated with glycine (125 mM in PBS) for 5 min to stop fixation and subsequently washed with cold PBS. Cells were harvested with PBS supplemented with PMSF (1 mM). After resuspension in lysis buffer (5 mM Tris–HCl, pH 8.0, 85 mM KCl, 0.5% Igepal-CA630 (v/v)

supplemented with protease inhibitor cocktail (Carl Roth) and 1 mM PMSF), cells were incubated on ice for 20 min. Cells were centrifuged to collect the nuclear pellet. Following resuspension in Sonication buffer (50 mM Tris–HCl, pH 8.1, 0.3% SDS (w/v), 10 mM EDTA supplemented with 1 mM PMSF and Protease Inhibitor Cocktail) and incubation on ice for 30 min, samples were sonicated using the Covaris S220 Sonicator (PIP 105, Duty Factor 2%, CPB 200, 2 min). Samples were centrifuged to pellet cell debris and the supernatant was collected. After diluting 80 µg of chromatin with dilution buffer (16.7 mM Tris–HCl, 167 mM NaCl, 0.01% SDS (w/v), 1.2 mM EDTA, 1.1% Triton (v/v), 1 mM PMSF, Protease Inhibitor Cocktail), samples were incubated overnight rotating at 4°C with 5 µg p53 antibody (FL-393, Santa Cruz) or a control IgG antibody (Normal rabbit IgG, EMD Millipore). The next day, 25 µL of Dynabeads Protein G (Thermo Fisher Scientific) were added for 2 h at 4 °C to collect the immunocomplexes. The beads were washed with following buffers to reduce non-specific binding: Low salt washing buffer (0.1% SDS (w/v), 2 mM EDTA, 20 mM Tris–HCl pH 8.1, 1% Triton X-100 (v/v), and 150 mM NaCl), high salt washing buffer (0.1% SDS (w/v), 2 mM EDTA, 20 mM Tris–HCl pH 8.1, 1% Triton X-100 (v/v), and 500 mM NaCl), LiCl washing buffer (10 mM Tris–HCl pH 8.1, 1 mM EDTA, 1% IGEPAL CA630 (v/v), 1% deoxycholic acid (w/v), 250 mM LiCl) and TE-Buffer (10 mM Tris–HCl pH 8.1, 1 mM EDTA). For DNA elution, the beads were incubated for 30 min at 37 °C with Elution buffer (1% SDS (w/v), 0.1 M NaHCO3) twice. To reverse crosslinks between proteins and DNA, 200 mM NaCl were added and samples were incubated at 65°C overnight. To remove RNAs, 50 µg/mL RNase A were added for 30 min at 37°C. Next, samples were mixed with 100 µg/mL Proteinase K, 10 mM EDTA and 40 mM Tris–HCl pH 6.5 and incubated for 3 h at 45°C. DNA was purified using the Monarch PCR & DNA Cleanup Kit (NEB). 3 µL of each sample were used for the subsequent qPCR (see section 5.8.2) with the primers shown in Table 5.10.1. Data obtained from qPCR was normalized to the respective input samples taken prior to immunoprecipitation according to equation (5) and additionally normalized to the 3h time point.

$$\%Input = 100 \times 2^{Ct_{adjusted\ input} - Ct_{IP}} \quad (5)$$

Table 5.10.1: Primers for ChIP.

Primer	Sequence (5'-3')	Reference
BAX forward	AACCAGGGGATCTCGGAAG	(Sánchez *et al.*, 2014)
BAX reverse	AGTGCCAGAGGCAGGAAGT	(Sánchez *et al.*, 2014)
CDKN1A forward	AGCCTTCCTCACATCCTCCT	(Sánchez *et al.*, 2014)
CDKN1A reverse	GGAATGGTGAAAGGTGGAAA	(Sánchez *et al.*, 2014)

5.11 Single molecule fluorescence in-situ hybridization (smFISH)

smFISH experiments were performed by Dhana Friedrich (for details see Friedrich, 2019; Friedrich *et al.*, 2019). In brief, cells were rinsed on ice with sterile, ice-cold PBS and fixed using 2% PFA (EM-grade, Electron Microscopy Sciences) for 10 min at RT. Next, cells were permeabilized overnight with 70% Ethanol at 4°C. All buffers used in the upcoming steps were prepared with RNAse/DNAse-free H_2O (QIAGEN). For the design of custom probe sets for smFISH, the online tool for Stellaris probe design (Biosearch Technologies Inc.) was employed. For exon probe sets, CAL Fluor Red 610 was used as conjugated dye, for intron probe sets Quasar 670 was used. Hybridization was performed according to the manufacturer's protocol for 16 h at 37°C with a final probe concentration of 0.1 µM. The next day, cells were rinsed with 2x SSC (Applichem GmBH) and subsequently incubated with Alexa Fluor 488 N-Hydroxysuccinimid (NHS-AF88, Molecular Probes/Life Technologies) for 10 min at RT to unspecifically stain cytoplasmic proteins. To counterstain the nucleus, Hoechst 33342 (Molecular Probes/Life Technologies) was used and afterwards, cover glasses were embedded in 15 µL Prolong Gold Antifade (Molecular probes/Life technologies). Imaging was performed using a Nikon Eclipse Ti-E inverted microscope and a 60x plan apo objective (NA 1.4) and controlled via the Nikon Elements software. 21 z-stacks were taken for each cell with a step width of 300 nm. The following filter sets were used: Quasar 670: 640/30 nm excitation (EX), 660 nm dichroic beam splitter (BS), 690/50 nm emission (EM); Alexa Fluor 488: 470/40 nm EX, 495 nm BS, 525/50 nm EM; CAL Fluor 610: 580/25 nm EM, 600 nm BS, 625 EX; Hoechst: 387/11 nm EX, 409 nm BS, 447/60 nm EM.

RNA counts per cell were quantified via the FISH-quant tool (Mueller *et al.*, 2013) as well as custom-written MATLAB software. Co-localization of exon and intron signals in nuclei indicated transcriptional start sides (TSS). The fraction of active promoters (f) was used as a proxy for burst frequency and was calculated via equation 6 with *n* being the number of genetic loci.

$$f = \frac{\#TSS}{n} \tag{6}$$

As a proxy for burst size the transcription rate at active transcription sites (µ) was used. The transcription rate per hour can be calculated according to equation 7 based on the occupancy of RNAP2 (*M*), the RNAP2 elongation speed (v) and the gene length of the respective target (*l*). The occupancy of RNAP2 itself can be derived from the quotient of summed TSS intensity values (Int_{TSS}) and the median intensity of a cytoplasmic mRNA spot ($mInt_{mRNA}$) also considering correction factors for the probe position (η) and a fixed value of 1.5 ($\varkappa$) for correcting RNAP2 occupancies as described before (Bahar Halpern *et al.*, 2015).

$$\mu = M \cdot \frac{v}{l} \quad (7)$$

$$M = \frac{Int_{TSS}}{\varkappa \cdot \eta \cdot mInt_{mRNA}} \quad (8)$$

In turn, the number of RNAs per cell (X_{RNA}) can be inferred from the transcription rate at active sites (μ), the fraction of active promoters (f) and the RNA degradation rate (δ_{RNA}) as seen in equation 9.

$$X_{RNA} = \frac{n \cdot f \cdot \mu}{\delta_{RNA}} \quad (9)$$

6 REFERENCES

6 REFERENCES

Adams, C. J. *et al.* (2008) 'ATM and Chk2 kinase target the p53 cofactor Strap', *EMBO Reports*, 9(12), pp. 1222–1229. doi: 10.1038/embor.2008.186.

Adighibe, O. and Pezzella, F. (2018) 'The Role of JMY in p53 Regulation', *Cancers*, 10(6), p. 173. doi: 10.3390/cancers10060173.

Ahn, J. and Prives, C. (2002) 'Checkpoint Kinase 2 (Chk2) Monomers or Dimers Phosphorylate Cdc25C after DNA Damage Regardless of Threonine 68 Phosphorylation', *Journal of Biological Chemistry*, 277(50), pp. 48418–48426. doi: 10.1074/jbc.M208321200.

Ahn, J., Urist, M. and Prives, C. (2003) 'Questioning the role of checkpoint kinase 2 in the p53 DNA damage response', *Journal of Biological Chemistry*, 278(23), pp. 20480–20489. doi: 10.1074/jbc.M213185200.

Ahn, J. Y. *et al.* (2000) 'Threonine 68 Phosphorylation by Ataxia Telangiectasia Mutated Is Required for Efficient Activation of Chk2 in Response to Ionizing Radiation', *Cancer Research*, 60(21), pp. 5934–5936.

Arva, N. C. *et al.* (2005) 'A chromatin-associated and transcriptionally inactive p53-Mdm2 complex occurs in mdm2 SNP309 homozygous cells', *Journal of Biological Chemistry*, 280(29), pp. 26776–26787. doi: 10.1074/jbc.M505203200.

Badciong, J. C. and Haas, A. L. (2002) 'MdmX Is a RING Finger Ubiquitin Ligase Capable of Synergistically Enhancing Mdm2 Ubiquitination', *Journal of Biological Chemistry*, 277(51), pp. 49668–49675. doi: 10.1074/jbc.M208593200.

Bahar Halpern, K. *et al.* (2015) 'Bursty Gene Expression in the Intact Mammalian Article Bursty Gene Expression in the Intact Mammalian Liver', *Molecular Cell*, 58(1), pp. 147–156. doi: 10.1016/j.molcel.2015.01.027.

Bahassi, E. M. *et al.* (2002) 'Mammalian Polo-like kinase 3 (Plk3) is a multifunctional protein involved in stress response pathways', *Oncogene*, 21(43), pp. 6633–6640. doi: 10.1038/sj.onc.1205850.

Bahassi, E. M. *et al.* (2006) 'Priming phosphorylation of Chk2 by polo-like kinase 3 (Plk3) mediates its full activation by ATM and a downstream checkpoint in response to DNA damage', *Mutation Research*, 596(1–2), pp. 166–176. doi: 10.1016/j.mrfmmm.2005.12.002.

Bakkenist, C. J. and Kastan, M. B. (2004) 'Initiating Cellular Stress Responses', *Cell*, 118(1), pp. 9–17. doi: 10.1016/j.cell.2004.06.023.

Ball, H. L. *et al.* (2007) 'Function of a Conserved Checkpoint Recruitment Domain in ATRIP Proteins', *Molecular and Cellular Biology*, 27(9), pp. 3367–3377. doi: 10.1128/mcb.02238-06.

Banin, S. *et al.* (1998) 'Enhanced phosphorylation of p53 by ATM in response to DNA damage', *Science*, 281(5383), pp. 1674–1677. doi: 10.1126/science.281.5383.1674.

Bar-Or, R. L. *et al.* (2000) 'Generation of oscillations by the p53-Mdm2 feedback loop: A theoretical and experimental study', *Proceedings of the National Academy of Sciences of the United States of America*, 97(21), pp. 11250–11255. doi: 10.1073/pnas.210171597.

Barak, Y. *et al.* (1993) 'Mdm2 Expression is induced by wild type p53 activity', *EMBO Journal*, 12(2), pp. 461–468. doi: 10.1002/j.1460-2075.1993.tb05678.x.

Barlev, N. A. *et al.* (2001) 'Acetylation of p53 activates transcription through recruitment of coactivators/histone acetyltransferases', *Molecular Cell*, 8(6), pp. 1243–1254. doi: 10.1016/S1097-2765(01)00414-2.

Batchelor, E. *et al.* (2008) 'Recurrent Initiation: A Mechanism for Triggering p53 Pulses in Response to DNA Damage', *Molecular Cell*, 30(3), pp. 277–289. doi: 10.1016/j.molcel.2008.03.016.

Batchelor, E. *et al.* (2011) 'Stimulus-dependent dynamics of p53 in single cells', *Molecular Systems Biology*, 7(488), pp. 1–8. doi: 10.1038/msb.2011.20.

Batchelor, E. and Loewer, A. (2017) 'Recent progress and open challenges in modeling p53 dynamics in single cells', *Current Opinion in Systems Biology*, 3, pp. 54–59. doi: 10.1016/j.coisb.2017.04.007.

Batchelor, E., Loewer, A. and Lahav, G. (2010) 'The ups and downs of p53: Understanding protein dynamics in single cells', *Nat Rev Cancer*, 9(5), pp. 371–377. doi: 10.1038/nrc2604.The.

Beucher, A. *et al.* (2009) 'ATM and Artemis promote homologous recombination of radiation-induced DNA double-strand breaks in G2', *EMBO Journal*, 28(21), pp. 3413–3427. doi: 10.1038/emboj.2009.276.

Bhoumik, A. *et al.* (2005) 'ATM-Dependent Phosphorylation of ATF2 Is Required for the DNA Damage Response', *Molecular Cell*, 18(5), pp. 577–587. doi: 10.1016/j.molcel.2005.04.015.

Biderman, L. *et al.* (2012) 'MdmX Is Required for p53 Interaction with and Full Induction of the Mdm2 Promoter after Cellular Stress', *Molecular and Cellular Biology*, 32(7), pp. 1214–1225. doi: 10.1128/mcb.06150-11.

Blackford, A. N. and Jackson, S. P. (2017) 'ATM, ATR, and DNA-PK: The Trinity at the Heart of the DNA Damage Response', *Molecular Cell*, 66(6), pp. 801–817. doi: 10.1016/j.molcel.2017.05.015.

Borcherds, W. *et al.* (2014) 'Disorder and residual helicity alter p53-Mdm2 binding affinity and signaling in cells', *Nature Chemical Biology*, 10(12), pp. 1000–1002. doi: 10.1038/nchembio.1668.

Bourdon, J. C. *et al.* (1997) 'Further characterisation of the p53 responsive element - identification of new candidate genes for trans-activation by p53', *Oncogene*, 14(1), pp. 85–94. doi: 10.1038/sj.onc.1200804.

Brummelkamp, T. R., Bernards, R. and Agami, R. (2016) 'A System System for for Stable

Stable Expression Expression of of Short Short Interfering Interfering RNAs RNAs in in Mammalian Cells', *Science*, 296(5567), pp. 550–553.

Buscemi, G. *et al.* (2004) 'Activation of ATM and Chk2 kinases in relation to the amount of DNA strand breaks', *Oncogene*, 23(46), pp. 7691–7700. doi: 10.1038/sj.onc.1207986.

Buscemi, G. *et al.* (2006) 'DNA Damage-Induced Cell Cycle Regulation and Function of Novel Chk2 Phosphoresidues', *Molecular and Cellular Biology*, 26(21), pp. 7832–7845. doi: 10.1128/mcb.00534-06.

Campisi, J. and d'Adda di Fagagna, F. (2007) 'Cellular senescence: when bad things happen to good cells', *Molecular Cell Biology*, 8(9), pp. 729–740. doi: 10.1038/nrm2233.

Canman, C. E. *et al.* (1998) 'Activation of the ATM kinase by Ionizing Radiation and Phosphorylation of p53', *Science*, 281(5383), pp. 1677–1679. doi: 10.1126/science.281.5383.1677.

Carpenter, A. E. *et al.* (2006) 'CellProfiler : image analysis software for identifying and quantifying cell phenotypes', *Genome Biology*, 7(10), p. R100. doi: 10.1186/gb-2006-7-10-r100.

Castellino, R. C. *et al.* (2008) 'Medulloblastomas overexpress the p53-inactivating oncogene WIP1/PPM1D', *Journal of Neuro-Oncology*, 86(3), pp. 245–256. doi: 10.1007/s11060-007-9470-8.

Chang, H. H. Y. *et al.* (2017) 'Non-homologous DNA end joining and alternative pathways to double-strand break repair', *Nature Reviews Molecular Cell Biology*, 18, pp. 495–506. doi: 10.1038/nrm.2017.48.

Chehab, N. H. *et al.* (1999) 'Phosphorylation of Ser-20 mediates stabilization of human p53 in response to DNA damage', *Proceedings of the National Academy of Sciences of the United States of America*, 96(24), pp. 13777–13782. doi: 10.1073/pnas.96.24.13777.

Chen, J. (2012) 'The Roles of MDM2 and MDMX Phosphorylation in Stress Signaling to p53', *Genes and Cancer*, 3(3–4), pp. 274–282. doi: 10.1177/1947601912454733.

Chen, L. *et al.* (2005) 'ATM and Chk2-dependent phosphorylation of MDMX contribute to p53 activation after DNA damage', *EMBO Journal*, 24(19), pp. 3411–3422. doi: 10.1038/sj.emboj.7600812.

Chen, S. H., Forrester, W. and Lahav, G. (2016) 'Schedule-dependent interaction between anticancer treatments', *Science*, 351(6278), pp. 1204–1208. doi: 10.1126/science.aac5610.

Chen, X. *et al.* (2013) 'DNA damage strength modulates a bimodal switch of p53 dynamics for cell-fate control', *BMC Biology*, 11(73), pp. 1–11. doi: 10.1186/1741-7007-11-73.

Chi, S. *et al.* (2005) 'Structural Details on mdm2-p53 Interaction', *Journal of Biological*

Chemistry, 280(46), pp. 38795–38802. doi: 10.1074/jbc.M508578200.

Chuikov, S. *et al.* (2004) 'Regulation of p53 activity through lysine methylation', *Nature*, 432(7015), pp. 353–360. doi: 10.1038/nature03117.

Ciccia, A. and Elledge, S. J. (2010) 'The DNA Damage Response: Making It Safe to Play with Knives', *Molecular Cell*. Elsevier Inc., 40(2), pp. 179–204. doi: 10.1016/j.molcel.2010.09.019.

Ciliberto, A. *et al.* (2005) 'Steady States and Oscillations in the p53/Mdm2 Network', *Cell Cycle*, 4(3), pp. 488–493. doi: 10.4161/cc.4.3.1548.

Cohen, A. A. *et al.* (2008) 'Dynamic Proteomics of Individual Cancer Cells in Response to a Drug', *Science*, 322(5907), pp. 1511–1516. doi: 10.1126/science.1160165.

Davison, T. S. *et al.* (1998) 'Characterization of the oligomerization defects of two p53 mutants found in families with Li-Fraumeni and Li-Fraumeni-like syndrome', *Oncogene*, 17(5), pp. 651–656. doi: 10.1038/sj.onc.1202062.

Demonacos, C. *et al.* (2004) 'A new effector pathway links ATM kinase with the DNA damage response.', *Nature cell biology*, 6(10), pp. 968–976. doi: 10.1038/ncb1170.

Demonacos, C., Krstic-Demonacos, M. and Thangue, N. B. La (2001) 'A TPR Motif Cofactor Contributes to p300 Activity in the p53 Response', *Molecular Cell*, 8(1), pp. 71–84. doi: 10.1016/s1097-2765(01)00277-5.

Deng, W. *et al.* (2020) 'The role of PPM1D in cancer and advances in studies of its inhibitors', *Biomedicine and Pharmacotherapy*, 125, p. 109956. doi: 10.1016/j.biopha.2020.109956.

Diella, F. *et al.* (1993) 'Absence of p53 point mutations in nontransformed human mammary epithelial cell lines', *Life Sci. Adv. Biochem*, 12, pp. 47–51.

Donovan, B. T. *et al.* (2019) 'Live-cell imaging reveals the interplay between transcription factors , nucleosomes , and bursting', *The EMBO Journal*, 38(12), pp. 1–18. doi: 10.15252/embj.2018100809.

Dozier, C. *et al.* (2004) 'Regulation of Chk2 phosphorylation by interaction with protein phosphatase 2A via its B ′ regulatory subunit', *Biology of the Cell*, 96(7), pp. 509–517. doi: 10.1016/j.biolcel.2004.04.010.

El-Deiry, W. S. *et al.* (1992) 'Definition of a consensus binding site for p53', *Nature Genetics*, 1(1), pp. 45–49. doi: 10.1038/ng0492-45.

Eliaš, J. and Maxnamara, C. K. (2021) 'Mathematical Modelling of p53 Signalling during DNA Damage Response : A Survey', *International Journal of Molecular Sciences*, 22(19), p. 10590. doi: 10.3390/ijms221910590.

Espinosa, J. M. (2008) 'Mechanisms of regulatory diversity within the p53 transcriptional network', *Oncogene*, 27(29), pp. 4013–4023. doi: 10.1038/onc.2008.37.

Falcicchio, M. *et al.* (2020) 'Regulation of p53 by the 14-3-3 protein interaction network : new opportunities for drug discovery in cancer', *Cell Death Discovery*, 6(126). doi: 10.1038/s41420-020-00362-3.

Falck, J. *et al.* (2001) 'The ATM - Chk2 - Cdc25A checkpoint pathway guards against radioresistant DNA synthesis', *Nature*, 410(6830), pp. 842–847. doi: 10.1038/35071124.

Fernandez-Fernandez, M. R., Veprintsev, D. B. and Fersht, A. R. (2005) 'Proteins of the S100 family the regulate the oligomerization of p53 tumor suppressor', *Proceedings of the National Academy of Sciences of the United States of America*, 102(13), pp. 4735–4740. doi: 10.1073/pnas.0501459102.

Finzel, A. *et al.* (2016) 'Hyperactivation of ATM upon DNA-PKcs inhibition modulates p53 dynamics and cell fate in response to DNA damage', *Molecular Biology of the Cell*, 27(15), pp. 2360–2367. doi: 10.1091/mbc.E16-01-0032.

Fiscella, M. *et al.* (1997) 'Wip1, a novel human protein phosphatase that is induced in response to ionizing radiation in a p53-dependent manner', *Proceedings of the National Academy of Sciences of the United States of America*, 94(12), pp. 6048–6053. doi: 10.1073/pnas.94.12.6048.

Fischer, M. (2017) 'Census and evaluation of p53 target genes', *Oncogene*, 36(28), pp. 3943–3956. doi: 10.1038/onc.2016.502.

Fischer, N. W. *et al.* (2016) 'P53 Oligomerization Status Modulates Cell Fate Decisions Between Growth, Arrest and Apoptosis', *Cell Cycle*. Taylor & Francis, 15(23), pp. 3210–3219. doi: 10.1080/15384101.2016.1241917.

Francoz, S. *et al.* (2006) 'Mdm4 and Mdm2 cooperate to inhibit p53 activity in proliferating and quiescent cells in vivo', *Proceedings of the National Academy of Sciences of the United States of America*, 103(9), pp. 3232–3237. doi: 10.1073/pnas.0508476103.

Freeman, A. K. *et al.* (2010) 'Negative regulation of CHK2 activity by protein phosphatase 2A is modulated by DNA damage', *Cell Cycle*, 9(4), pp. 736–747. doi: 10.4161/cc.9.4.10613.

Friedel, L. and Loewer, A. (2022) 'The guardian's choice: how p53 enables context-specific decision-making in individual cells', *FEBS Journal*, 289(1), pp. 40–52. doi: 10.1111/febs.15767.

Friedler, A. *et al.* (2005) 'Modulation of Binding of DNA to the C-Terminal Domain of p53 by Acetylation', *Structure*, 13(4), pp. 629–636. doi: 10.1016/j.str.2005.01.020.

Friedrich, D. *et al.* (2019) ' Stochastic transcription in the p53-mediated response to DNA damage is modulated by burst frequency ', *Molecular Systems Biology*, 15(12), pp. 1–20. doi: 10.15252/msb.20199068.

Friedrich, D. (2019) *Oscillatory transcription factors and stochastic gene expression From pulsatile p53 dynamics to bursty transcription in the DNA*. Humboldt University

Berlin.

Fujimoto, H. *et al.* (2006) 'Regulation of the antioncogenic Chk2 kinase by the oncogenic Wip1 phosphatase', *Cell Death and Differentiation*, 13(7), pp. 1170–1180. doi: 10.1038/sj.cdd.4401801.

Fuku, T. *et al.* (2007) 'Increased wild-type p53-induced phosphatase 1 (Wip1 or PPM1D) expression correlated with downregulation of checkpoint kinase 2 in human gastric carcinoma', *Pathology International*, 57(9), pp. 566–571. doi: 10.1111/j.1440-1827.2007.02140.x.

Funk, W. D. *et al.* (1992) 'A transcriptionally active DNA-binding site for human p53 protein complexes', *Molecular and Cellular Biology*, 12(6), pp. 2866–2871. doi: 10.1128/mcb.12.6.2866-2871.1992.

Gaglia, G. *et al.* (2013) 'Activation and control of p53 tetramerization in individual living cells', *Proceedings of the National Academy of Sciences of the United States of America*, 110(38), pp. 15497–15501. doi: 10.1073/pnas.1311126110.

García-santisteban, I. *et al.* (2021) 'Sustained CHK2 activity , but not ATM activity , is critical to maintain a G1 arrest after DNA damage in untransformed cells', *BMC Biology*, 19(1), p. 35. doi: 10.1186/s12915-021-00965-x.

Gately, D. P. *et al.* (1998) 'Characterization of ATM Expression , Localization , and Associated DNA-dependent Protein Kinase Activity', *Molecular and Cellular Biology*, 9(9), pp. 2361–2374. doi: 10.1091/mbc.9.9.2361.

Geva-Zatorsky, N. *et al.* (2006) 'Oscillations and variability in the p53 system', *Molecular Systems Biology*, 2(1), pp. 2006–0033. doi: 10.1038/msb4100068.

Ghate, N. B. *et al.* (2019) 'P32 Is a Negative Regulator of P53 Tetramerization and Transactivation', *Molecular Oncology*, 13(9), pp. 1976–1992. doi: 10.1002/1878-0261.12543.

Giard, D. J. *et al.* (1973) 'In Vitro Cultivation of Human Tumors : Establishment of Cell Lines Derived From', *Journal of the National Cancer Institute*, 51(5), pp. 1417–1423.

Golding, I. *et al.* (2005) 'Real-time kinetics of gene activity in individual bacteria', *Cell*, 123(6), pp. 1025–1036. doi: 10.1016/j.cell.2005.09.031.

Gu, B. and Zhu, W. (2012) 'Surf the Post-translational Modification Network of p53 Regulation', *International Journal of Biological Sciences*, 8(5), pp. 672–684. doi: 10.7150/ijbs.4283.

Gu, W. and Roeder, R. G. (1997) 'Activation of p53 sequence-specific DNA binding by acetylation of the p53 C-terminal domain', *Cell*, 90(4), pp. 595–606. doi: 10.1016/S0092-8674(00)80521-8.

Guo, X. *et al.* (2010) 'Interdependent phosphorylation within the kinase domain T-loop regulates CHK2 activity', *Journal of Biological Chemistry*, 285(43), pp. 33348–33357. doi: 10.1074/jbc.M110.149609.

Hafner, A. *et al.* (2017) 'p53 pulses lead to distinct patterns of gene expression albeit similar DNA-binding dynamics', *Nature Structural & Molecular Biology*, 24(10), pp. 840–847. doi: 10.1038/nsmb.3452.

Hafner, A. *et al.* (2019) 'The multiple mechanisms that regulate p53 activity and cell fate', *Nature Reviews Molecular Cell Biology*, 20(4), pp. 199–210. doi: 10.1038/s41580-019-0110-x.

Hafner, A. *et al.* (2020) 'Quantifying the Central Dogma in the p53 Pathway in Live Single Cells Quantifying the Central Dogma in the p53 Pathway in Live Single Cells', *Cell Systems*, 10(6), pp. 495–505. doi: 10.1016/j.cels.2020.05.001.

Hamstra, D. A. *et al.* (2006) 'Real-time evaluation of p53 oscillatory behavior in vivo using bioluminescent imaging', *Cancer Research*, 66(15), pp. 7482–7489. doi: 10.1158/0008-5472.CAN-06-1405.

Hanson, R. L., Porter, J. R. and Batchelor, E. (2019) 'Protein stability of p53 targets determines their temporal expression dynamics in response to p53 pulsing', *Journal of Cell Biology*, 218(4), pp. 1282–1297. doi: 10.1083/jcb.201803063.

Helleday, T. *et al.* (2007) 'DNA double-strand break repair : From mechanistic understanding to cancer treatment', *DNA Repair*, 6(7), pp. 923–935. doi: 10.1016/j.dnarep.2007.02.006.

Heltberg, M. L. *et al.* (2019) 'Inferring Leading Interactions in the p53 / Mdm2 / Mdmx Circuit through Live-Cell Imaging and Modeling', *Cell Systems*, 9(6), pp. 548-558.e5. doi: 10.1016/j.cels.2019.10.010.

Hendy, O. *et al.* (2017) 'Differential context-specific impact of individual core promoter elements on transcriptional dynamics', *Molecular Biology of the Cell*, 28(23), pp. 3260–3370. doi: 10.1091/mbc.E17-06-0408.

Hirao, A. *et al.* (2000) 'DNA damage-induced activation of p53 by the checkpoint kinase Chk2', *Science*, 287(5459), pp. 1824–1827. doi: 10.1126/science.287.5459.1824.

Hoeijmakers, J. H. J. (2009) 'DNA Damage, Aging, and Cancer', *The New England journal of medicine*, 361(15), pp. 1475–1485. doi: 10.1056/NEJMra0804615.

Hofmann, T. G. *et al.* (2002) 'Regulation of p53 activity by its interaction with homeodomain-interacting protein kinase-2', *Nature Cell Biology*, 4(1), pp. 1–10. doi: 10.1038/ncb715.

Huang, J. *et al.* (2006) 'Repression of p53 activity by Smyd2-mediated methylation', *Nature*, 444(7119), pp. 629–632. doi: 10.1038/nature05287.

Huang, Q. *et al.* (2018) 'MDMX acidic domain inhibits p53 DNA binding in vivo and regulates tumorigenesis', *Proceedings of the National Academy of Sciences of the United States of America*, 115(15), pp. E3368–E3377. doi: 10.1073/pnas.1719090115.

Hustedt, N. and Durocher, D. (2017) 'The control of DNA repair by the cell cycle', *Nature Cell Biology*, 19(1), pp. 1–9. doi: 10.1038/ncb3452.

Imagawa, T. *et al.* (2009) 'Evaluation of transcriptional activity of p53 in individual living mammalian cells', *Analytical Biochemistry*, 387(2), pp. 249–256. doi: 10.1016/j.ab.2009.01.030.

Ito, A. *et al.* (2002) 'MDM2-HDAC1-mediated deacetylation of p53 is required for its degradation', *The EMBO Journal*, 21(22), pp. 6236–6245. doi: 10.1093/emboj/cdf616.

Ivanov, G. S. *et al.* (2007) 'Methylation-Acetylation Interplay Activates p53 in Response to DNA Damage', *Molecular and Cellular Biology*, 27(19), pp. 6756–6769. doi: 10.1128/mcb.00460-07.

Jaiswal, H. *et al.* (2017) ' ATM /Wip1 activities at chromatin control Plk1 re-activation to determine G2 checkpoint duration ', *The EMBO Journal*, 36(14), pp. 2161–2176. doi: 10.15252/embj.201696082.

Jallepalli, P. V. *et al.* (2003) 'The Chk2 tumor suppressor is not required for p53 responses in human cancer cells', *Journal of Biological Chemistry*, 278(23), pp. 20475–20479. doi: 10.1074/jbc.M213159200.

Jang, E. R. *et al.* (2010) 'Phosphorylation of p300 by ATM controls the stability of NBS1', *Biochemical and Biophysical Research Communications*, 397(4), pp. 637–643. doi: 10.1016/j.bbrc.2010.05.060.

Jang, E. R., Duk, J. and Lee, J. (2011) 'Acetyltransferase p300 regulates NBS1-mediated DNA damage response', *FEBS Letters*. Federation of European Biochemical Societies, 585(1), pp. 47–52. doi: 10.1016/j.febslet.2010.11.034.

Jeggo, P. A., Geuting, V. and Löbrich, M. (2011) 'The role of homologous recombination in radiation-induced double-strand break repair', *Radiotherapy and Oncology*, 101(1), pp. 7–12. doi: 10.1016/j.radonc.2011.06.019.

Jimenez, G. S. *et al.* (1999) 'DNA-dependent protein kinase is not required for the p53-dependent response to DNA damage', *Nature*, 400(6739), pp. 81–83. doi: 10.1038/21913.

Johnson, S. A., You, Z. and Hunter, T. (2007) 'Monitoring ATM kinase activity in living cells', *DNA Repair*, 6(9), pp. 1277–1284. doi: 10.1016/j.dnarep.2007.02.025.

Jones, S. N. *et al.* (1995) 'Rescue of embryonic lethality in Mdm2-deficient mice by absence of p53', *Nature*, 378(6553), pp. 206–208. doi: 10.1038/378206a0.

Kaeser, M. D. and Iggo, R. D. (2002) 'Chromatin immunoprecipitation analysis fails to support the latency model for regulation of p53 DNA binding activity in vivo', *Proceedings of the National Academy of Sciences of the United States of America*, 99(1), pp. 95–100. doi: 10.1073/pnas.012283399.

Kao, S.-H. *et al.* (2015) 'Analysis of Protein Stability by the Cycloheximide Chase Assay', *Bio-Protocol*, 5(1), pp. 1–5. doi: 10.21769/bioprotoc.1374.

Kastan, M. and Bakkenist, C. (2003) 'DNA damage activates ATM through intermolecular autophosphorylation and dimmer association', *Nature*, 421(6922), pp. 499–506.

doi: 10.1038/nature01368.

Kawaguchi, T. *et al.* (2005) 'The relationship among p53 oligomer formation, structure and transcriptional activity using a comprehensive missense mutation library', *Oncogene*, 24(46), pp. 6976–6981. doi: 10.1038/sj.onc.1208839.

Khosravi, R. *et al.* (1999) 'Rapid ATM-dependent phosphorylation of MDM2 precedes p53 accumulation in response to DNA damage', *Proceedings of the National Academy of Sciences of the United States of America*, 96(26), pp. 14973–14977. doi: 10.1073/pnas.96.26.14973.

Kilic, S. *et al.* (2019) 'Phase separation of 53 BP 1 determines liquid-like behavior of DNA repair compartments', *EMBO Journal*, 38(16), p. e101379. doi: 10.15252/embj.2018101379.

Knights, C. D. *et al.* (2006) 'Distinct p53 acetylation cassettes differentially influence gene-expression patterns and cell fate', *Journal of Cell Biology*, 173(4), pp. 533–544. doi: 10.1083/jcb.200512059.

Kruiswijk, F., Labuschagne, C. F. and Vousden, K. H. (2015) 'P53 in survival, death and metabolic health: A lifeguard with a licence to kill', *Nature Reviews Molecular Cell Biology*, 16(7), pp. 393–405. doi: 10.1038/nrm4007.

Kruse, J.-P. P. and Gu, W. (2009) 'Modes of p53 regulation', *Cell*, 137(4), pp. 609–622. doi: 10.1016/j.cell.2009.04.050.

Kumar, N., Singh, A. and Kulkarni, R. V. (2015) 'Transcriptional Bursting in Gene Expression: Analytical Results for General Stochastic Models', *PLoS Computational Biology*, 11(10), pp. 1–22. doi: 10.1371/journal.pcbi.1004292.

Lahav, G. *et al.* (2004) 'Dynamics of the p53-Mdm2 feedback loop in individual cells', *Nature Genetics*, 36(2), pp. 147–150. doi: 10.1038/ng1293.

Lakin, N. D., Hann, B. C. and Jackson, S. P. (1999) 'The ataxia-telangiectasia related protein ATR mediates DNA-dependent phosphorylation of p53', *Oncogene*, 18(27), pp. 3989–3995. doi: 10.1038/sj.onc.1202973.

Landgraf, P. *et al.* (2014) 'BONCAT : Metabolic Labeling , Click Chemistry , and Affi nity Purifi cation of Newly Synthesized Proteomes', in *Methods in molecular biology (Clifton, N.J.)*, pp. 199–215. doi: 10.1007/978-1-4939-2272-7.

Laptenko, O. *et al.* (2015) 'The p53 C Terminus Controls Site-Specific DNA Binding and Promotes Structural Changes within the Central DNA Binding Domain', *Molecular Cell*, 57(6), pp. 1034–1046. doi: 10.1016/j.molcel.2015.02.015.

Laptenko, O. *et al.* (2016) 'The Tail That Wags the Dog : How the Disordered C-Terminal Domain Controls the Transcriptional Activities of the p53 Tumor-Suppressor Protein', *Trends in Biochemical Sciences*, 41(12), pp. 1022–1034. doi: 10.1016/j.tibs.2016.08.011.

Lee, J. H. and Paull, T. T. (2004) 'Direct Activation of the ATM Protein Kinase by the Mre11/Rad50/Nbs1 Complex', *Science*, 304(5667), pp. 93–96. doi:

10.1126/science.1091496.

Lee, J. H. and Paull, T. T. (2021) 'Cellular functions of the protein kinase ATM and their relevance to human disease', *Nature Reviews Molecular Cell Biology*, 22(12), pp. 796–814. doi: 10.1038/s41580-021-00394-2.

Lees-Miller, S. P. *et al.* (1992) 'Human DNA-activated protein kinase phosphorylates serines 15 and 37 in the amino-terminal transactivation domain of human p53.', *Molecular and Cellular Biology*, 12(11), pp. 5041–5049. doi: 10.1128/mcb.12.11.5041.

Lees-Miller, S. P., Chen, Y. R. and Anderson, C. W. (1990) 'Human cells contain a DNA-activated protein kinase that phosphorylates simian virus 40 T antigen, mouse p53, and the human Ku autoantigen.', *Molecular and Cellular Biology*, 10(12), pp. 6472–6481. doi: 10.1128/mcb.10.12.6472.

Lehman, T. A. *et al.* (1991) 'p53 Mutations, ras Mutations, and p53-Heat Shock 70 Protein Complexes in Human Lung Carcinoma Cell Lines', *Cancer Research*, 51(15), pp. 4090–4096.

Li, M. *et al.* (2003) 'Mono- Versus Polyubiquitination: Differential Control of p53 Fate by Mdm2', *Science*, 302(5652), pp. 1972–1975. doi: 10.1126/science.1091362.

Linares, L. K. *et al.* (2003) 'HdmX stimulates Hdm2-mediated ubiquitination and degradation of p53', *Proceedings of the National Academy of Sciences of the United States of America*, 100(21), pp. 12009–12014. doi: 10.1073/pnas.2030930100.

Lionnet, T. and Singer, R. H. (2012) 'Transcription goes digital', *EMBO Reports*, 13(4), pp. 313–21. doi: 10.1038/embor.2012.31.

Liu, S. and Kong, D. (2021) 'End resection : a key step in homologous recombination and DNA double - strand break repair', *Genome Instability & Disease*. Springer Singapore, 2(1), pp. 39–50. doi: 10.1007/s42764-020-00028-5.

Liu, Y., Tavana, O. and Gu, W. (2019) 'p53 modifications : exquisite decorations of the powerful guardian', *Journal of molecular cell biology*, 11(7), pp. 564–577. doi: 10.1093/jmcb/mjz060.

Loewer, A. *et al.* (2010) 'Basal Dynamics of p53 Reveal Transcriptionally Attenuated Pulses in Cycling Cells', *Cell*, 142(1), pp. 89–100. doi: 10.1016/j.cell.2010.05.031.

Loewer, A. *et al.* (2013) 'The p53 response in single cells is linearly correlated to the number of DNA breaks without a distinct threshold', *BMC Biology*, 11(1), p. 114. doi: 10.1186/1741-7007-11-114.

Löffler, R. (2021) *Modellierung des oszillierenden P53- Autoregulationsnetzwerkes*. Technical University Darmstadt.

Loffreda, A. *et al.* (2017) 'Live-cell p53 single-molecule binding is modulated by C-terminal acetylation and correlates with transcriptional activity', *Nature Communications*, 8(1), pp. 1–12. doi: 10.1038/s41467-017-00398-7.

Lou, Z. *et al.* (2006) 'MDC1 Maintains Genomic Stability by Participating in the Amplification of ATM-Dependent DNA Damage Signals', *Molecular Cell*, 21(2), pp. 187–200. doi: 10.1016/j.molcel.2005.11.025.

Lu, J. *et al.* (2021) 'Emerging Roles of Liquid–Liquid Phase Separation in Cancer: From Protein Aggregation to Immune-Associated Signaling', *Frontiers in Cell and Developmental Biology*, 9, p. 631486. doi: 10.3389/fcell.2021.631486.

Lu, X., Nannenga, B. and Donehower, L. (2005) 'PPM1D dephosphorylates Chk1 and p53 and abrogates cell cycle checkpoints', *Genes & Development*, 19(10), pp. 1162–1174. doi: 10.1101/gad.1291305.tein.

Lu, X., Nguyen, T. A. and Donehower, L. A. (2005) 'Reversal of the ATM/ATR-mediated DNA damage response by the oncogenic phosphatase PPM1D', *Cell Cycle*, 4(8), pp. 4060–4064. doi: 10.4161/cc.4.8.1876.

Luna, R. M. D. O., Wagner, D. S. and Lozano, G. (1995) 'Rescue of early embryonic lethality in mdm2-deficient mice by deletion of p53', *Nature*, 378(6553), pp. 203–206. doi: 10.1038/378203a0.

Luo, J. *et al.* (2004) 'Acetylation of p53 augments its site-specific DNA binding both in vitro and in vivo', *Proceedings of the National Academy of Sciences of the United States of America*, 101(8), pp. 2259–2264. doi: 10.1073/pnas.0308762101.

Ma, L. *et al.* (2005) 'A plausible model for the digital response of p53 to DNA damage', *Proceedings of the National Academy of Sciences of the United States of America*, 102(40), pp. 4–9. doi: 10.1073/pnas.0501352102.

Matsuoka, S., Huang, M. and Elledge, S. J. (1998) 'Linkage of ATM to Cell Cycle Regulation by the Chk2 Protein Kinase', *Science*, 282(5395), pp. 1893–1897. doi: 10.1126/science.282.5395.1893.

Maya, R. *et al.* (2001) 'ATM-dependent phosphorylation of Mdm2 on serine 395: Role in p53 activation by DNA damage', *Genes and Development*, 15(9), pp. 1067–1077. doi: 10.1101/gad.886901.

McKinney, K. *et al.* (2004) 'p53 Linear Diffusion along DNA Requires Its C Terminus', *Molecular Cell*, 16(3), pp. 413–424. doi: 10.1016/j.molcel.2004.09.032.

Migliorini, D. *et al.* (2002) 'Mdm4 (Mdmx) Regulates p53-Induced Growth Arrest and Neuronal Cell Death during Early Embryonic Mouse Development', 22(15), pp. 5527–5538. doi: 10.1128/MCB.22.15.5527.

Miller Jenkins, L. M. *et al.* (2012) 'p53 N-terminal phosphorylation : a defining layer of complex regulation', *Carcinogenesis*, 33(8), pp. 1441–1449. doi: 10.1093/carcin/bgs145.

Minsky, N. and Oren, M. (2004) 'The RING domain of Mdm2 mediates histone ubiquitylation and transcriptional repression', *Molecular Cell*, 16(4), pp. 631–639. doi: 10.1016/j.molcel.2004.10.016.

Molina, N. *et al.* (2013) 'Stimulus-induced modulation of transcriptional bursting in a

single mammalian gene', *Proceedings of the National Academy of Sciences of the United States of America*, 110(51), pp. 20563–20568. doi: 10.1073/pnas.1312310110.

Monk, N. A. M. (2003) 'Oscillatory Expression of Hes1 , p53 , and NF- kB Driven by Transcriptional Time Delays', *Current Biology*, 13(16), pp. 1409–1413. doi: 10.1016/S.

Mönke, G. *et al.* (2017) 'Excitability in the p53 network mediates robust signaling with tunable activation thresholds in single cells', *Scientific Reports*, 7, p. 46571. doi: 10.1038/srep46571.

Mordes, D. A. and Cortez, D. (2008) 'Activation of ATR and related PIKKs', *Cell Cycle*, 7(18), pp. 2809–2812. doi: 10.4161/cc.7.18.6689.

Mueller, F. *et al.* (2013) 'FISH-quant: Automatic counting of transcripts in 3D FISH images', *Nature Methods*, 10(4), pp. 277–278. doi: 10.1038/nmeth.2406.

Muller, P. *et al.* (2018) 'Evidence for allosteric effects on p53 oligomerization induced by phosphorylation', *Protein Science*, 27(2), pp. 523–530. doi: 10.1002/pro.3344.

Muller, P. A. J. and Vousden, K. H. (2013) 'P53 Mutations in Cancer', *Nature Cell Biology*, 15(1), pp. 2–8. doi: 10.1038/ncb2641.

Murray-Zmijewski, F., Slee, E. A. and Lu, X. (2008) 'A complex barcode underlies the heterogeneous response of p53 to stress', *Nature Reviews Molecular Cell Biology*, 9(9), pp. 702–712. doi: 10.1038/nrm2451.

Nakamura, S. and Roth, J. A. (2000) 'Multiple Lysine Mutations in the C-Terminal Domain of p53 Interfere with MDM2-Dependent Protein Degradation and Ubiquitination', *Molecular and Cellular Biology*, 20(24), pp. 9391–9398. doi: 10.1128/MCB.20.24.9391-9398.2000.

Natsume, T. and Kanemaki, M. T. (2017) 'Conditional Degrons for Controlling Protein Expression at the Protein Level', *Annual Review of Genetics*, 51, pp. 83–102. doi: 10.1146/annurev-genet-120116-024656.

Nicolas, D., Phillips, N. E. and Naef, F. (2017) 'What shapes eukaryotic transcriptional bursting?', *Molecular BioSystems*, 13(7), pp. 1280–1290. doi: 10.1039/C7MB00154A.

Nyati, S. *et al.* (2018) 'Quantitative and Dynamic Imaging of ATM Kinase Activity', *Methods in Molecular Biology*, 1596, pp. 131–145. doi: 10.1007/978-1-4939-6940-1.

Ohkubo, S. *et al.* (2006) 'Excess HDM2 impacts cell cycle and apoptosis and has a selective effect on p53-dependent transcription', *Journal of Biological Chemistry*, 281(25), pp. 16943–16950. doi: 10.1074/jbc.M601388200.

Okamoto, K. *et al.* (2005) 'DNA Damage-Induced Phosphorylation of MdmX at Serine 367 Activates p53 by Targeting MdmX for Mdm2-Dependent Degradation', *Molecular and Cellular Biology*, 25(21), pp. 9608–9620. doi:

10.1128/mcb.25.21.9608-9620.2005.

Oliva-Trastoy, M. *et al.* (2007) 'The Wip1 phosphatase (PPM1D) antagonizes activation of the Chk2 tumour suppressor kinase', *Oncogene*, 26(10), pp. 1449–1458. doi: 10.1038/sj.onc.1209927.

Ou, Y. *et al.* (2005) 'p53 C-Terminal Phosphorylation by CHK1 and CHK2 Participates in the Regulation of DNA-Damage-induced C-Terminal Acetylation', *Molecular Biology of the Cell*, 16(4), pp. 1684–1695. doi: 10.1091/mbc.E04.

Paek, A. L. *et al.* (2016) 'Cell-to-Cell Variation in p53 Dynamics Leads to Fractional Killing', *Cell*, 165(3), pp. 631–642. doi: 10.1016/j.cell.2016.03.025.

Parant, J. *et al.* (2001) 'Rescue of embryonic lethality in Mdm4 -null mice by loss of Trp53 suggests a nonoverlapping pathway with MDM2 to regulate p53', *Nature Genetics*, 29(1), pp. 92–95. doi: 10.1038/ng714.

Paull, T. T. (2015) 'Mechanisms of ATM activation', *Annual Review of Biochemistry*, 84(December), pp. 711–738. doi: 10.1146/annurev-biochem-060614-034335.

Pei, D., Zhang, Y. and Zheng, J. (2012) 'Regulation of p53 : a collaboration between Mdm2 and MdmX', *Oncogene*, 3(3), pp. 228–235. doi: 10.18632/oncotarget.443.

te Poele, R. H. *et al.* (2002) 'DNA Damage Is Able to Induce Senescence in Tumor Cells in Vitro and in Vivo', *Cancer research*, 62(6), pp. 1876–1883.

Popp, A. P., Hettich, J. and Gebhardt, J. C. M. (2021) 'Altering transcription factor binding reveals comprehensive transcriptional kinetics of a basic gene', *Nucleic acids research*, 49(11), pp. 6249–6266.

Porter, Joshua R, Fisher, B. E. and Batchelor, E. (2016) 'p53 Pulses Diversify Target Gene Expression Dynamics in an mRNA Half-Life-Dependent Manner and Delineate Co-regulated Target Gene Subnetworks', *Cell Systems*, 2(4), pp. 272–282. doi: 10.1016/j.cels.2016.03.006.

Porter, Joshua R., Fisher, B. E. and Batchelor, E. (2016) 'P53 Pulses Diversify Target Gene Expression Dynamics in an mRNA Half-Life-Dependent Manner and Delineate Co-regulated Target Gene Subnetworks', *Cell Systems*, 2(4), pp. 272–282. doi: 10.1016/j.cels.2016.03.006.

Purvis, J. E. *et al.* (2012) 'p53 Dynamics Control Cell Fate', *Science*, 336(6087), pp. 1440–1444. doi: 10.1126/science.1218351.

Purvis, J. E. and Lahav, G. (2013) 'Encoding and Decoding Cellular Information through Signaling Dynamics', *Cell*, 152(5), pp. 945–956. doi: 10.1016/j.cell.2013.02.005.

Raj, A. *et al.* (2006) 'Stochastic mRNA Synthesis in Mammalian Cells', *PLoS biology*, 4(10), p. e309. doi: 10.1371/journal.pbio.0040309.

Rajagopalan, S. *et al.* (2008) '14-3-3 activation of DNA binding of p53 by enhancing its association into tetramers', 36(18), pp. 5983–5991. doi: 10.1093/nar/gkn598.

Rajagopalan, S. *et al.* (2010) 'Mechanistic differences in the transcriptional activation of p53 by 14-3-3 isoforms', *Nucleic Acids Research*, 38(3), pp. 893–906. doi: 10.1093/nar/gkp1041.

Riley, T. *et al.* (2008) 'Transcriptional control of human p53-regulated genes', *Nature Reviews Molecular Cell Biology*, 9(5), pp. 402–412. doi: doi: 10.1038/nrm2395. PMID: 18431400.

Rodriguez, M. S. *et al.* (2000) 'Multiple C-Terminal Lysine Residues Target p53 for Ubiquitin-Proteasome-Mediated Degradation', *Molecular and Cellular Biology*, 20(22), pp. 8458–8467. doi: 10.1128/mcb.20.22.8458-8467.2000.

Rogakou, E. P. *et al.* (1999) 'Megabase Chromatin Domains Involved in DNA Double-Strand Breaks In Vivo', *The Journal of Cell Biology*, 146(5), pp. 905–915. doi: 10.1083/jcb.146.5.905.

Rokudai, S. *et al.* (2013) 'MOZ increases p53 acetylation and premature senescence through its complex formation with PML', *Proceedings of the National Academy of Sciences of the United States of America*, 110(10), pp. 3895–3900. doi: 10.1073/pnas.1300490110.

Saito, S. N. I. *et al.* (2002) 'ATM mediates phosphorylation at multiple p53 sites, including Ser46, in response to ionizing radiation', *Journal of Biological Chemistry*, 277(15), pp. 12491–12494. doi: 10.1074/jbc.C200093200.

Sakaguchi, K. *et al.* (1997) 'Effect of phosphorylation on tetramerization of the tumor suppressor protein p53', *Journal of Protein Chemistry*, 16(5), pp. 553–556. doi: 10.1023/A:1026334116189.

Sakaguchi, K. *et al.* (1998) 'DNA damage activates p53 through a phosphorylation-acetylation cascade', *Genes and Development*, 12(18), pp. 2831–2841. doi: 10.1101/gad.12.18.2831.

Sakaguchi, K. *et al.* (2000) 'Damage-mediated Phosphorylation of Human p53 Threonine 18 through a Cascade Mediated by a Casein 1-like Kinase', *Journal of Biological Chemistry*, 275(13), pp. 9278–9283. doi: 10.1074/jbc.275.13.9278.

Sammons, M. A. *et al.* (2020) 'Tumor suppressor p53: from engaging DNA to target gene regulation', *Nucleic acids research*. Oxford University Press, 48(16), pp. 8848–8869. doi: 10.1093/nar/gkaa666.

Sánchez, Y. *et al.* (2014) 'Genome-wide analysis of the human p53 transcriptional network unveils a lncRNA tumour suppressor signature', *Nature communications*, 5, p. 5812. doi: 10.1038/ncomms6812.

Saramäki, A. *et al.* (2006) 'Regulation of the human p21(waf1/cip1) gene promoter via multiple binding sites for p53 and the vitamin D3 receptor', *Nucleic Acids Research*, 34(2), pp. 543–554. doi: 10.1093/nar/gkj460.

Schlereth, K. *et al.* (2010) 'DNA Binding Cooperativity of p53 Modulates the Decision between Cell-Cycle Arrest and Apoptosis', *Molecular Cell*, 38(3), pp. 356–368.

doi: 10.1016/j.molcel.2010.02.037.

Schlereth, K. *et al.* (2013) 'Characterization of the p53 Cistrome - DNA Binding Cooperativity Dissects p53's Tumor Suppressor Functions', *PLoS Genetics*, 9(8), p. e1003726. doi: 10.1371/journal.pgen.1003726.

Schwarz, J. K., Lovly, C. M. and Piwnica-worms, H. (2003) 'Regulation of the Chk2 Protein Kinase by Oligomerization- Mediated cis - and trans -Phosphorylation', *Molecular cancer research*, 1(8), pp. 598–609.

Seshacharyulu, P. *et al.* (2013) 'Phosphatase: PP2A structural importance, regulation and its aberrant expression in cancer', *Cancer Letters*, 335(1), pp. 9–18. doi: 10.1016/j.canlet.2013.02.036.Phosphatase.

Shankaran, H. *et al.* (2009) 'Rapid and sustained nuclear-cytoplasmic ERK oscillations induced by epidermal growth factor', *Molecular Systems Biology*, 5(332), pp. 1–13. doi: 10.1038/msb.2009.90.

Sharp, D. A. *et al.* (1999) 'Stabilization of the MDM2 oncoprotein by interaction with the structurally related MDMX protein', *Journal of Biological Chemistry*, 274(53), pp. 38189–38196. doi: 10.1074/jbc.274.53.38189.

Sheng, C. (2017) *Cellular heterogeneity in the DNA damage response is determined by cell cycle specific p21 degradation*. Technical University Darmstadt.

Sheng, C. *et al.* (2019) 'PCNA-Mediated Degradation of p21 Coordinates the DNA Damage Response and Cell Cycle Regulation in Individual Cells', *Cell Reports*, 27(1), pp. 48-58.e7. doi: 10.1016/j.celrep.2019.03.031.

Shi, X. *et al.* (2007) 'Modulation of p53 function by SET8-mediated methylation at lysine 382', *Molecular Cell*, 27(4), pp. 636–646. doi: 10.1016/j.molcel.2007.07.012.Modulation.

Shibata, A. *et al.* (2011) 'Factors determining DNA double-strand break repair pathway choice in G2 phase', 30(6), pp. 1079–1092. doi: 10.1038/emboj.2011.27.

Shieh, S.-Y. *et al.* (1997) 'DNA Damage-Induced Phosphorylation of p53 Alleviates Inhibition by MDM2', *Cell*, 91(3), pp. 325–334. doi: 10.1016/s0092-8674(00)80416-x.

Shieh, S. *et al.* (2000) 'The human homologs of checkpoint kinases Chk1 and Cds1 (Chk2) phosphorylate p53 at multiple DNA damage-inducible sites', *Genes & Development*, 14(3), pp. 289–300.

Shieh, S. Y., Taya, Y. and Prives, C. (1999) 'DNA damage-inducible phosphorylation of p53 at N-terminal sites including a novel site, Ser20, requires tetramerization', *EMBO Journal*, 18(7), pp. 1815–1823. doi: 10.1093/emboj/18.7.1815.

Shikama, N. *et al.* (1999) 'A Novel Cofactor for p300 that Regulates the p53 Response', *Molecular Cell*, 4(3), pp. 365–376. doi: 10.1016/s1097-2765(00)80338-x.

Shin, Y. and Brangwynne, C. P. (2017) 'Liquid phase condensation in cell physiology and

disease', *Science*, 357(6357), p. eaaf4382. doi: 10.1126/science.aaf4382.

Shreeram, S. *et al.* (2006) 'Wip1 Phosphatase Modulates ATM-Dependent Signaling Pathways', *Molecular Cell*, 23(5), pp. 757–764. doi: 10.1016/j.molcel.2006.07.010.

Smeenk, L. *et al.* (2011) 'Role of p53 Serine 46 in p53 Target Gene Regulation', *PLoS ONE*, 6(3), p. e17574. doi: 10.1371/journal.pone.0017574.

Smith, L. and Thangue, N. B. La (2005) 'Signalling DNA Damage by Regulating p53 Co-Factor Activity', *Cell Cycle*, 4(1), pp. 30–32. doi: 10.4161/cc.4.1.1397.

Soule, H. D. *et al.* (1990) 'Isolation and Characterization of a Spontaneously Immortalized Human Breast', *Cancer Research*, 50(18), pp. 6075–6086.

Stavreva, D. A. *et al.* (2019) 'Transcriptional Bursting and Co-bursting Regulation by Steroid Hormone Release Pattern and Transcription Factor Mobility', *Molecular Cell*, 75(6), pp. 1161-1177.e11. doi: 10.1016/j.molcel.2019.06.042.

Stewart-Ornstein, J. and Lahav, G. (2017) 'p53 dynamics in response to DNA damage vary across cell lines and are shaped by efficiency of DNA repair and activity of the kinase ATM', *Science Signaling*, 10(476), pp. 1–11. doi: 10.1126/scisignal.aah6671.

Stommel, J. M. and Wahl, G. M. (2004) 'Accelerated MDM2 auto-degradation induced by DNA-damage kinases is required for p53 activation', *EMBO Journal*, 23(7), pp. 1547–1556. doi: 10.1038/sj.emboj.7600145.

Strasen, J. *et al.* (2018) ' Cell-specific responses to the cytokine TGF β are determined by variability in protein levels ', *Molecular Systems Biology*, 14(1), pp. 1–17. doi: 10.15252/msb.20177733.

Stucki, M. and Jackson, S. P. (2006) 'γH2AX and MDC1 : Anchoring the DNA-damage-response machinery to broken chromosomes', *DNA Repair*, 5(5), pp. 534–543. doi: 10.1016/j.dnarep.2006.01.012.

Suter, D. M. *et al.* (2011) 'Origins and consequences of transcriptional discontinuity', *Current Opinion in Cell Biology*, 23(6), pp. 657–662. doi: 10.1016/j.ceb.2011.09.004.

Sykes, S. M. *et al.* (2006) 'Acetylation of the p53 DNA-Binding Domain Regulates Apoptosis Induction', *Molecular Cell*, 24(6), pp. 841–851. doi: 10.1016/j.molcel.2006.11.026.

Tang, Y. *et al.* (2006) 'Tip60-Dependent Acetylation of p53 Modulates the Decision between Cell-Cycle Arrest and Apoptosis', *Molecular Cell*, 24(6), pp. 827–839. doi: 10.1016/j.molcel.2006.11.021.

Tang, Y. *et al.* (2008) 'Acetylation Is Indispensable for p53 Activation', *Cell*, 133(4), pp. 612–626. doi: 10.1016/j.cell.2008.03.025.

Tanimura, S. *et al.* (1999) 'MDM2 interacts with MDMX through their RING finger

domains', *FEBS Letters*, 447(1), pp. 5–9. doi: 10.1016/S0014-5793(99)00254-9.

Tay, S. *et al.* (2010) 'Single-cell NF-κB dynamics reveal digital activation and analog information processing in cells', *Nature*, 466(7303), pp. 267–271. doi: doi:10.1038/nature09145.

Terakawa, T., Kenzaki, H. and Takada, S. (2012) 'p53 Searches on DNA by Rotation-Uncoupled Sliding at C - Terminal Tails and Restricted Hopping of Core Domains', *Journal of the American Chemical Society*, 134(35), pp. 14555–62. doi: 10.1021/ja305369u.

Teufel, D. P., Bycroft, M. and Fersht, A. R. (2009) 'Regulation by phosphorylation of the relative affinities of the N-terminal transactivation domains of p53 for p300 domains and Mdm2', *Oncogene*, 28(20), pp. 2112–2118. doi: 10.1038/onc.2009.71.

Tiana, G., Jensen, M. H. and Sneppen, K. (2002) 'Time delay as a key to Apoptosis Induction in the p53 Network', *Eur. Phys. J. B*, 29(1), pp. 135–140.

Tibbetts, R. S. *et al.* (1999) 'A role for ATR in the DNA damage-induced phosphorylation of p53', *Genes and Development*, 13(2), pp. 152–157. doi: 10.1101/gad.13.2.152.

Timofeev, O. *et al.* (2013) 'P53 DNA Binding Cooperativity Is Essential for Apoptosis and Tumor Suppression InVivo', *Cell Reports*, 3(5), pp. 1512–1525. doi: 10.1016/j.celrep.2013.04.008.

Toettcher, J. E. *et al.* (2009) 'Distinct mechanisms act in concert to mediate cell cycle arrest', *Proceedings of the National Academy of Sciences of the United States of America*, 106(3), pp. 785–790. doi: 10.1073/pnas.0806196106.

Tunnacliffe, E. and Chubb, J. R. (2020) 'What Is a Transcriptional Burst ?', *Trends in Genetics*. Elsevier Ltd, 36(4), pp. 288–297. doi: 10.1016/j.tig.2020.01.003.

Tunnacliffe, E., Corrigan, A. M. and Chubb, J. R. (2018) 'Promoter-mediated diversification of transcriptional bursting dynamics following gene duplication', *Proceedings of the National Academy of Sciences of the United States of America*, 115(33), pp. 8364–8369. doi: 10.1073/pnas.1800943115.

Virshup, D. M. and Shenolikar, S. (2009) 'From Promiscuity to Precision : Protein Phosphatases Get a Makeover', *Molecular Cell*. Elsevier Inc., 33(5), pp. 537–545. doi: 10.1016/j.molcel.2009.02.015.

Vousden, K. H. (2000) 'p53 : Death Star', *Cell*, 103(5), pp. 691–694. doi: 10.1016/S0092-8674(00)00171-9.

Vugt, M. A. T. M. Van *et al.* (2010) 'A Mitotic Phosphorylation Feedback Network Connects Cdk1 , Plk1 , 53BP1 , and Chk2 to Inactivate the G 2 / M DNA Damage Checkpoint', *PLoS biology*, 8(1), p. e1000287. doi: 10.1371/journal.pbio.1000287.

Wade, M. and Wahl, G. M. (2010) 'Targeting Mdm2 and Mdmx in cancer therapy', *Molecular cancer research*, 7(1), pp. 1–11. doi: 10.1158/1541-7786.MCR-08-

0423.Targeting.

Wang, B. and Zhang, L. (2021) 'Liquid – liquid phase separation in human health and diseases', *Signal Transduction and Targeted Therapy*, 6(1), p. 290. doi: 10.1038/s41392-021-00678-1.

Wang, N. *et al.* (2015) 'A novel recurrent CHEK2 Y390C mutation identi fi ed in high-risk Chinese breast cancer patients impairs its activity and is associated with increased breast cancer risk', *Oncogene*, 34(40), pp. 5198–5205. doi: 10.1038/onc.2014.443.

Wang, Y. *et al.* (1995) 'Interaction of p53 with its consensus DNA-binding site.', *Molecular and Cellular Biology*, 15(4), pp. 2157–2165. doi: 10.1128/mcb.15.4.2157.

Wee, K. B. and Aguda, B. D. (2006) 'Akt versus p53 in a Network of Oncogenes and Tumor Suppressor Genes Regulating Cell Survival and Death', *Biophysical Journal*, 91(3), pp. 857–865. doi: 10.1529/biophysj.105.077693.

Wei, X. *et al.* (2016) 'Secondary interaction between MDMX and p53 core domain inhibits p53 DNA binding', *Proceedings of the National Academy of Sciences of the United States of America*, 113(19), pp. E2558–E2563. doi: 10.1073/pnas.1603838113.

Weinberg, R. L. *et al.* (2005) 'Comparative binding of p53 to its promoter and DNA recognition elements', *Journal of Molecular Biology*, 348(3), pp. 589–596. doi: 10.1016/j.jmb.2005.03.014.

West, A. G. and Attikum, H. Van (2006) 'Chromatin at the crossroads. Meeting on Signalling to Chromatin Epigenetics.', *EMBO Journal*, 7(12), pp. 1206–1210. doi: 10.1038/sj.embor.7400834.

Wu, X. *et al.* (1993) 'The p53-mdm2 autoregulatory feedback loop', *Genes & Development*, 7(7a), pp. 1126–1132. doi: 10.1101/gad.7.7a.1126.

Wu, X. and Chen, J. (2003) 'Autophosphorylation of Checkpoint Kinase 2 at Serine 516 Is Required for Radiation-induced Apoptosis', *Journal of Biological Chemistry*, 278(38), pp. 36163–36168. doi: 10.1074/jbc.M303795200.

Xia, J.-F. and Jia, Y. (2010) 'A mathematical model of a P53 oscillation network triggered by DNA damage A mathematical model of a P53 oscillation network triggered by DNA damage', *Chinese Physics B*, 19(4), p. 040506. doi: 10.1088/1674-1056/19/4/040506.

Xu, X., Tsvetkov, L. M. and Stern, D. F. (2002) 'Chk2 Activation and Phosphorylation-Dependent Oligomerization', *Molecular and Cellular Biology*, 22(12), pp. 4419–4432. doi: 10.1128/mcb.22.12.4419-4432.2002.

Xue, L. *et al.* (2009) 'Regulation of ATM in DNA double strand break repair accounts for the radiosensitivity in human cells exposed to high linear energy transfer ionizing radiation', *Mutation Research*, 670(1–2), pp. 15–23. doi:

10.1016/j.mrfmmm.2009.06.016.

Yissachar, N. *et al.* (2013) 'Dynamic Response Diversity of NFAT Isoforms in Individual Living Cells', *Molecular Cell*, 49(2), pp. 322–330. doi: 10.1016/j.molcel.2012.11.003.

Zannini, L., Delia, D. and Buscemi, G. (2014) 'CHK2 kinase in the DNA damage response and beyond', *Journal of Molecular Cell Biology*, 6(6), pp. 442–457. doi: 10.1093/jmcb/mju045.

Zhang, T. *et al.* (2007) 'Exploring Mechanisms of the DNA-Damage Response: p53 Pulses and their Possible Relevance to Apoptosis', *Cell Cycle*, 6(1), pp. 85–94. doi: 10.4161/cc.6.1.3705.

Zhao, Y. *et al.* (2006) 'Acetylation of p53 at Lysine 373/382 by the Histone Deacetylase Inhibitor Depsipeptide Induces Expression of p21Waf1/Cip1', *Molecular and Cellular Biology*, 26(7), pp. 2782–2790. doi: 10.1128/mcb.26.7.2782-2790.2006.

Zhou, Y. *et al.* (2017) 'Regulation of the DNA Damage Response by DNA-PKcs Inhibitory Phosphorylation of ATM', *Molecular Cell*, 65(1), pp. 91–104. doi: 10.1016/j.molcel.2016.11.004.

Zou, L. and Elledge, S. J. (2003) 'Sensing DNA damage through ATRIP recognition of RPA-ssDNA complexes', *Science*, 300(5625), pp. 1542–1548. doi: 10.1126/science.1083430.

7 APPENDIX

APPENDIX

7.1 Abbreviations

A

A	adenine/adenosine purine base
AHA	L-Azidohomoalanine
ATM	ataxia telangiectasia mutated
ATR	ataxia telangiectasia and Rad3-related protein
ATRIP	ATR interacting protein
A549	adenocarcinomic human alveolar basal epithelial cells

B

BAX	Bcl-2-associated X protein
bp	basepairs
BD	binding domain
BS	beam splitter
BSA	bovine serum albumin

C

C	cytosine/cytidine pyrimidine base
C	cysteine
Cas9	Caspase-9
CBP	CREB binding protein
CDC25	cell division cycle phosphatase 25
CDKN1A	cyclin dependent kinase inhibitor 1A (p21)
CFP	cyan fluorescent protein
ChIP	chromatin immunoprecipitation
CHK1	checkpoint kinase 1
CHK2	checkpoint kinase 2
Chr	chromosome
CHX	cycloheximide
CREB	cAMP response element binding protein
Ct	cycle threshold value
CTD	C-terminal domain
Ctrl	control

D

DBD	DNA binding domain
DMSO	dimethyl sulfoxide
DNA	deoxyribonucleic acid
DNA-PKcs	DNA-dependent protein kinase
DSB	double strand break

E

EGF	epidermal growth factor
EM	emission
EX	excitation

F

FCS	fetal calf serum
fc	fold change
FHA	forkhead-associated
FP	fixed point
FWHM	full width at half maximum

G

G	guanine/ guanosine pyrimidine base
GAPDH	glyceraldehyde 3-phosphate dehydrogenase
GFP	green fluorescent protein

	Gy	gray
H		
	H2AX	histone 2AX
	H2B	histone 2B
	HAT	histone-acetyltransferase
	HMT	Histone Methyl Transferase
	HR	homologous recombination
	HRP	horseradish peroxidase
	HS	horse serum
I		
	IF	immunofluorescence
	IR	ionizing radiation
J		
	JMY	junction-mediating and regulatory protein
K		
	K	lysine
	Kb	kilobases
M		
	mAID	mini auxin-inducible degron
	MCF7	Michigan Cancer Foundation-7 (breast cancer cell line)
	MCF10A	Michigan Cancer Foundation-10A (immortalized breast epithelial cell line)
	MDMX	mouse double minute 2, also known as MDM4 or HDMX
	MDM2	mouse double minute 2, also known as HDM2
	min	minutes
	MRN	Mre11, Rad50 and Nbs1
	mRNA	messenger ribonucleic acid
N		
	NA	numerical aperture
	NCS	neocarcinostatin
	NES	nuclear export sequence
	NFDM	Non-fat dried milk
	NHEJ	non-homologous end joining
O		
	OD	oligomerization domain
P		
	PAGE	polyacrylamide gel electrophoresis
	PBS	phosphate buffered saline
	PCR	polymerase chain reaction
	PDF	probability density function
	PFA	paraformaldehyde
	PIKK	phosphatidylinositide 3-kinase-related kinase
	MTp	rat metallothionein promoter
	PRD	proline-rich domain
	PTM	post-translational modification
	PPM1D	protein phosphatase Mg2+/Mn2+ dependent 1D, also known as WIP1
Q		
	qRT-PCR	quantitative real-time PCR
R		
	RD	redamaging
	RE	response element
	RNA	ribonucleic acid

	rpm	revolutions per minute
	RQ	relative quantity
	RT	room temperature
S		
	S	Serine
	SCD	SQ/TQ cluster
	SDS	sodium dodecyl sulfate
	SE	standard error of the mean
	shRNA	small hairpin ribonucleic acid
	SMASh	small Molecule-Assisted Shutoff
	smFISH	single-molecule fluorescence in-situ hybridization
	SSB	single strand breaks
	ssDNA	single stranded DNA
	STRAP	stress-responsive activator of p300
T		
	T	thymine/ thymidine pyrimidine nucleobase
	T	amino acid threonine
	t	time
	TAD	trans-activation domain (of the p53 protein)
	TBS	tris buffered saline
	TBS-T	tris buffered saline with Tween
	TF	transcription factor
	TSS	transcriptional start site
U		
	UbCp	ubiquitine C promoter
	UTR	untranslated region
	UV	ultraviolet (radiation)
W		
	WT	wild type
Y		
	Y	amino acid tyrosine
	YFP	yellow fluorescent protein
0-9		
	53BP1	p53 binding protein 1
	9-1-1	RAD9-HUS1-RAD1
	3DOT	3D orbital tracking

7.2 List of Figures

7.3 List of Tables

7.4 Supplementary Tables

Table 7.4.1: Number of cells analysed in the respective experiments.

Figure	Experiment	Condition	Cell #
Figure 3.1.1A-B	Re-damaging	0.2 µg/mL NCS	671
		0.4 µg/mL NCS	668
		0.2 + 0.2 µg/mL NCS	689
Figure 3.1.1C-G	Re-damaging at different time points	Ctrl	682
		Re-damaging at 1 h	673
		Re-damaging at 2.5 h	773
		Re-damaging at 4 h	834
		Re-damaging at 5.5 h	744
		Re-damaging at 7 h	711
Figure 3.2.1C-D	P53 dynamics upon ATM inhibition (A549 Reporter)	DMSO	709
		ATMi at -1 h	714
		ATMi at 1 h	840
Figure 3.2.2B	P53 dynamics upon ATM inhibition (MCF10A Reporter)	DMSO	440
		ATMi at -1 h	552
		ATMi at 3 h	884
Figure 3.3.1A-B	P53 dynamics upon ATRi or DNA-PKi (A549 Reporter)	DMSO	709
		DNA-PKi at -1 h	820
		DNA-PKi + ATMi at 1 h	745
		ATRi at -1h	295
		ATRi + ATMi at 1 h	242
Figure 3.3.2A-C	P53 dynamics upon CHK2 inhibition (A549 Reporter)	DMSO	709
		CHK2i at -1 h	676
Figure 3.3.3B	P53 dynamics upon CHK2 inhibition (MCF10AReporter)	DMSO	440
		CHK2i at 3 h	853
Figure 3.3.3C	P53 dynamics upon CHK2 depletion	Untreated	167
		Control siRNA	249
		CHK2 siRNA	412
Figure 3.3.4	P53 dynamics in different cell cycle phases	DMSO G1	308
		DMSO S/G2	177
		ATMi G1	407
		ATMi S/G2	394

		CHK2i G1	340
		CHK2i S/G2	298
Figure 3.3.5	P53 dynamics in different cell cycle phases	CHK2i + ATMi G1	306
		CHK2i + ATMi S/G2	246
Figure 3.3.6A	P53 dynamics upon CHK2/ATM inhibition and re-damaging	DMSO	444
		DMSO Re-damaging	455
		ATMi	468
		ATMi Re-damaging	633
		CHK2i	463
		CHK2i Re-damaging	541
Figure 3.3.6C-D	P53 upon WIP1 depletion	DMSO Control	400
		DMSO Scrambled siRNA	467
		DMSO WIP1 siRNA	863
		CHK2i Control	817
		CHK2i Scrambled siRNA	621
		CHK2i WIP1 siRNA	980
Figure 3.3.7	P53 dynamics upon CHK2i inhibition at 5 h	DMSO	239
		CHK2i at 5h	333
Figure 3.7.1	Wash-off of CHK2 inhibition	DMSO	567
		ATMi + CHK2i	497
		ATMi + CHK2i + WO	386
		ATMi + CHK2i + WO ATMi	449
Figure 3.7.4B	P53 dynamics upon increasing doses of IR	0.5 Gy	522
		1 Gy	510
		2 Gy	822
		5 Gy	1068
		10 Gy	1159
Figure 3.7.4C-D	P53 dynamics upon ATM inhibition at different time points	DMSO	287
		ATMi at 15 min	433
		ATMi at 30 min	315
		ATMi at 60 min	406
		ATMi at 120 min	262

Table 7.4.2: Thresholds for pulse analysis.

Figure	Experiment	Threshold
Figure 3.1.1A-B	Re-damaging	0.2
Figure 3.1.1C-G	Re-damaging at different time points	0.2
Figure 3.2.1C-D	P53 dynamics upon ATM inhibition	0.2
Figure 3.3.1A-B	P53 dynamics upon ATR or DNA-PK inhibition (A549 Reporter)	0.2
Figure 3.3.2A-C	P53 dynamics upon CHK2 inhibition (A549 Reporter)	0.2
Figure 3.3.4	P53 dynamics in different cell cycle phases	0.15
Figure 3.3.5	P53 dynamics in different cell cycle phases upon CHK2 and ATM inhibition	0.15
Figure 3.3.6C-D	P53 upon WIP1 depletion	0.3
Figure 3.3.7	P53 dynamics upon CHK2i inhibition at 5 h	0.2
Figure 3.7.1	Wash-off of CHK2 inhibition	0.2
Figure 3.7.4B	P53 dynamics upon increasing doses of IR	0.3
Figure 3.7.4C-D	P53 dynamics upon ATM inhibition at different time points	0.3

7.5 Supplementary Figures

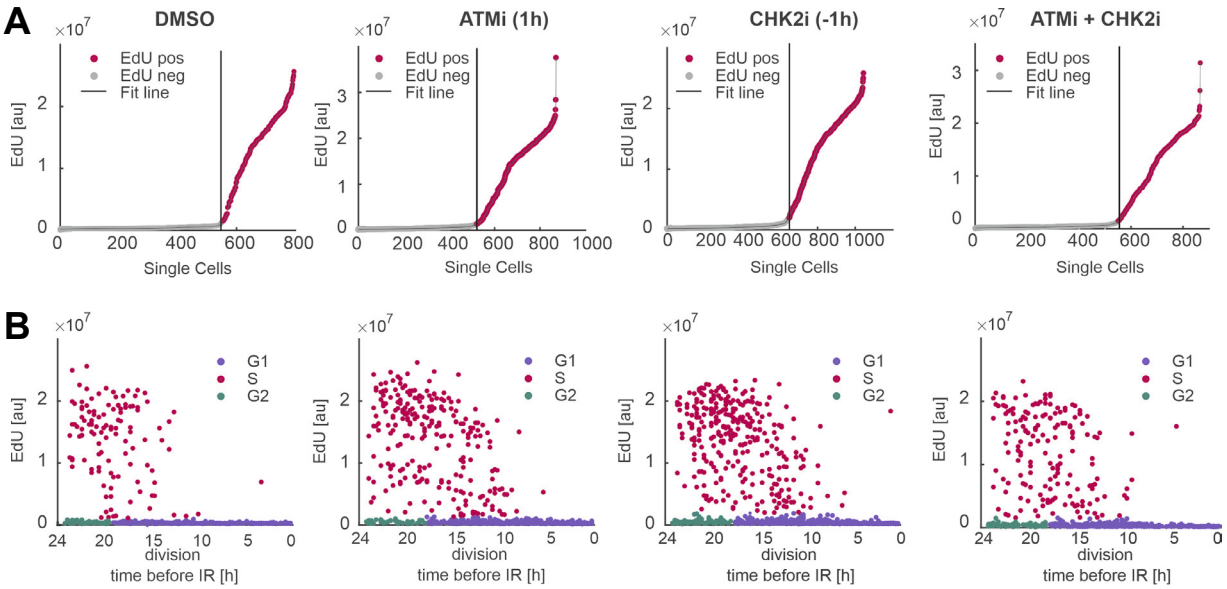

Figure 7.5.1: Determination of the cell cycle phase at time of irradiation.

A. Detection of S-phase cell by EdU staining. Cells were sorted according to their EdU signal and fitted along the X-axis to remove noise. S-phase cells were determined using an edge detection algorithm (Sheng, 2017). **B.** Timepoint of last cell division before irradiation (IR) was determined for all cells. Cells that divided before S-phase cells were sorted as G2 phase cells, cells that divided after S-phase cells were sorted as G1-phase cells.

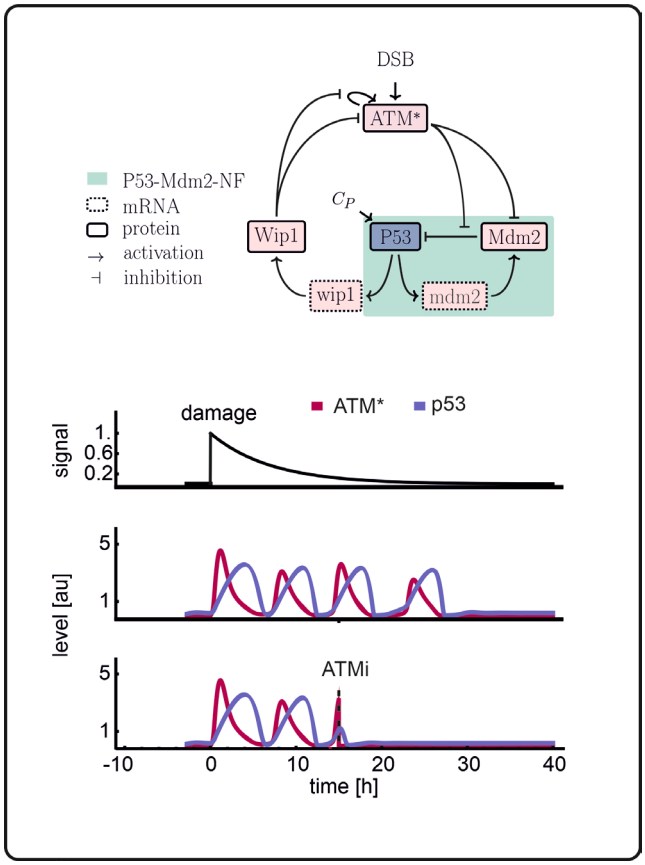

Figure 7.5.2: Model of the p53 pathways based on Mönke *et al.*, 2017.

A. Network scheme for the model. ATM activation is induced by DNA DSB. Active ATM (ATM*) fosters the formation of more ATM*. Active ATM destabilizes MDM2 by phosphorylation. P53 activates transcription of WIP1 and MDM2. WIP1 dephosphorylates ATM and interferes with positive feedback on ATM. **B.** Simulated time series. Pulses occur until the damage signal falls below a threshold value. ATMi inhibition immediately terminates the p53 response. **Modeling from Raphael Löffler.**

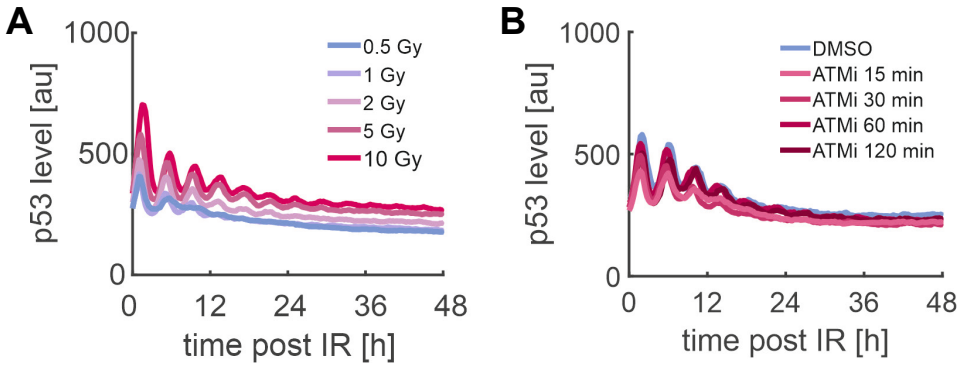

Figure 7.5.3: The total number of pulses increases with the damage dose.

A. A549 reporter cells were irradiated with increasing doses (0.5 to 10 Gy) and followed via time-lapse live-cell microscopy. Trajectories show the median nuclear fluorescence intensity of p53. **B.** A549 reporter cells were treated with an ATM inhibitor at different time points post 5 Gy IR (15-120 min) and tracked via time-lapse live-cell microscopy. Trajectories show the median nuclear fluorescence intensity of p53. The number of cells analysed per condition as well as the threshold used for pulse analysis can be found in Table 7.4.1 and Table 7.4.2.

ACKNOWLEDGEMENT

During the work on this project, I learned more but also faced more challenges than ever before. This would not have been possible without the support of many people, both in the lab and in my personal life.

First and foremost, I want to thank Prof. Alexander Löwer for introducing me to the fascinating world of p53 and systems biology. I really appreciated your input and patience during more discussions than I can count and especially your support during the challenging times of my project. I could not have wished for a better supervisor.

I would also like to thank Prof. Markus Löbrich for his input during retreats and TAC meeting and for agreeing to review my thesis.

Furthermore, I want to thank Prof. Barbara Drossel, Isabella Mendler and Raphael Löffler for a lot of fruitful discussions and for expanding and even changing my view on the p53 network.

Importantly, I want to thank the Löwer group and all their current and former members for taking me in and making my PhD an incredible time. You opened so many doors for me. Special thanks to Anna, not only for the many hours in the lab, in an office full of unicorns or in Austria making floral wreaths. Also for listening and supporting me, whenever I needed you. Thank you to Stefan for office evenings with tea and baskets full of tangerines and for your support in the very beginning of my project and at the end. Thank you to Petra, not only for backing me up in the lab but also for listening to my complaints and your moral encouragement. It meant a lot to me. Thank you to Bettina for your almost magical technical assistance. Ann-Kathrin, Zixin, Flavia, Jenny, Theresa, Sonja, Sara, Anne, Caibin and Marcel: Thank you for lunch breaks in the botanical garden, (Singstar) parties and head-sized bufala mozzarellas and for lending me a helping hand, whenever I needed it. I hope you know, how much I appreciated it. Thank you to Dhana Friedrich for sharing your scientific passion and enthusiasm with me. It was a pleasure to work with you.

Moreover, I would like to thank Maria and Francesco for their support and supply with evenings full of tasty food and laughter. Without you, I sometimes literally would not have been able to get to work.

Besonderer Dank gilt meinen Eltern. Ich kann immer auf eure bedingungslose Unterstützung und euer Verständnis zählen, egal in welcher Situation, egal zu welcher Uhrzeit. Ohne euch wäre diese Arbeit nicht möglich gewesen. Kristina und Julia, ich bin froh euch zu haben!

Finally, I want to thank Lorenzo for his sheer endless support during this journey. I do not know where to start. Thank you for driving with me to work on snowy weekends, for waiting with a warm dinner for me whenever I was coming home late, for making me laugh every day and for the countless other things you did and still do to support me. I am so happy to have you in my life.

EHRENWÖRTLICHE ERKLÄRUNG

Ich erkläre hiermit, dass ich die vorliegende Arbeit entsprechend den Regeln guter wissenschaftlicher Praxis selbstständig und ohne unzulässige Hilfe Dritter angefertigt habe.

Sämtliche aus fremden Quellen direkt oder indirekt übernommenen Gedanken sowie sämtliche von Anderen direkt oder indirekt übernommenen Daten, Techniken und Materialien sind als solche kenntlich gemacht. Die Arbeit wurde bisher bei keiner anderen Hochschule zu Prüfungszwecken eingereicht. Die eingereichte elektronische Version stimmt mit der schriftlichen Version überein.

Darmstadt, den ……

……..
Laura Friedel

„Expecto Patronum“